UNIVERSITY OF CALIFORNIA SAN DIEGO

Cell Density Regulates the Golgi through Hippo, the STRIPAK Complex, and GOLPH3

A dissertation submitted in partial satisfaction of the requirements for the degree

Doctor of Philosophy

in

Biology

by

Thuy Thi Thu Tran

Committee in charge:

Professor Seth J. Field, Chair
Professor Amy Kiger, Co-chair
Professor Kun-liang Guan
Professor Tony Hunter
Professor Maho Niwa

2018

The dissertation of **Thuy Thi Thu Tran** is approved, and it is acceptable in quality and form for publication on microfilm and electronically:

_____

_____

_____

_____
Co-chair

_____
Chair

University of California San Diego

2018

DEDICATION

I dedicate this dissertation to my husband, Tu Viet Nguyen, who got his PhD in Electrical Engineering from Jacob School of Engineering, UCSD in 2013, then immediately started enduring all the struggles of doing a PhD in Biology with me. Two PhDs end-to-end, how many people could go through that much.

TABLE OF CONTENTS

LIST OF ABBREVIATIONS

GOLPH3	Golgi Phosphoprotein 3
MYO18A	Myosin 18A
STRIPAK	Striatin Interacting Phosphatase And Kinase
STRN3	Striatin 3
PP2A	Protein Phosphatase 2A
PP2Ac	Protein Phosphatase 2A catalytic subunit
CTTNBP2NL	Cortactin-Binding Protein 2 N-Terminal Like
STRIP1	Striatin-Interacting Protein 1
MST1	Mammalian STE20-like 1
MST2	Mammalian STE20-like 2
LATS1	Large Tumor Suppressor Kinase 1
LATS2	Large Tumor Suppressor Kinase 2
PDGFA	Platelet Derived Growth Factor Subunit A
GAPDH	Glyceraldehyde 3-Phosphate Dehydrogenase
GM130	Golgi Matrix Protein 130
ManII	Mannosidase II
GFP	Green Fluorescent Protein
VSVG	Vesicular Stomatitis Virus G Protein
IP	Immunoprecipitation
IF	Immunofluorescence
DIC	Differential Interference Contrast

LIST OF FIGURES

LIST OF TABLES

ACKNOWLEDGEMENTS

At the end of this journey looking back, I still could not believe what I have been through it. I could not imagine how much I have transformed in the past six years and a half. Gone is the girl who was very naïve, easy to believe, did not know how to ask questions. Now it is a much tougher woman, no less stubborn, but even more determined. I would like to thank all the people who has been in and out the journey with me.

I would like to thank my advisor Dr. Seth Field especially. He has guided me through my dissertation project. I would like to thank my committee members: my co-chair Dr. Amy Kiger, Dr. Maho Niwa, Dr. Kun-Liang Guan, and Dr. Tony Hunter who have been very kind and helpful through their advice on my project. I am grateful to Dr. Kun-Liang Guan for his input for my project and letting people in his lab show me how to do some new experiments. I would like to thank Dr. Huilin Zhou of Ludwig Cancer Research, La Jolla and his scientist Dr. Claudio Ponte de Albuquerque. Although my collaboration with their lab is not mentioned in this dissertation, I appreciate their kindness and generousness in teaching me many out-of-scope experimental techniques to satisfy my scientific curiosity.

I would like to thank past and present members of the Field's lab, who have given me the best support and a good environment to finish my project. Through conversation with them, I learned a lot about U.S culture and learned how much people hold divergent backgrounds, thoughts, and actions.

I would like to thank my family, who from afar, gives me all the freedom to do whatever I want but reminds me that I need to finish and go home soon.

Finally yet importantly, I would like to thank the Chair of the Graduate study in the Biological Sciences program, Dr. Jens Lykke-Andersen, who is always there to help graduate students with their various problems. I am lucky to have administrative staffs of the Biological Sciences program who give constant support to graduate students in the program.

Chapter 2 is the complete text and figures of the manuscript by Tran, T.T.T, Dippold, H.C., Makowski, S.L., Buschman, M.D., Tanaka, H., Guan, K.-L., and Field, S.J. (2018). Cell Density Regulates the Golgi Through Hippo, the STRIPAK Complex, and GOLPH3. Manuscript is in review with Developmental Cell. I, Thuy Thi Thu Tran, is the primary investigator and author of this paper.

VITA

2007 – 2011	Bachelor of Biomedical Science, National University of Singapore, Singapore.
2011 – 2012	Research assistant, Codexis Laboratories, Singapore.
2012 – 2018	Doctor of Philosophy in Biology, University of California San Diego, USA.

PUBLICATIONS

"**Tran, T.T.T**, Dippold, H.C., Makowski, S.L., Buschman, M.D., Tanaka, H., Guan, K.-L., and Field, S.J. (2018). Cell Density Regulates the Golgi Through Hippo, the STRIPAK Complex, and GOLPH3. Manuscript is in review with Developmental Cell."

"Makowski, S.L., **Tran, T.T.T.**, and Field, S.J. (2017). Emerging themes of regulation at the Golgi. Curr. Opin. Cell Biol. 45, 17–23."

"Zhang, J., Yang, L., Ang, Z., Yoong, S.L., **Tran, T.T.T.**, Anand, G.S., Tan, N.S., Ho, B., and Ding, J.L. (2010). Secreted M-Ficolin Anchors onto Monocyte Transmembrane G Protein-Coupled Receptor 43 and Cross Talks with Plasma C-Reactive Protein to Mediate Immune Signaling and Regulate Host Defense. Journal of Immunology 185, 6899–6910."

ABSTRACT OF THE DISSERTATION

Cell Density Regulates the Golgi through Hippo, the STRIPAK Complex, and GOLPH3

by

Thuy Thi Thu Tran

Doctor of Philosophy in Biology

University of California San Diego, 2018

Professor Seth Field, Chair
Professor Amy Kiger, Co-chair

The Golgi is the main hub for the modification, sorting, and transport of proteins to various intra- and extracellular destinations. Against conventional belief that most of Golgi trafficking was constitutive, our data show regulation of Golgi morphology and trafficking in response to cell density and extracellular cues.

Studies in our lab showed that the Golgi phosphoprotein 3 (GOLPH3) functions at the Golgi in the GOLPH3 complex to regulate Golgi trafficking. GOLPH3 is recruited to

the Golgi by binding to phosphatidylInositol-4-phosphate (PI(4)P), which is enriched at the *trans*-Golgi. GOLPH3 also interacts with Myosin 18A (MYO18A), which in turn binds F-actin. The linkages of PI(4)P-GOLPH3-MYO18A-F-actin make the basis of the GOLPH3 complex, which provides a tensile force applied onto Golgi membranes to aid in vesicles budding for protein transport. The consequence of that process is the Golgi being stretched in the form of an extended ribbon that surrounds the nucleus. We have shown that interfering with the GOLPH3 complex reduces cellular transport and alters Golgi morphology.

Here, we identify a signaling pathway that transduces cell density signal through the Hippo proteins MST1/2 and the Striatin interacting phosphatases and kinases (STRIPAK) complex to the GOLPH3 complex to regulate Golgi forward trafficking. In sparsely growing cells, the MST1/2 protein kinases, independently of their kinase activity and the canonical Hippo pathway, act to promote the localization of Striatin 3 (STRN3) to the Golgi where STRN3 directly interacts with GOLPH3 bridging it with other members of the STRIPAK complex. The PP2A phosphatase activity of STRIPAK promotes GOLPH3's interaction with MYO18A, which together drive Golgi forward trafficking and impart its normal, extended ribbon shape. On the other hand, high cell density inhibits interaction between STRIPAK complex to GOLPH3, taking away the effect of PP2A, which results in a weaken GOLPH3-MYO18A interaction. Inhibition of GOLPH3-MYO18A interaction results in a compact Golgi and reduced Golgi trafficking in high cell density.

Through control of secretion, cell density signaling through MST1/2, STRIPAK, and GOLPH3 complex regulate paracrine growth factor signaling, providing a means to affect the proliferation of neighboring cells.

CHAPTER 1: INTRODUCTION TO THE GOLPH3 COMPLEX, THE HIPPO PATHWAY, AND CELL DENSITY SIGNALING

1.1 The Golgi structure and trafficking.

First discovered in year 1897 by Camillo Golgi, hence the name, the Golgi is an universal organelle found in most eukaryotic cells (Review: (Dröscher, 1998)). Observing under electron microscope, the Golgi was described as flatten cisternae of membrane piled on top of each other to form stacks (Dalton and Felix, 1954; Sjöstrand and Hanzon, 1954). The Golgi is a main organelle that functions in protein modification and secretion. Most of the plasma membrane resident and secretory proteins need to go through the Golgi before reaching their destinations (Farhan and Rabouille, 2011). Figure 1.1A shows a 3D reconstruction of an *Arabidopsis* Golgi stack (Staehelin and Kang, 2008) which represents a typical Golgi stack. A typical Golgi stack composes of four general sub compartments: *cis*-Golgi, which includes cisternae that are close to the nucleus; *trans*-Golgi, which includes cisternae that are away from the nucleus; *medial*-Golgi, of which cisternae are in between *cis*- and *trans*-Golgi; and Trans Golgi Network (TGN), the outer most cisterna, which has the most vesicle-budding activity. Identity of each Golgi sub compartment is maintained by resident enzymes, membrane binding proteins, and lipid composition of cisternae membrane (Munro, 2005; Puthenveedu and Linstedt, 2005). The structure of Golgi stacks is well conserved across many eukaryotic species, from amoeba to human. Figure 1.1B shows Golgi stacks of the simple, single-cell-eukaryote amoeba (Wise and Flickinger, 1970). Figure 1.1C shows a Golgi stack of tobacco plants (Staehelin and Kang, 2008). Figure 1.1D shows a Golgi stack of yeast *Pichia pastoris* (Rossanese

et al., 1999). Figure 1.1E shows structure of a human Golgi stack, of which appearance is similar to Golgi stacks of other higher eukaryotes (Dippold et al., 2009).

Although most college textbooks depict a eukaryotic cell with a single Golgi stack, each eukaryotic cell contains many more of those stacks in the cytoplasm. For example, an amoeba cell or a plant root cap cell could contain several hundred Golgi stacks (Dupree and Sherrier, 1998; Wise and Flickinger, 1970). The number of Golgi stacks in a cell varies with cell types and species. Animal cells typically have ten to a few dozen Golgi stacks. While Golgi stacks in amoeba and plants disperse throughout the cytoplasm, mammalian Golgi stacks are connected by membraneous tubules to form a ribbon in the perinuclear region. Research shows that Golgi ribbon formation depends on microtubules that link all mini stacks (Wehland et al., 1983; Thyberg and Moskalewski, 1985; Valm et al., 2017); also, within each stack, cisternae are glued together by GRASP55 and GRASP65, which also contribute to the integrity of the ribbon and Golgi function (Review: (Zhang and Wang, 2016)).

Figure 1.2 sketches transportation of proteins to other organelles or outside of the cells as well as back to the ER. The anterograde (forward) trafficking process starts with protein production in the ER. COPII vesicles bring proteins from the ER to *cis*-Golgi. From *cis*-Golgi, proteins continue to be transported to *med*- and *trans*-Golgi. By traveling along Golgi sub-compartments, proteins are further modified and sorted to make sure they reach correct destinations, either other organelles, the plasma membrane, or outside of the cells. In the retrograde (reverse) trafficking process, mis-transported resident enzymes specific for ER or each Golgi-sub compartment are returned to the correct sub

compartment in COPI vesicles (Appenzeller-Herzog and Hauri, 2006; Strating and Martens, 2009).

Despite important roles of the Golgi in protein transport, little is known about how this process is regulated (Snyder et al., 2006). Recent evidences suggest that Golgi binding proteins and Golgi lipid composition function in regulation of Golgi trafficking (Kuna and Field, 2018; Makowski et al., 2017; Munro, 2005). In 2009, our lab published characterization of a GOLPH3 complex at the Golgi that regulates Golgi forward trafficking.

1.2 GOLPH3 complex and Golgi forward trafficking

Our findings showed that the GOLPH3 complex at the Golgi facilitate Golgi forward trafficking. In the GOLPH3 complex, GOLPH3 binds to PI(4)P, GOLPH3 also binds to MYO18A, and MYO18A binds to F-actin. These linkages create a tensile force which is exerted on the Golgi membrane to facilitate vesicle budding from the *trans*-Golgi (Dippold et al., 2009; Farber-Katz et al., 2014; Ng et al., 2013; Xing et al., 2016) (Figure 1.3A).

The phosphatidylinositol-4-phosphate (PI(4)P) is generated by phosphorylation of phosphatidylinositol at carbon position 4 on inositol ring. Despite having low levels elsewhere, PI(4)P is abundant at the Golgi, especially on *trans*-Golgi (Di Paolo and De Camilli, 2006; van Meer et al., 2008). The level of PI(4)P at the Golgi is maintained by kinases and phosphatases that make and degrade PI(4)P. PI4KIIIα, PI4KIIIβ, and PI4KIIα kinases have been shown to localize to the Golgi to increase PI(4)P level (Balla et al., 2002; Barylko et al., 2001; Minogue et al., 2001). On the other hand, Sac I, an ER-resident phosphatase, translocates to the Golgi to reduce PI(4)P level upon serum starvation (Blagoveshchenskaya et al., 2008). Manipulating PI(4)P level at the Golgi by interfering

with PI4K kinases and phosphatases reveals the function of PI(4)P in promoting Golgi forward trafficking (Hama et al., 1999; Wang et al., 2003). Although many effectors of PI(4)P have been identified, strikingly, most of them function in non-vesicular lipid transport such as CERT which transports ceramide from the ER to the *trans*-Golgi, OSBP which transports cholesterol from the ER to the *trans*-Golgi, and FAPP2 which transports glucosylceramide from the *cis*-Golgi to the *trans*-Golgi (Review: (Makowski et al., 2017)). Different from other PI(4)P effectors, GOLPH3 protein binds PI(4)P to facilitate Golgi trafficking.

The Golgi phosphoprotein 3 (GOLPH3) was first identified in biochemical assays by two independent groups, (Wu et al., 2000) and (Bell et al., 2001). They subjected the Golgi fraction of rat liver cells (which have predominant Golgi) to mass spectroscopy and identified a protein of about 33 – 34 kDa, which conserves from yeast to human. They named it GMx33 and GPP34 respectively. In further experiments, both groups showed that GOLPH3 localizes to the *trans*-Golgi. GOLPH3 was shown to be phosphorylated at multiple sites in a 2D gel (Wu et al., 2000). While GOLPH3 later was shown to associate with Golgi tubules (Snyder et al., 2006), no one at that time was sure about what GOLPH3 would do to the Golgi.

Efforts have been made to crystalize GOLPH3 (Figure 1.3B). The crystal structure of the yeast homolog of GOLPH3, Vps74 reveal a single globular domain with many α-helices and two protruding outward β-strands (Schmitz et al., 2008; Wood et al., 2009). The protruding β-strands are called a β-hairpin. Interestingly, the Vps74 structure is very similar to the Vps36 structure. Because Vps36 uses its β-hairpin to insert into a binding pocket at the center of the ESCRTII complex, the β-hairpin of Vps74 is predicted to insert

in some unknown of structure. Together with yeast Vps74, mammalian GOLPH3 has been crystallized, and also has a protruding β-hairpin (Figure 1.3B).

Our published work (Dippold et al., 2009; Ng et al., 2013; Xing et al., 2016) led to the discovery of GOLPH3 as a main effector of PI(4)P in a proteomic screen for PI(4)P binding proteins. GOLPH3 of human, fly, and yeast all bind to PI(4)P. Disabling Pik1, the yeast PI(4)P kinase responsible for making PI(4)P, leads to GOLPH3 disassociation from the Golgi. A similar effect was observed with expression of a PI(4)P phosphatase that localizes to the Golgi. We showed that knockdown of GOLPH3 leads to collapse of the Golgi ribbon and reduced total protein secretion as measured by the ^{35}S-amino acid pulse chase assay (Dippold et al., 2009; Ng et al., 2013; Xing et al., 2016) (Figures 1.3C&1.3E).

In a complex with GOLPH3, Myosin 18A (MYO18A) was shown to bind directly to GOLPH3 (Buschman and Field, 2017; Dippold et al., 2009; Farber-Katz et al., 2014; Taft et al., 2013). First cloned from a stromal cell lines, MYO18A is considered a non-conventional Myosin with an “extra” PDZ domain before the N-terminal motor domain (Furusawa et al., 2000). MYO18A has been shown to bind F-actin directly. However, unlike other myosins, which hydrolyze ATP to move along F-actin, whether MYO18A has motor activity is still a topic of debate (Guzik-Lendrum et al., 2013; Isogawa et al., 2005; Taft et al., 2013). Nevertheless, (Billington et al., 2015) showed the ability of MYO18A to form mixed bipolar filaments with myosin II, which suggests that MYO18A could still move along F-actin. Our lab reported that knocking down of MYO18A, similar to knocking down of GOLPH3, leads to a compact Golgi, reduces Golgi exit frequency and total protein secretion (Buschman and Field, 2017; Dippold et al., 2009; Kuna and Field, 2018; Ng et al., 2013; Xing et al., 2016) (Figures 1.3D&1.3E).

When our lab looked into regulation of Golgi trafficking through the GOLPH3 complex, we identified another critical component, the STRIPAK complex.

1.3 The STRIPAK complex

The STRiatin-Interacting-Phosphatase and kinases (STRIPAK) complex consists of the STRN3 scaffolding protein bringing together MOB4, PP2A, STRIP1/2, CCM3, GCKIII, and CTTNBP2/CTTNBP2NL or SIKE/SLMAP. STRN3 was suggested to bind directly to MOB4, PP2A, STRIP1/2, and CCM3. Then STRIP1/2 bridge either CTTNBP2/NL or SIKE/SLMAP to STRN3 in a mutually exclusive manner. CCM3 links GCKIII to STRN3 (Goudreault et al., 2009; Hauri et al., 2013) (Figure 1.4A). However, recent views of the STRIPAK complex from different mass spectrometry experiments suggest more interdependent interactions between STRIPAK members, in which MOB4 could also bind GCKs, STRIP1/2 could also interact with PP2A, and SIKE could also bind directly to STRN3 (Review: (Shi et al., 2016)) (Figure 1.4B).

At the core of the STRIPAK complex is STRN3. STRN3 was first detected as a nuclear antigen in S and G2 phase of HepG2 cells being stained with serum of a patient with non-invasive bladder carcinoma (Muro et al., 1995). Hence, STRN3 was first named SG2NA. The domain structure of STRN3 consists of six tandem WD-40 motifs at the C-terminal end, and camodulin (CaM), caveolin (CaV), and a coiled coil (C-C) domain at the N-terminal end. The WD-40 motifs are often observed in scaffolding proteins, in which an array of WD-40 forms a β-propeller structure which interacts with other proteins (Smith, 2008). Later work by Pallas and colleagues showed that STRN3 binds calmodulin and is in a complex with PP2A phosphatase. However, both interaction of STRN3 with PP2A and PP2A phosphatase activity do not depend on Ca^{++} (Moreno et al., 2000). Informatics

prediction showed the N-terminus of STRN3 to contain not only calmodulin (CaM) but also caveolin (CaV) and coiled coil (C-C) motifs. All three are collectively called the Striatin domain (Gaillard et al., 2001; Moreno et al., 2001). A schematic representation of the STRN3 protein is in Figure 1.5.

The STRIPAK complex contains PP2A holoenzyme. PP2A is a serine/threonine phosphatase ubiquitously expresses in all eukaryotic cells. PP2A complex includes a catalytic subunit, a scaffolding subunit, and a regulatory subunit. PP2A catalytic subunit (PP2Ac) occurs in two isoforms α and β, which have high sequence homology (97%). Similarly, PP2A scaffolding subunit PP2A A also has two isoforms α and β, again with high sequence homology (86%). More divergent is the PP2A regulatory subunit PP2A B. There are four different families of regulatory subunit B, denoted B, B', B'', and B'''. A second way of naming them is B55/PR55, B56/PR61, PR48/PR72/PR130, and PR93/PR110. Although it looks more complicated, the second way of naming shows the relative molecular weight of each subunit. STRN3 belongs to B'''/PR93/PR110 group (Figure 1.6A) (Review: (Seshacharyulu et al., 2013)). By making their own antibodies again PP2Ac, PP2A B', and STRN3, Pallas and his group showed co-IP of STRN3 with the PP2A A/C complex and vice versa. The co-IP experiment was done with lysates of transformed NIH3T3 cells overexpressing Ha-tagged mutant or wildtype PP2Ac (Moreno et al., 2000). STRIPAK complex has been shown to interact with the Hippo kinases MST1/2 in mammals, and its PP2A functions in deactivating Hippo kinases (Bae et al., 2017; Couzens et al., 2013; Hauri et al., 2013; Ribeiro et al., 2010; Zheng et al., 2017). Beside, PP2A has been indicated in many dephosphorylation processes in cells,

especially in regulating activity of more than thirty other protein kinases (Millward et al., 1999).

Okadaic acid (OKA) and Calyculin A (Cal A) are the two toxins most commonly used to inhibit PP2A activity. Structures of OKA and Cal A are presented in Figure 1.6B, adapted from (Cohen et al., 1990). OKA was first isolated from two marine sponges (Tachibana et al., 1981). OKA was linked to diarrheic shellfish poisoning associated with consuming shellfish (Yasumoto et al., 1984). Phosphatase assays on ^{32}P labeled-substrates myosin light chain and phosphorylase a showed a great specificity of OKA to inhibit PP2A with ID_{50} = 1 nM. PP1 was inhibited to a lesser extent with ID_{50} = 0.1 – 0.5 µM. PP2B was quite resistant to OKA with ID_{50} = 4 – 5 µM. PP2C was not affected by OKA (Bialojan and Takai, 1988; Cohen et al., 1989). Structure of OKA showed high hydrophobicity which means OKA is able to cross the plasma membrane. This prompted experiments in intact cells to examine the effects of phosphatase inhibition. Isolated hepatocytes and adipocytes were labeled with ^{32}P then treated with different concentrations of OKA. After 15 min incubation, OKA was shown to have maximal effect to promote phosphorylation in cells at 1 µM, while half maximal (ED_{50}) was obtained with 200 nM (Hardie et al., 1991). OKA was shown to be more specific in inhibiting PP2A than PP1 with about 10 folds difference in specificity (Bialojan and Takai, 1988; Cohen et al., 1989; Hardie et al., 1991). Various concentrations of OKA have been used to treat different types of cells with different time points. For example, primary cultures of rat cortical neurons were treated with 10 nM OKA for 4 – 24 hours (Yoon et al., 2006). With 30 min incubation, concentration of OKA required to inhibit swelling activated the K^+-influx channel in human erythrocytes was 65 nM (Kaji and Tsukitani, 1991). Between 10 nm to

1000 nm of OKA was used to treat human hepatocytes to increase glucose output (Haystead et al., 1989). On the other hand, Cal A was shown to efficiently inhibit PP1 at similar concentration as OKA inhibits PP2A (Cohen et al., 1990; Ishihara et al., 1989).

1.4 Cell density signaling and the Hippo pathway

Density-dependent cell growth and proliferation have been observed for decades, in which cells in culture dish stop or slow their proliferation upon “touching” other cells (Eagle and Levine, 1967; Holley, 1975; Stoker and Rubin, 1967). In contrast, cancer cells are able to escape density-regulated cell proliferation; they acquire enhanced ability to invade host tissues and metastasize (Hanahan and Weinberg, 2000). Characterization of density-dependent cell growth and proliferation would involve identification of cell surface receptors with their respective signaling cascades, and the mechanism of interaction between each member (Holley, 1975).

The Hippo signaling pathway, as depicted in Figure 1.7, consists of Hippo kinases MST1 and MST2 in mammals and a single Hippo (Hpo) kinase in *Drosophila*. In high cell density, MST1/2 phosphorylate LATS1/2, which in turn phosphorylate YAP/TAZ. Phosphorylated YAP/TAZ are inactive and kept in cytoplasm by binding to 14-3-3 or subjected to degradation. In low cell density, the Hippo pathway is inactive, so unphosphorylated YAP/TAZ translocate into the nucleus to activate transcription of growth promotion genes. The Hippo pathway is also implicated in regulation of organ size. Enhancing activity of YAP leads to organ overgrowth in both *Drosophila* and mice (Dong et al., 2007; Pan, 2007; Zhao et al., 2011). There are many excellent reviews on the Hippo pathway such as (Halder and Johnson, 2011; Avruch et al., 2012; Park and Guan, 2013; Mo et al., 2014; Meng et al., 2016).

The Hpo kinase was first isolated in *Drosophila* genetic screen for genes that inhibit cell growth. Its kinase domain reveals Hpo as a member of the Ste20 family of Ser/Thr kinases and belongs to group II GCK subfamily. Hpo associates with and phosphorylates Sav. The Hpo/Sav complex promotes Wts (LATS1/2) phosphorylation (Harvey et al., 2003; Udan et al., 2003; Wu et al., 2003). Hpo is most closely related to human kinases MST2 (60%) and MST1 (58%) which were first isolated by Chernoff's group (Creasy and Chernoff, 1995a, 1995b). Independently, another group identified MST1/2 as kinases that are activated under extreme stress in NIH3T3 cells (Taylor et al., 1996).

The domain structures of MST1/2 are represented in Figure 1.8. Global alignment of MST1 and MST2 sequences reveals 87.95% similarity. The kinase domain alone shows 94.4% similarity (Figure 1.9). The ATP binding pocket, surface properties, and substrate selectivity are very similar between MST1 and MST2 (Record et al., 2010). Human MST1 is encoded by the *STK4* gene, and human MST2 is encoded by the *STK3* gene. They are 487 and 491 amino acids in length respectively. Both MST1 and MST2 contain an N-terminal kinase domain, an autoinhibitory domain (sometimes called the linker region), and a C-terminal SARAH domain. The autophosphorylation sites T183 and T180 on MST1 and MST2 respectively are critical for kinase activity. Mutants bearing T180A or T183A are kinase deficient (Glantschnig et al., 2002; Praskova et al., 2004). TAOK1-3 have been shown to phosphorylate T183 and T180 to activate MST1/2 (Boggiano et al., 2011). Crystal structures of the active MST1 kinase domain and the inactive MST2 kinase domain reveals conformational changes upon phosphorylation of T183 and T180 leading to substrate binding. The SARAH domain enables MST1/2 to form homodimer that is capable of trans-autophosphorylation at T183 and T180, leading to

kinase activation (Jin et al., 2012; Ni et al., 2013). One layer of MST1/2 kinase activity control is the formation of heterodimers between MST1/2 and RASSF proteins through SARAH domains, which is thought to disrupt MST1/2 homodimers, thus reducing autophosphorylation activation (Creasy et al., 1996; Hwang et al., 2007, 2014; Polesello et al., 2006). It is worth noting that there have not been any reports on whether MST1 and MST2 can form heterodimers with each other. Other phosphorylation events also contribute to regulation of MST1/2 activity. MST1 T387 has been shown to be phosphorylated by Akt to inhibit MST1 activity (Jang et al., 2007). PHLPP phosphatases counter Akt's effect by dephosphorylating T387 on MST1 while physically interacting with MST1 in Hela cells (Jung et al., 2014; Qiao et al., 2010; Rawat and Chernoff, 2015). MST1/2 also autophosphorylate their linker region, which creates a docking site for Mob1 which serves to enhance downstream LATS1/2 phosphorylation. On the other hand, phosphorylation of the linker region also leads to docking of the STRIPAK complex, which brings PP2A to dephosphorylate and thus deactivate MST1/2 (Bae et al., 2017; Zheng et al., 2017).

Studies of a particular kinase often involve the use of a corresponding kinase-dead version as a negative control. The kinase-dead MST1/2 are generated by mutating the lysine at position 59 and 56 within the kinase domain of MST1 and MST2 respectively to arginine, because this lysine is critical for ATP binding in a kinase reaction. Many groups have used MST1K59R and MST2K56R as negative controls for kinase activity of MST1 and MST2, and during the process showed that MST1K59R and MST2K56R do not retain kinase activity. MST1K59R is unable to phosphorylate myelin basic protein in vitro (Creasy et al., 1996). MST1K59R and MST2K56R are unable to phosphorylate its

substrate Mob1 in vivo (Praskova et al., 2008). MST2K56R is unable to phosphorylate cdc2(6–20)F15K19 synthetic peptide in vitro (Deng et al., 2003). Mutants bearing T180A or T183A are kinase deficient comparable to that of K59R or K56R mutants (Glantschnig et al., 2002; Praskova et al., 2004).

Given the canonical role of the Hippo pathway in regulating cell proliferation and organ growth and the explosive amount of literature on the topic, many have the impression that MST1/2 kinases function primarily in the Hippo pathway. Although it may be true in the fly model, evidence in humans suggests that MST1/2 can be functionally redundant and deviated from those in fly. For example, MST1/2 have functions in the immune system. They have been reported to phosphorylate Mob1 to restrain proliferation of naïve T cells in mice (Zhou et al., 2008) or loss of MST1 leads to progressive loss of naïve T cells in human (Nehme et al., 2012). Unlike in *Drosophila*, MST1/2 are redundant in activating LATS1/2 kinases. MAP4K family kinases can act on LATS1/2 in parallel with MST1/2. Knocking down MST1/2 has minimal effect on YAP phosphorylation in human cells (Meng et al., 2015). An interesting observation is that the Hippo pathway also exerts non-cell autonomous effect on neighboring cells. The non-cell autonomous effect of the Hippo pathway was shown to mostly occur through regulation of autocrine/paracrine signaling (Del Re et al., 2010; Sarikaya and Extavour, 2015; Zhang et al., 2009).

Here, we report that under conditions of low cell density, the Hippo protein MST1/2 interact with the STRIPAK complex, which leads to STRIPAK localization to the Golgi via interaction with GOLPH3. At the Golgi, dephosphorylation by PP2A leads to enhanced GOLPH3-MYO18A interaction, thus promoting vesicle trafficking, and as a consequence, an extended Golgi. On the other hand, at high cell density when the canonical Hippo

pathway is activated, the STRIPAK complex leaving the Golgi leads to weakening of GOLPH3-MYO18A interaction, which results in inhibition of Golgi-dependent protein secretion and a compact Golgi. We find that cell density, by controlling secretion via MST1/2, STRIPAK, GOLPH3, and MYO18A, regulates paracrine growth factor secretion and signaling, providing a means to affect the proliferation of neighboring cells.

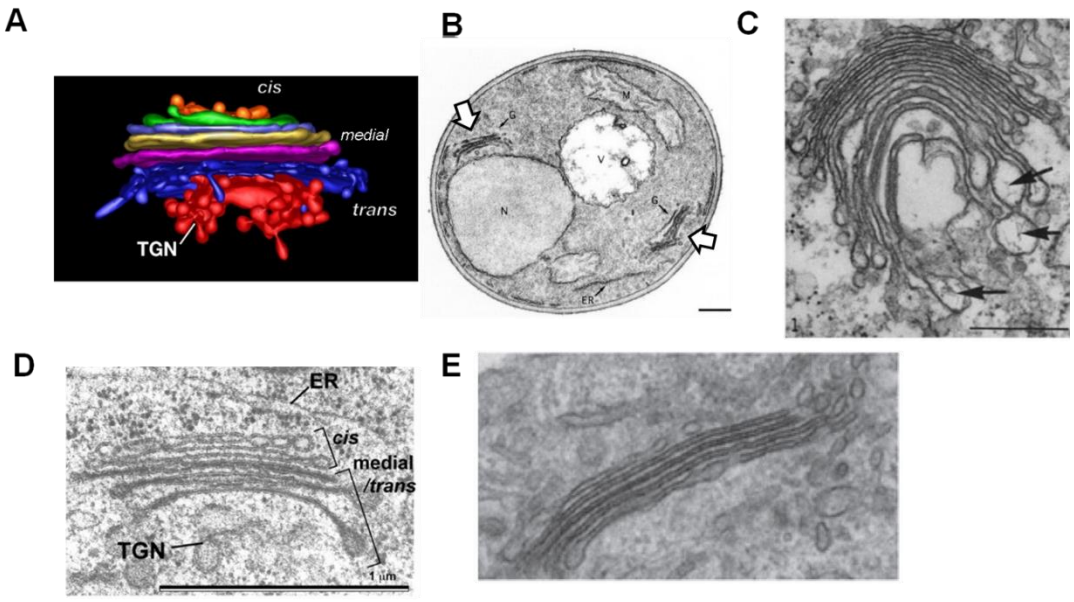

Figure 1.1: The Structure of Golgi Stacks.
(A) 3D reconstruction of *Arabidopsis*' Golgi representing a typical Golgi with four general sub compartments: *cis*-Golgi, *medial*-Golgi, *trans*-Golgi and Trans Golgi Network (TGN). TGN is where the most vesicle-budding activity happens. (B) Golgi stacks of the simple, single-cell-eukaryote amoeba. (C) A Golgi stack of tobacco plant. (D) A Golgi stack of yeast *Pichia pastoris*. (E) A human Golgi stack. Adapted from (Staehelin and Kang, 2008; Wise and Flickinger, 1970; Rossanese et al., 1999; Dippold et al., 2009).

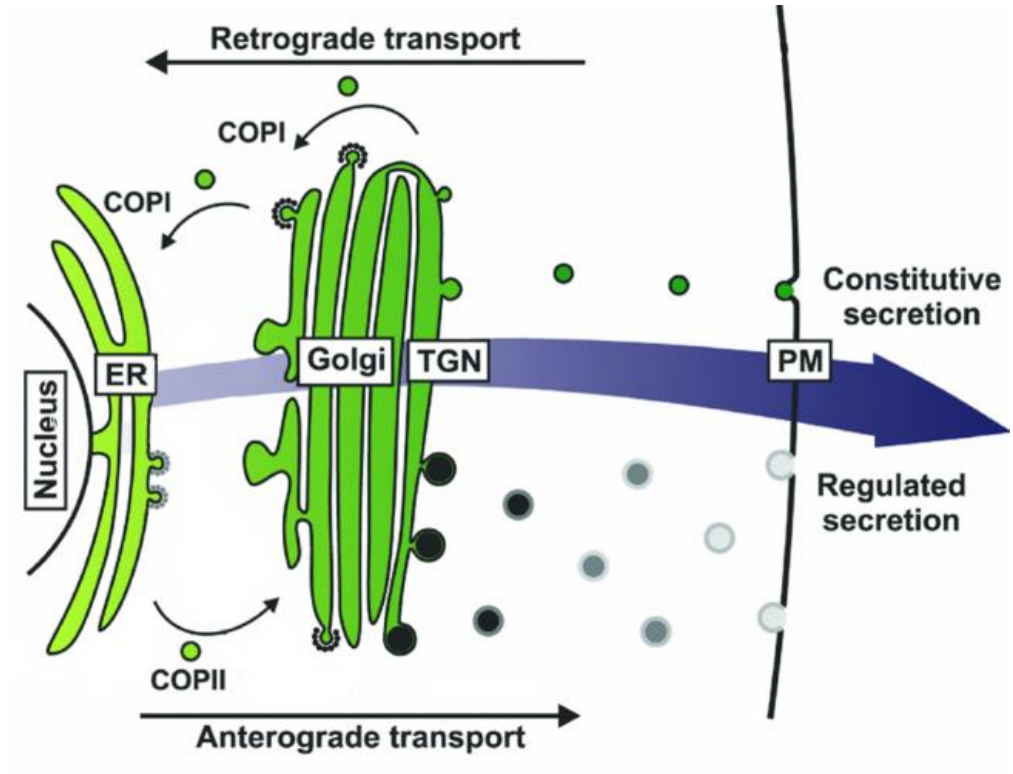

Figure 1.2: Protein Transportation at The Golgi.
The anterograde (forward) trafficking process starts with protein production in the ER. COPII vesicles bring protein from the ER to *cis*- Golgi. From *cis*-Golgi, proteins are continued to be transported to *med*- and *trans*- Golgi. By traveling along Golgi sub compartments, proteins are further modified and sorted to make sure they reach correct destinations: either other organelles or outside of the cells. In the retrograde (reverse) trafficking process, if some enzymes specific for ER or each Golgi-subcompartment are mis-carried to the next compartment, they will return in COPI vesicles. Figure was retrieved from the book Biology of the Cell with modification (Volume 101, Issue 9, pages 495-509, 3 JAN 2012 DOI: 10.1042/BC20080233.
http://onlinelibrary.wiley.com/doi/10.1042/BC20080233/full#f1)

Figure 1.3: The GOLPH3 Complex Regulates Golgi Morphology and Function.
(A) The GOLPH3 complex consists of GOLPH3 protein binding to PI(4)P; GOLPH3 also binds MYO18A which binds F-actin. These linkages create a tensile force which applies onto Golgi membrane to facilitate vesicle budding from *trans*-Golgi. (B) Crystal structure and electrostatic model of human GOLPH3 and yeast ortholog Vps74 show high similarity. They both have the appearance of a globular protein with a protruding β-hairpin, and a highly hydrophilic pocket crystalizing with SO_4^{2-} resembles PI(4)P binding site. (C) Knocking down GOLPH3 using three different siRNAs lead to compact Golgi. (D) Knocking down MYO18A using three different siRNAs lead to compact Golgi. (E) Cells with GOLPH3 or MYO18A knockdown or F-actin destroyed by Latrunculin B have impaired vesicle exit at the Golgi. Adapted from (Dippold et al., 2009) and (Wood et al., 2009).

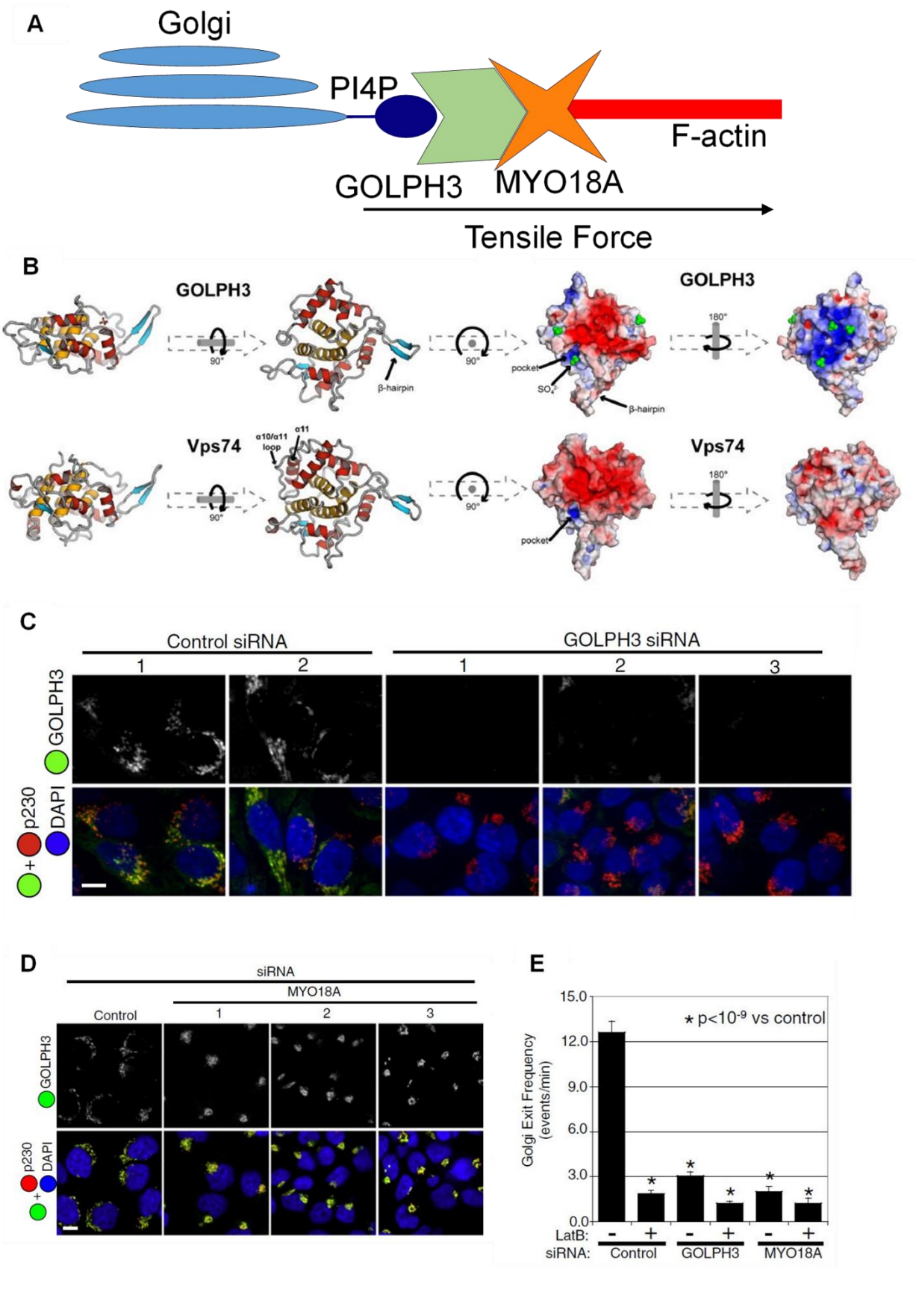
A
Golgi
PI4P
F-actin
GOLPH3
MYO18A
Tensile Force
B
GOLPH3
90°
β-hairpin
pocket
SO4
180°
Vps74
α10/α11 loop
α11
C
Control siRNA
GOLPH3 siRNA
1
2
3
GOLPH3
p230
DAPI
D
siRNA
MYO18A
Control
E
* p<10-9 vs control
Golgi Exit Frequency (events/min)
15.0
12.0
9.0
6.0
3.0
0.0
LatB:
siRNA:
Control
GOLPH3
MYO18A

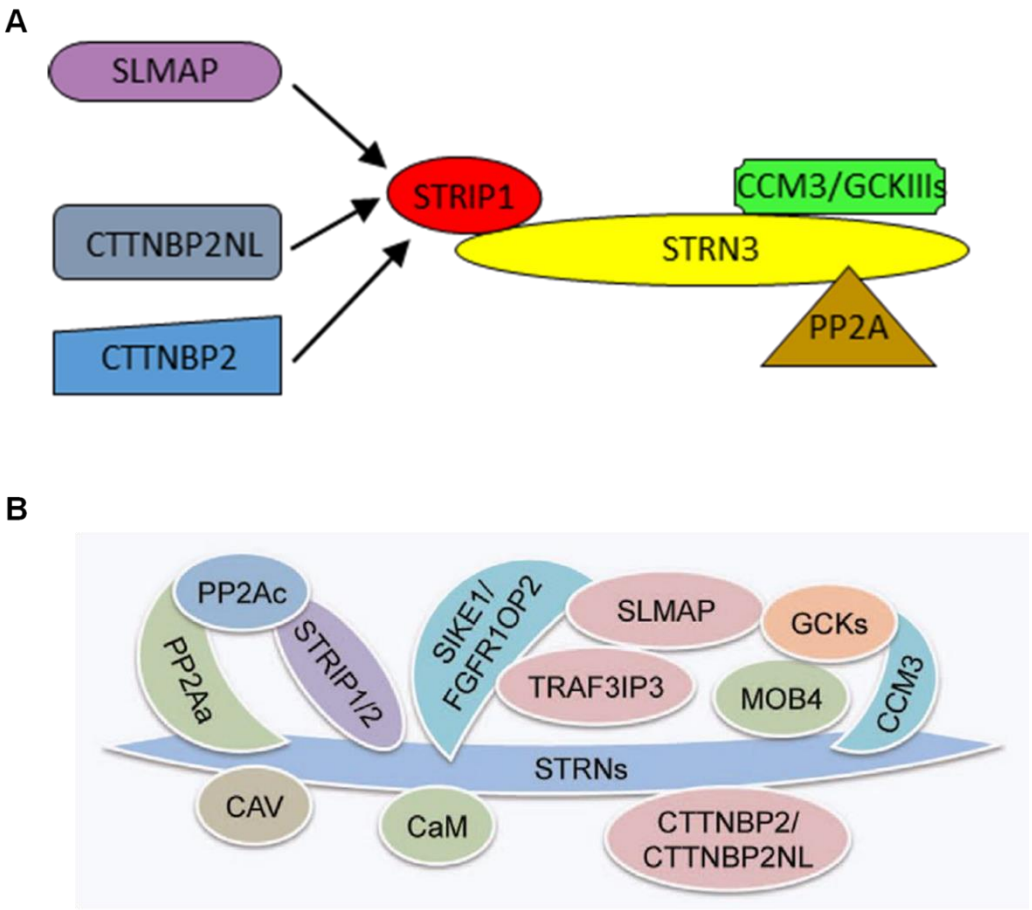

Figure 1.4: Architecture of the STRIPAK Complex.
(A) The STRiatin-Interacting-Phosphatase and kinases (STRIPAK) consists of STRN3 bringing together MOB4, PP2A, STRIP1/2, CCM3, GCKIII, and CTTNBP2/CTTNBP2NL or SIKE/SLMAP. STRN3 binds directly to MOB4, PP2A, STRIP1/2, and CCM3. STRIP1/2 bridge either CTTNBP2/NL or SIKE/SLMAP to STRN3 in a mutually exclusive manner. CCM3 links GCKIII to STRN3 (Adapt with modification Hwang and Pallas, 2014). (B) More interdependent interactions among STRIPAK members. MOB4 could also bind GCKs, STRIP1/2 interact with PP2A, and SIKE could bind directly to STRN3 (Shi et al., 2016)

Figure 1.5: Schematic Structure of STRN3.
STRN3 carries calmodulin (CaM), caveolin (CaV), and coiled coil (C-C) motifs at the N-terminal, which are collectively termed striatin domain. STRN3 carries a tandem of six WD-40 motifs at the C-terminal. WD-40 can form a β-propeller structure, which is often observed in scaffolding proteins. The coiled coil domain enables STRN3 to form homodimer.

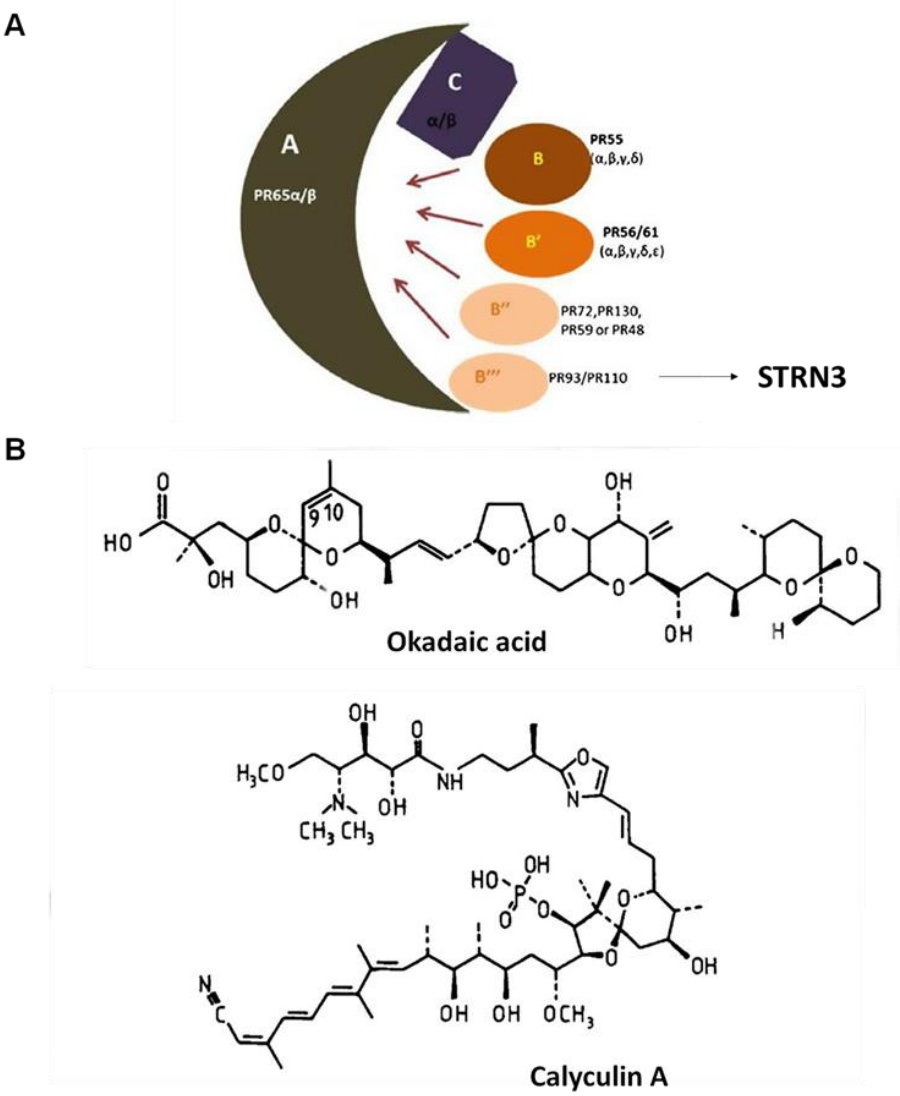

Figure 1.6: Structure of PP2A, Okadaic Acid, and Calyculin A.
(A) The catalytic subunit of PP2A, PP2Ac, occurs in two isoforms α and β, which have high sequence homology (97%). The scaffolding subunit PP2A A also has two isoforms α and β with high sequence homology (86%). More diverted is the PP2A regulatory subunit, PP2A B. There are four different families of regulatory subunit B, denoted B, B', B'', and B''' or B55/PR55, B56/PR61, PR48/PR72/PR130, and PR93/PR110. STRN3 belongs to the B''' group. (B) Structure of Okadaic acid (OKA) and Calyculin A (Cal A) showed high hydrophobicity, which allows them to cross cell membrane. OKA is a potent inhibitor of PP2A. OKA could inhibit PP2A about 10-100 times better than inhibiting PP1 at an effective concentration for PP2A. Cal A is a potent inhibitor of both PP2A and PP1 at nano-molar scale. Cal A could inhibit both PP2A and PP1 equally well. Adapted from (Seshacharyulu et al., 2013) and (Cohen et al., 1990).

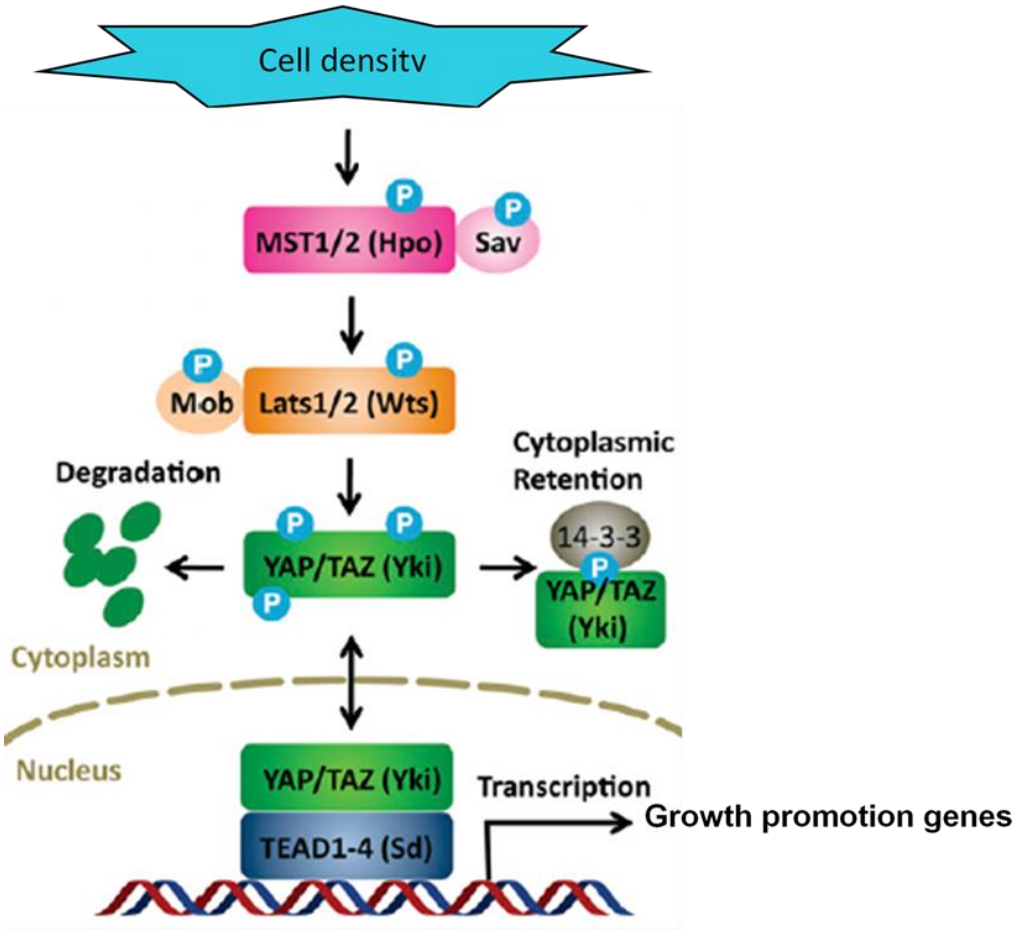

The Hippo pathway (Yu &Guan, 2013)

Figure 1.7: The Hippo Signaling Pathway That Responds to Cell Density to Regulate Cellular Growth.

The canonical Hippo pathway starts from Hippo kinases MST1/2. When Hippo pathway is active, MST1/2 phosphorylate LATS1/2, which in turn phosphorylate YAP/TAZ. Phosphorylated YAP/TAZ are inactivated and kept in cytoplasm by binding to 14-3-3 or subjected to degradation. When Hippo pathway is inactive, unphosphorylated YAP/TAZ translocate into the nucleus to activate transcription of growth promotion genes.

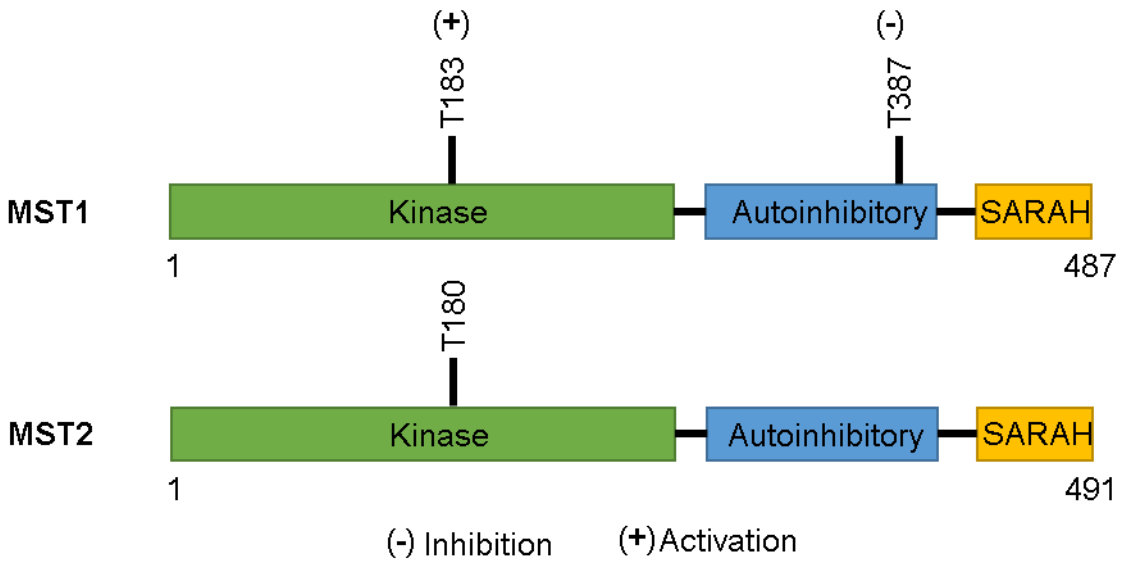

Figure 1.8: Schematic Structure of MST1/2.
MST1 contains an N-terminal kinase domain, an autoinhibitory domain (linker region), and a C-terminal SARAH domain. MST1 and MST2 are activated by phosphorylation at T183 and T180 on MST1 and MST2 respectively by TAOK1-3 or by autophosphorylation. Akt is reported to inactivate MST1 by phosphorylating T387. This action is countered by PHLPP phosphatases (Rawat and Chernoff, 2015).

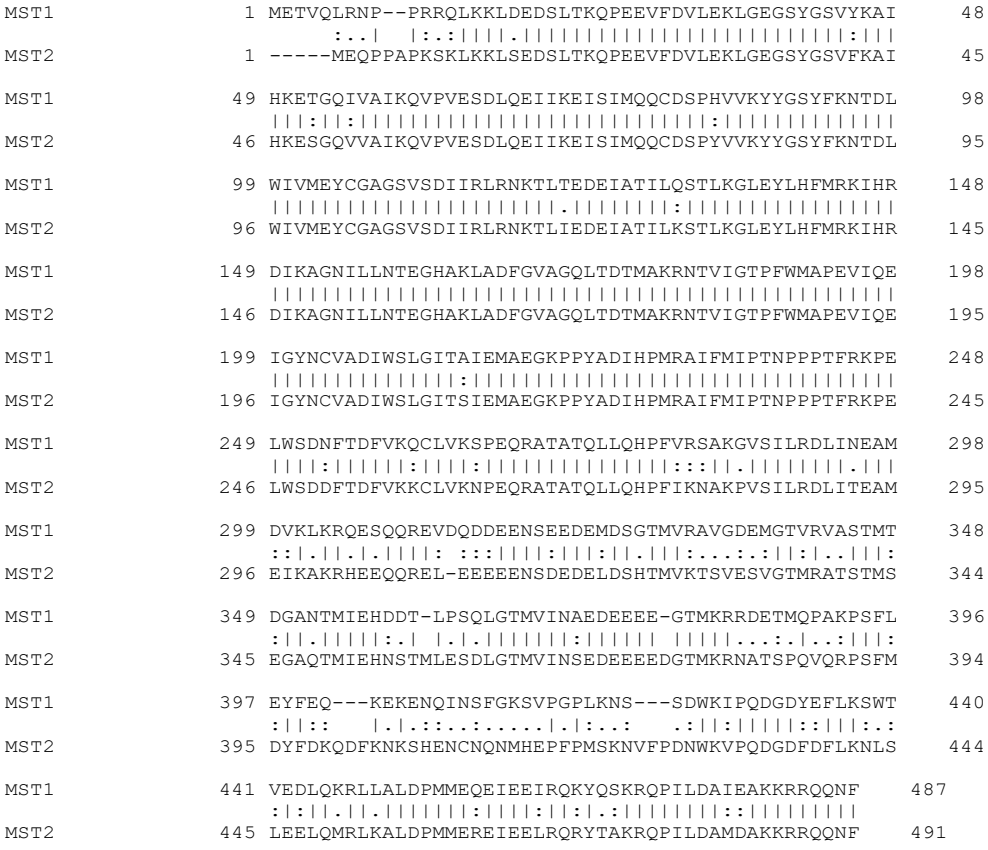

Figure 1.9: Global Alignment of MST1 and MST2 Protein Sequences.
Protein sequences of MST1 and MST2 bear 87.95% similarity. The kinase domains alone bear 94.4% similarity. ATP binding pocket, surface properties and substrate selectivity are very similar between MST1 and MST2 (Alignment using EMBOSS Needle).

CHAPTER 2: CELL DENSITY REGULATION OF THE GOLGI THROUGH HIPPO, THE STRIPAK COMPLEX, AND GOLPH3

2.1 Introduction

Exit from the Golgi for trafficking to the plasma membrane (PM) is a key step in secretion whose regulation is poorly understood (Buschman et al., 2015a, 2015b; Makowski et al., 2017). Discovery of the role of the GOLPH3 complex in Golgi vesicle exit has provided a conceptual framework to understand regulation of the Golgi. GOLPH3 is tightly localized to the *trans*-Golgi and to vesicles budding from it (Bell et al., 2001; Dippold et al., 2009; Snyder et al., 2006). This localization is a consequence of GOLPH3's interaction with the phosphoinositide PI4P (Dippold et al., 2009), which is highly enriched at the *trans*-Golgi (Godi et al., 1999, 2004). GOLPH3 further binds to the unconventional myosin, MYO18A, which binds F-actin to apply a tensile force to the Golgi. This force is required for efficient vesicle budding from the *trans*-Golgi for trafficking to the PM (Bishé et al., 2012; Dippold et al., 2009; Ng et al., 2013; Xing et al., 2016). As a side-effect, this force also gives the Golgi its characteristic appearance as an extended ribbon, as observed by light microscopy, and flattened cisternae, as observed by electron microscopy (Dippold et al., 2009; Ng et al., 2013). A large body of data make it clear that in higher organisms, the majority of Golgi-to-PM trafficking occurs through the GOLPH3 pathway (Bishé et al., 2012; Dippold et al., 2009; Ng et al., 2013; Xing et al., 2016).

Cell density sensing provides a critical control on cell growth. The Hippo pathway, first identified in flies but conserved throughout metazoa, senses increasing cell crowding to shut off cell proliferation (Avruch et al., 2012; Meng et al., 2016). This behavior is observed in cell culture, but *in vivo* manifests to regulate organ size. In mammals, the

upstream signals are uncertain, but cell crowding leads to activation of the protein kinase activity of the MST1 and MST2 orthologs of the *Drosophila* Hippo protein (Zhao et al., 2007). Activation of MST1 and MST2 involves SAV1-dependent relief of inhibitory dephosphorylation by the protein phosphatase PP2A (Bae et al., 2017; Couzens et al., 2013; Ribeiro et al., 2010; Zheng et al., 2017). PP2A is bound to STRN3 in the STRiatin Interacting Phosphatases and Kinases (STRIPAK) complex that interacts with MST1/2. In crowded cells, activated MST1/2 phosphorylate the LATS1 and LATS2 protein kinases, in a manner that depends on the MOB1 protein (Chan et al., 2005; Praskova et al., 2008). LATS1 and LATS2, in turn, phosphorylate the YAP and TAZ transcriptional co-activators. When phosphorylated, YAP and TAZ are retained in the cytoplasm and are degraded, resulting in shut-off of nuclear target genes, and exit from the cell cycle. Although this regulation of transcription is well known, whether other aspects of cell function are regulated in response to cell crowding remains unknown. In particular, the coordinated regulation required to control organ size is likely to depend on secreted, diffusible extracellular signals (Hariharan, 2015; Penzo-Méndez and Stanger, 2015). Indeed, in addition to its cell autonomous regulation of transcription, Hippo has non-cell autonomous effects on cell proliferation (Del Re et al., 2010; Sarikaya and Extavour, 2015; Zhang et al., 2009)

Here, we report that the Golgi is regulated by cell density. This regulation involves signaling through MST1/2 to STRN3/STRIPAK to enhance the interaction between GOLPH3 and MYO18A. In sparse cells, MST1/2 promote STRN3 interaction with GOLPH3. The PP2A catalytic subunit within STRIPAK dephosphorylates the GOLPH3 complex, which promotes the interaction between GOLPH3 and MYO18A, resulting in

enhanced Golgi-to-PM trafficking and extension of the Golgi ribbon around the nucleus. Surprisingly, in this regard, MST1 and MST2 act independently of their kinase activity, and independently of LATS1/2. With increasing cell density, the lack of signal from MST1/2 results in dissociation of STRN3 from GOLPH3, resulting in impaired interaction of GOLPH3 with MYO18A, and thus reduces Golgi-to-PM trafficking and compaction of the Golgi ribbon. Notably, this global regulation of the secretory pathway includes regulation of growth factor secretion, providing a mean for controlling cell proliferation in neighboring cells. This signaling pathway, by which cell density regulates the Golgi, involves a novel role for MST1/2 (Hippo) and has implications for understanding the biology of regulation of cell proliferation and organ size and the roles that these proteins play in cancer.

2.2 Results

2.2.1 High Cell Density Causes Golgi Compaction and Impaired Golgi-to-PM Trafficking

While studying the Golgi, we noted changes in Golgi morphology that correlated with cell density. We plated HeLa cells at different densities and observed Golgi morphology using immunofluorescence (IF) to the Golgi marker GM130 (Figure 2.1A). At low density, the Golgi ribbon extended partially around the nucleus. However, with increasing cell density, the Golgi condensed into a compact ball. To quantify the effect of cell density, we measured the area of the Golgi (area of the smallest encircling ellipse). Golgi area decreased significantly with increasing cell density (Figure 2.1B). In addition to HeLa, Golgi compaction in response to high cell density occurred in HEK293 human

kidney cells (Figures 2.1C and 2.1D), MDA-MB-231 human breast cancer cells (Figures S2.1A and S2.1B), and NRK normal rat kidney cells (Figures S2.1C and S2.1D).

We examined whether regulation of the Golgi by cell density affects secretion. First, we measured global secretion of endogenous proteins using a ^{35}S-amino acid pulse-chase experiment. After pulse-chase, we measured the appearance of labeled protein secreted into the media, as well as incorporation of label into proteins in the cell lysate. We calculated relative secretion as a fraction of total protein synthesis, and compared cells plated at low and high density. For all cell lines examined, HEK293, HeLa, and NIH3T3, high cell density caused a significant reduction in global secretion of endogenous proteins (Figure 2.1E).

Next, we observed trafficking of the experimental cargo ts045-VSVG-GFP, a temperature sensitive mutant of the Vesicular Stomatitis Virus G glycoprotein, that, upon shift to the permissive temperature, is released from the ER to the Golgi and then to the PM (Presley et al., 1997; Scales et al., 1997). In unpermeabilized cells, an antibody to the extracellular domain detects VSVG at the PM. In sparsely plated cells, we observed robust trafficking to the PM and minimal intracellular accumulation of VSVG-GFP, as expected (Figures 2.1F and 2.1G). Although the regulation of this viral protein was muted compared to endogenous proteins, we observed a significant reduction in VSVG trafficking to the PM in densely plated cells, with accumulation in the Golgi. We conclude that in densely plated cells, VSVG is able to exit the ER, but then accumulates at the Golgi, unable to traffic efficiently to the PM. Taken together, these data demonstrate novel regulation of the Golgi as a common feature of the mammalian cellular response to high cell density.

2.2.2 High Cell Density Inhibits the GOLPH3 Complex at The Golgi

Golgi compaction and impaired forward trafficking are hallmarks of inhibition of the PI4P/GOLPH3/MYO18A/F-actin complex that we previously found functions to promote vesicle exit from the *trans*-Golgi (Bishé et al., 2012; Dippold et al., 2009; Ng et al., 2013; Xing et al., 2016). Because of the similarity to Golgi phenotypes in response to high cell density, we examined the GOLPH3 complex. By western blot (WB), GOLPH3 and MYO18A expression were unaffected by cell density (Figure S2.1E). Furthermore, GOLPH3 localization to the Golgi was unaffected by cell density (Figure S2.1F). Since GOLPH3 localizes to the Golgi via binding to PI4P, we infer that PI4P levels at the Golgi and the recruitment of GOLPH3 to the Golgi are unaffected by cell density.

Next, we examined whether the interaction between GOLPH3 and MYO18A is regulated by cell density. We immunoprecipitated (IPed) endogenous GOLPH3 from low density HeLa cells, observing robust co-IP of endogenous MYO18A (Figure 2.1H). However, IP of GOLPH3 from high density HeLa cells co-IPed significantly less MYO18A (Figures 2.1H and 2.1I). A similar decrease in the association of GOLPH3 with MYO18A at high cell density occurred in HEK293 cells (Figure S2.1G). We conclude that high cell density leads to impaired interaction between GOLPH3 and MYO18A. Notably, impaired interaction between GOLPH3 and MYO18A is known to result in Golgi compaction and arrest of Golgi-to-PM trafficking (Dippold et al., 2009; Farber-Katz et al., 2014; Ng et al., 2013; Xing et al., 2016) and thus explains the response of the Golgi to high cell density.

2.2.3 STRN3 Interacts with GOLPH3 at the Golgi

We predicted that one or more proteins that interact with the GOLPH3/MYO18A complex are involved in relaying the cell density signal. Thus, we performed large scale

IP of endogenous GOLPH3, followed by mass spectrometry (MS), which identified multiple peptides of striatin 3 (STRN3) (Figure S2.2A). STRN3 is the core of the STRIPAK complex (Goudreault et al., 2009; Kean et al., 2011). Notably, STRN3 binds to the MST1/2 (Hippo) kinases (Couzens et al., 2013; Hauri et al., 2013; Ribeiro et al., 2010), which are regulated by cell density (Avruch et al., 2012; Meng et al., 2016). Thus, we further investigated the interaction between GOLPH3 and STRN3.

By IP/WB, endogenous STRN3 robustly co-IPed with endogenous GOLPH3 in both HeLa and HEK293 cells (Figures 2.1H, 2.2A, and S2.1G). Furthermore, by IF endogenous STRN3 localized, in part, to the Golgi (Figure 2.2B), consistent with previous literature (Baillat et al., 2001). We confirmed the specificity of the IF signal by knockdown of STRN3 with three different siRNAs. Strikingly, STRN3 localization to the Golgi depended on GOLPH3, as siRNA knockdown of GOLPH3 (confirmed by parallel WB, Figure 2.2D) caused STRN3 to dissociate from the Golgi (Figure 2.2E). However, STRN3 localization to the Golgi was independent of MYO18A (Figures 2.2D and 2.2E). A co-IP experiment confirmed that the interaction between GOLPH3 and STRN3 occurs independently of MYO18A, unaffected by siRNA knockdown of MYO18A (Figure 2.2F). These results establish that STRN3 complexes with GOLPH3, resulting in its Golgi localization, in a manner independent of MYO18A.

2.2.4 STRN3 Regulates the Golgi by Promoting the Interaction of GOLPH3 with MYO18A

With the discovery that STRN3 interacts with GOLPH3, we wondered whether it plays a role in regulation of the structure and function of the Golgi, as is true for the GOLPH3 complex. Knockdown of STRN3 using three different siRNAs efficiently reduced

STRN3 levels as observed by IF (Figure 2.2B) and WB (Figure S2.3A). Knockdown of STRN3 caused compaction of the Golgi (Figures 2.2B and 2.2C). Furthermore, expression of siRNA-resistant STRN3 in knockdown cells restored STRN3 expression (Figures 2.2G and S2.3B) and restored normal Golgi morphology (Figures 2.2G and 2.2H). Thus, the Golgi phenotype is not an off-target effect of the siRNA, but rather Golgi compaction is a consequence of loss of STRN3.

Next, we used a ^{35}S-amino acid pulse-chase experiment to assess the effect of loss of STRN3 on global secretion of endogenous proteins. Similar to the effect of knockdown of MYO18A, knockdown of STRN3 by either of two siRNAs impaired overall secretion (Figures 2.3A and 2.3B). We also examined the effect of STRN3 knockdown (Figure S2.3C) on trafficking of ts045-VSVG-GFP (Figures 2.3C and 2.3D). While the regulation of trafficking of this viral protein was muted compared to endogenous proteins, trafficking was still significantly impaired upon knockdown of STRN3. We observed accumulation of VSVG-GFP at the Golgi, with a significant reduction in the amount delivered to the PM. Thus, knockdown of STRN3 results in Golgi compaction and arrest of Golgi-to-PM trafficking, which are the hallmarks of inhibition of the GOLPH3 complex.

We investigated whether knockdown of STRN3 affects the GOLPH3 complex. First, knockdown of STRN3 did not affect the expression of GOLPH3 or MYO18A proteins (Figure S2.3E). Likewise, siRNA knockdown of STRN3 that was sufficient to cause Golgi compaction did not alter the Golgi localization of GOLPH3 (Figures S2.3D and S2.3E), indicating that PI4P levels and GOLPH3 recruitment to the Golgi are unaffected by loss of STRN3. Next, we assessed the interaction between GOLPH3 and MYO18A. siRNA knockdown of STRN3 resulted in a significant decrease in the co-IP of MYO18A with

GOLPH3 (Figures 2.3E and 2.3F). The decrease in the interaction of GOLPH3 with MYO18A upon knockdown of STRN3 explains the Golgi compaction and arrest of Golgi-to-PM trafficking that occurs with loss of STRN3, and mimics the effect of high cell density.

2.2.5 STRN3 Interaction with GOLPH3 is Regulated by Cell Density

Since loss of STRN3 recapitulates the Golgi phenotype caused by cell crowding, and STRN3 is known to interact with the Hippo proteins, MST1/2, that are part of a cell density-sensing pathway (Couzens et al., 2013; Hauri et al., 2013), we wondered if the GOLPH3-STRN3 interaction is regulated by cell density. Compared to cells at low density, co-IP of STRN3 with GOLPH3 was significantly reduced in cells plated at high density (Figures 2.1H and 2.1K). Experiments in HEK293 cells revealed a similar reduction in the co-IP of STRN3 with GOLPH3 in densely plated cells (Figure S2.1G). We conclude that increasing cell density results in dissociation of STRN3 from GOLPH3. Since STRN3 is required for efficient interaction between GOLPH3 and MYO18A, loss of STRN3 from the GOLPH3 complex in response to increasing cell density explains the decrease in the GOLPH3-MYO18A interaction that occurs in response to increasing cell density.

2.2.6 Hippo Proteins MST1/2 Regulate the Golgi

In light of the known interaction between STRN3 and MST1/2 (Hippo), we examined whether MST1 or MST2 regulate the Golgi. Knockdown of MST1, MST2, or both (Figure S2.4A) resulted in compaction of the Golgi (Figures 2.4A and 2.4B). Furthermore, expression of siRNA-resistant MST1 or MST2 (corresponding to the appropriate siRNA) restored normal Golgi morphology (Figures 2.4C, 2.4D, S2.4B, 2.4E, 2.4F, and S2.4C), indicating that Golgi compaction was not an off-target effect of the siRNA. Next, siRNA knockdown of MST1 or MST2 each significantly impaired Golgi-to-

PM trafficking of ts045-VSVG-GFP (Figures 2.4G, 2.4H, and S2.4D). Thus, loss of MST1 or MST2 causes Golgi compaction and impaired trafficking, the hallmarks of inhibition of the GOLPH3 complex, and similar to the effect of high cell density or loss of STRN3.

2.2.7 MST1/2 Regulate the Golgi via GOLPH3 and STRN3, Independently of Their Kinase Activity and Canonical Hippo Signaling

The known role of MST1 and MST2 in the regulation of gene transcription in response to changing cell density depends on their kinase activity to phosphorylate the LATS1 and LATS2 proteins (Avruch et al., 2012; Meng et al., 2016). Specifically, at high cell density, MST1/2 kinases phosphorylate LATS1/2, activating them to phosphorylate the transcriptional co-activators YAP/TAZ, causing exit from the nucleus and reduced transcription of target genes. We already observed a discrepancy with this canonical role of MST1/2 in that they are active to shut down transcription under conditions of high cell density, whereas we find that they are active to promote Golgi function under conditions of low cell density. Furthermore, MST1 and MST2 act redundantly to regulate transcription, whereas we observe that they are both required for Golgi function. To begin to understand this discrepancy, we examined the role of MST1/2 kinase activity for its regulation of the Golgi. We performed knockdown/rescue experiments comparing the ability to restore Golgi morphology by WT MST1 and MST2 versus kinase-dead mutants of MST1 (MST1-K59R) and MST2 (MST2-K56R) that are unable to phosphorylate substrates *in vitro* or *in vivo* (Creasy et al., 1996; Deng et al., 2003; Praskova et al., 2008). Expression of kinase-dead MST1 or MST2 each rescued Golgi morphology as well as the wild-type proteins (Figures 2.4C, 2.4D, S2.4B, 2.4E, 2.4F, and S2.4C).

To further test whether MST1/2 kinase activity is dispensable for MST1/2 regulation of the Golgi, we used the inhibitor XMU-MP-1 (Fan et al., 2016; Zheng et al., 2017). Unlike control cells, XMU-MP-1-treated cells continued to exhibit nuclear YAP even when plated at high density, indicating that XMU-MP-1 was efficiently inhibiting MST1/2 kinase activity (Figure 2.5A). By contrast, in the same cells, Golgi morphology was regulated normally, with an extended Golgi at low cell density, and a compact Golgi at high cell density, regardless of inhibition of MST1/2 kinase activity by XMU-MP-1 (Figures 2.5A and 2.5B).

To further assess whether MST1/2 regulation of the Golgi occurs independently of canonical Hippo pathway signaling, we tested whether loss of LATS1/2 phenocopies loss of MST1/2. Compared to parental WT cells, LATS1/2 double-knockout cells [engineered using CRISPR/Cas9 (Meng et al., 2015) (Figure S2.5A)] exhibited normal regulation of Golgi morphology, appearing extended in sparsely plated cells, but compact in densely plated cells (Figures S2.5B and S2.5C). Taken together, our data indicate that MST1/2 function to promote Golgi function in a manner independent of their kinase activity and independent of the canonical downstream Hippo signaling pathway.

Since MST1/2 interact with STRN3 (Bae et al., 2017; Couzens et al., 2013; Hauri et al., 2013; Zheng et al., 2017), we examined whether MST1/2 regulation of the Golgi occurs through STRN3, GOLPH3, and MYO18A. Attempts to overexpress MST1 or MST2 resulted in cell death (data not shown). But, overexpression of kinase-dead FLAG-MST1-K59R or HA-MST2-K56R did not cause cell death, consistent with published data (Graves et al., 1998; Lee et al., 2001). Furthermore, in cells plated at moderate density they caused significant expansion of the Golgi (Figures 2.5C and 2.5D). We then performed

epistasis analysis to determine whether the ability of MST1 and MST2 to affect the Golgi is dependent on STRN3, GOLPH3, and MYO18A. Knockdown of STRN3, GOLPH3, or MYO18A (Figure S2.5D) each completely eliminated the ability of MST1 or MST2 to affect the Golgi (Figures 2.5C and 2.5D). Thus, overexpression of kinase-dead MST1/2 is sufficient to overcome Golgi compaction caused by increasing cell density, restoring the extended Golgi ribbon by acting via STRN3, GOLPH3, and MYO18A.

Since high cell density causes dissociation of STRN3 from GOLPH3 and the Golgi, and MST1/2 act via STRN3 and GOLPH3, we examined whether MST1/2 regulate the association of STRN3 with GOLPH3 and the Golgi. siRNA knockdown of MST1 or MST2 (validated by parallel WB, Figure S2.5E) caused STRN3 to significantly dissociate from the Golgi (Figures 2.5E and 2.5F). Thus, loss of MST1 or MST2 recapitulates the effect of high cell density with dissociation of STRN3 from the Golgi, resulting in Golgi compaction and impairment of trafficking. In light of MST1 and MST2's known role in signaling in response to changes in cell density, taken together with our data, we conclude that MST1/2 relay the cell density signal to STRN3, which regulates GOLPH3-MYO18A interaction to regulate Golgi structure and function.

2.2.8 STRN3 Brings PP2Ac to the GOLPH3 Complex to Promote the Interaction of GOLPH3 with MYO18A

To provide further insight into the mechanism by which STRN3 promotes the interaction of GOLPH3 with MYO18A, we characterized the nature of the STRN3/STRIPAK complex bound to GOLPH3. STRN3 is the core of STRIPAK, including alternative complexes with STRIP1/2 (also known as FAM40A/B) and CTTNBP2NL versus with SLMAP or CTTNBP2 (Goudreault et al., 2009; Hwang and Pallas, 2014). Our

MS analysis of large scale IP of GOLPH3 also identified multiple peptides from CTTNBP2NL (Figure S2.2B). We further characterized the nature of the STRN3/STRIPAK complex bound to GOLPH3 using IP/WB. Endogenous GOLPH3 co-IPed endogenous STRIP1, CTTNBP2NL, and PP2Ac, the catalytic subunit of PP2A (Figure 2.6A). By contrast, we did not detect CTTNBP2 or SLMAP in the IP of GOLPH3 (Figure S2.6A), consistent with published data that the STRIP1/2-CTTNBP2NL and SLMAP or CTTNBP2 complexes with STRN3 are mutually exclusive (Goudreault et al., 2009).

Next, we examined the connectivity of the complex. siRNA knockdown of STRN3 eliminated the interaction of STRIP1, CTTNBP2NL, and PP2Ac with GOLPH3 (Figure 2.6A). By IF, endogenous CTTNBP2NL localized, in part, to the Golgi (Figures 2.6B and S6B) and that signal was lost upon knockdown of CTTNBP2NL by each of three different siRNAs (Figure S2.6B, knockdown confirmed by paralleled WB, Figure S2.6C). Strikingly, the localization of CTTNBP2NL to the Golgi was dependent on GOLPH3 and STRN3, as siRNA knockdown of each (confirmed by parallel WB, Figure S2.6D) caused CTTNBP2NL to dissociate from the Golgi (Figure 2.6B). While CTTNBP2NL localization to the Golgi was dependent on GOLPH3 and STRN3, it was independent of MYO18A (Figures 2.6B and S2.6D). By contrast, co-IP of STRN3 with GOLPH3 occurs independently of CTTNBP2NL (Figure 2.6C). STRIP1 has been proposed to directly interact with STRN3 and bridge CTTNBP2NL to STRN3 (Goudreault et al., 2009; Kean et al., 2011); however, we observed that co-IP of STRIP1 with GOLPH3 is partly dependent on CTTNBP2NL (Figure 2.6C). Our data indicate that STRN3 interacts with

GOLPH3 independently of CTTNBP2NL and STRIP1, while CTTNBP2NL, STRIP1, and PP2Ac interact with GOLPH3 via STRN3.

To examine whether the interaction between GOLPH3 and STRN3 is direct, we observed bacterially expressed, purified proteins *in vitro*. GST-STRN3, but not GST alone, pulled-down GOLPH3 (Figure 2.6D). We conclude that GOLPH3 directly interacts with STRN3, which bridges to other STRIPAK proteins, including PP2Ac, STRIP1, and CTTNBP2NL (Figure 2.6E).

We next sought insight into how STRN3/STRIPAK regulates the interaction between GOLPH3 and MYO18A, such that dissociation of STRN3 from GOLPH3 in cells at high density causes dissociation of MYO18A from GOLPH3. First, we examined the STRIPAK complex itself, finding that IP of endogenous STRN3 robustly co-IPed STRIP1, CTTNBP2NL, and PP2Ac equally well in sparse and dense cells (Figure S2.6D). PP2Ac is a core subunit of the STRIPAK complex that dephosphorylates MST1/2 in sparse cells (Bae et al., 2017; Couzens et al., 2013; Ribeiro et al., 2010; Zheng et al., 2017). Indeed, as shown above, PP2Ac is in the complex that co-IPs with GOLPH3 (Figure 2.6A). To examine whether PP2A plays a role in regulation of the Golgi, we treated sparsely plated cells with the PP2A inhibitors Okadaic acid or Calyculin A. Each caused significant compaction of the Golgi (Figures 2.7A and 2.7B). These data imply that PP2A phosphatase activity in STRIPAK may enhance the interaction between GOLPH3 and MYO18A. To further test whether dephosphorylation of the GOLPH3/MYO18A complex results in enhanced interaction, we examined the effects of dephosphorylation of the complex *in vitro*. Treatment with phosphatase strongly enhanced co-IP of MYO18A with GOLPH3 (Figure 2.7C). Thus, at low cell density STRN3 binding to GOLPH3 recruits the

STRIPAK phosphatase PP2Ac. PP2Ac-dependent dephosphorylation enhances the interaction between GOLPH3 and MYO18A. This enhanced interaction between GOLPH3 and MYO18A promotes Golgi-to-PM trafficking and causes extension of the Golgi ribbon (Figure 2.6E).

2.2.9 Cell Density Regulation of Secretion Provides an Explanation for Non-Cell Autonomous Growth Regulation by Hippo

The Hippo signaling pathway is known for its role to determine organ size *in vivo*, while in cell culture, it is observed to regulate cell proliferation in response to changing cell density (Avruch et al., 2012; Meng et al., 2016). Presumably, the ability to regulate overall organ size involves extracellular signals that coordinate overall organ growth. Indeed, Hippo signaling is known to exert both cell autonomous and non-cell autonomous control of cell proliferation (Del Re et al., 2010; Sarikaya and Extavour, 2015; Zhang et al., 2009). It occurs to us that regulation of secretory trafficking could allow for regulation in one cell to have consequences for neighboring cells. To determine if cell density regulation of Golgi function (via MST1/2-STRN3/STRIPAK-GOLPH3/MYO18A) affects growth factor secretion, we assessed secretion of PDGFA by MDA-MB-231-LM2 (LM2) cells (Minn et al., 2005). These cells secrete PDGFA in a manner dependent on PI4P (Halberg et al., 2016). We collected conditioned media from equal numbers of LM2 cells plated at low versus high density, and assessed PDGFA secretion. While cells grown at low and high densities expressed similar levels of intracellular PDGFA protein, the low density cells secreted significantly more than did the high density cells (Figure 2.7D and 7E). Next, we found that the secretion of PDGFA was dependent on GOLPH3 and STRN3 (Figures 2.7F, 2.7G, and S2.7).

Thus, we observe that growth factor secretion is modulated in response to cell density via the STRN3/GOLPH3 pathway that we found to be regulated by cell density via the Hippo signaling proteins, MST1 and MST2. Our data provide an explanation for the ability of cell density and the Hippo pathway to control cell proliferation at a distance.

2.3 Discussion

2.3.1 Novel Regulation of the Golgi by Cell Density

Remarkably little has been published regarding control of Golgi function in response to extracellular or intracellular signaling (Makowski et al., 2017). Here, we provide a striking example of previously unknown regulation of the Golgi in response to changing cell density. Our findings reveal that in low cell density, the Hippo proteins MST1 and MST2 function to promote STRN3/STRIPAK association with GOLPH3 at the Golgi. At the Golgi, the STRIPAK subunit PP2Ac promotes enhanced GOLPH3-MYO18A interaction, which drives active vesicle trafficking to the PM. In contrast, when cells become crowded, MST1/2 no longer promote STRIPAK association with GOLPH3 (and instead signal to LATS1/2 (Zhao et al., 2007)), resulting in weakening of the GOLPH3-MYO18A interaction, and thus compaction of the Golgi ribbon and reduced secretory trafficking. The defect in secretion that occurs as a result of increasing cell density affects overall trafficking, as observed by unbiased experiments that assess secretion of all endogenous cargoes. Importantly, the defect in secretion caused by high cell density includes reduced secretion of PDGFA, thus demonstrating a mechanism by which cell density and Hippo signaling can affect proliferation of neighboring cells.

2.3.2 Non-Canonical Activity of MST1/2

The canonical Hippo pathway in mammalian cells requires the kinase activity of MST1 and MST2 to phosphorylate the downstream substrates, LATS1 and LATS2, along with the associated protein, MOB1 (Avruch et al., 2012; Meng et al., 2016). Notably, the kinases MST1 and MST2 are functionally redundant in this activity and they are active in their role to activate LATS1/2 in cells at high density. By contrast, here we find that MST1/2 regulation of the Golgi involves an active role in cells at low density, and requires both MST1 and MST2. Furthermore, this activity occurs independently of LATS1/2 and independently of MST1 and MST2 kinase activity. MST1 and MST2 are known to directly interact with STRN3/STRIPAK (Bae et al., 2017; Couzens et al., 2013; Ribeiro et al., 2010; Zheng et al., 2017), and we find that MST1/2 regulation of the Golgi occurs via STRN3, controlling its interaction with GOLPH3 at the Golgi. Understanding the detailed nature of MST1/2 regulation of STRN3/STRIPAK remains an important unsolved question for future investigation.

2.3.3 GOLPH3 Pathway is a Hub for Signals that Regulate the Golgi

Until recently, in the literature the Golgi has been treated as a constitutive organelle, functioning without input in response to changes in intracellular and extracellular conditions (Makowski et al., 2017). However, recent examples demonstrate regulation of the Golgi by several signaling pathways (Buschman et al., 2015a, 2015b; Makowski et al., 2017). Growth factor signaling, via regulation of the subcellular localization of the SAC1 PI4P-phosphatase, results in increased Golgi PI4P, accompanied by increased Golgi extension and activation of Golgi-to-PM trafficking (Bajaj Pahuja et al., 2015; Blagoveshchenskaya et al., 2008). The Golgi is also regulated in

response to cellular DNA damage (Farber-Katz et al., 2014). Activated DNA-PK directly phosphorylates GOLPH3 to enhance the interaction between GOLPH3 and MYO18A, resulting in increased vesiculation and subsequent dispersal of the Golgi. Cell differentiation state also regulates the Golgi (Ng et al., 2013). GOLPH3L is a paralog of GOLPH3 that acts as an endogenous dominant negative inhibitor of GOLPH3-MYO18A. GOLPH3L expression is restricted to highly secretory cell-types, where it acts as a throttle for the GOLPH3-MYO18A complex. Here, we report regulation of the Golgi in response to changing cell density downstream of the mammalian Hippo proteins, MST1 and MST2. Taken together, we see that the GOLPH3 complex is a hub through which multiple input signals converge to regulate the Golgi.

2.3.4 Role in Cancer

GOLPH3 and MYO18A have both been identified as oncogenic cancer drivers for many types of cancer (Buschman and Field, 2017; Buschman et al., 2015a; Kuna and Field, 2018; Makowski et al., 2017; Scott et al., 2009; Xing et al., 2016). Furthermore, the PI transfer protein family, implicated in PI delivery to Golgi PI-4-kinases, including PITPNC1, is an oncogenic cancer driver found to act via GOLPH3 (Halberg et al., 2016; Kuna and Field, 2018). By contrast, null mutations in mice have demonstrated that components of the Hippo pathway, including MST1/2 and LATS1/2, can act as tumor suppressors (John et al., 1999; Yabuta et al., 2013; Zhou et al., 2009). Our data indicate that MST1/2 differ from LATS1/2, because only MST1/2 act as positive regulators of the GOLPH3 complex. Since the GOLPH3 complex promotes cancer, the prediction is that MST1/2 should have features both as tumor suppressors and as oncogenes. Indeed, data from TCGA demonstrate that while homozygous loss of function mutations of LATS1 or

LATS2 are common in cancer, homozygous loss of MST1 or MST2 is uncommon (Cerami et al., 2012; Gao et al., 2013; Weinstein et al., 2013). In fact, unlike LATS1/2, amplification of MST1 or MST2 is seen in many cancers. The TCGA observations are only correlative, with many possible explanations. However, in light of our findings, the role in cancer of regulation of the GOLPH3 complex by MST1 and MST2 becomes an interesting topic for future research.

AUTHOR CONTRIBUTIONS

S.J.F. and T.T.T.T. conceived the project, designed, and analyzed experiments. H.C.D. did some of the GOLPH3 IP experiments, IP-MS experiments, and cloned STRN3. S.L.M. did GOLPH3 IP/CTTNBP2NL knockdown experiments, STRN3 IPs, and PDGFA assays. M.D.B. did the ^{35}S-amino acid pulse-chase assays. H.T did the XMU-MP-1 experiments. K.L.G. provided LATS1/2 knockout cells and assisted with data interpretation. T.T.T.T. performed all other experiments. S.J.F. and T.T.T.T. wrote the paper with input from all authors.

2.4 Materials and Methods

2.4.1 Key resources tables

Table 2.1: Key Antibodies

ANTIBODIES	SOURCE	IDENTIFIER
Rabbit polyclonal anti-GOLPH3	(Dippold et al., 2009)	N/A
Rabbit polyclonal anti-MYO18A	Dr. Zissis Chroneos (University of Texas, Tyler, TX)	N/A
Mouse monoclonal anti-STRN3 (clone S68)	Novus biologicals	Cat#NB110-74572
Rabbit polyclonal anti-STRN3	Sigma	Cat#HPA004636

Table 2.1: Key Antibodies, cont.

ANTIBODIES	SOURCE	IDENTIFIER
Rabbit polyclonal anti-STRN3	Millipore	Cat# not yet available
Mouse monoclonal anti-FAM40A (STRIP1) (Clone 7B8)	OriGene	Cat#TA502310
Rabbit polyclonal anti-CTTNBP2NL	Proteintech	Cat#25523-1-AP
Rabbit monoclonal anti-STK3 (MST2) (EP1466Y)	Abcam	Cat#ab52641
Rabbit polyclonal anti-MST1	Cell Signaling Technology	Cat#3862S
Rabbit polyclonal anti-LATS1	Bethyl Laboratories	Cat#A300-477A
Rabbit polyclonal anti-LATS2	Bethyl Laboratories	Cat#A300-479A
Rabbit polyclonal anti-PDGFA	Origene	Cat#AP20635 PUN
Mouse monoclonal anti-VSV-G (8G5F11)	Kerafast	Cat#EB0010
Rabbit polyclonal anti-YAP (H-125)	Santa Cruz Biotechnology	Cat#sc-15407
Mouse monoclonal anti-GM130	BD Transduction Laboratories	Cat#610823
Mouse monoclonal anti-p230	BD Transduction Laboratories	Cat#611281
Rabbit polyclonal anti-Giantin	Covance	Cat#PRB-114C
Sheep polyclonal anti-TGN46	Bio-rad	Cat#AHP500GT
Rabbit polyclonal anti-HA (Y-11)	Santa Cruz Biotechnology	Cat#sc-805
Rabbit monoclonal anti-FLAG (D6W5B)	Cell Signaling Technology	Cat#14793
Mouse monoclonal anti-FLAG (M2)	Sigma	Cat#F1804
Mouse monoclonal anti-MYC (9B11)	Cell Signaling Technology	Cat#2276
Rabbit monoclonal anti-GAPDH (D16H11)	Cell Signaling Technology	Cat#5174
Mouse monoclonal anti-rabbit IgG, HRP-linked antibody	Jackson ImmunoResearch	Cat#211-032-171
Horse polyclonal anti-mouse IgG, HRP-linked antibody	Cell signaling Technology	Cat#7076

Table 2.1: Key Antibodies, cont.

ANTIBODIES	SOURCE	IDENTIFIER
Goat anti-rabbit AlexaFluor-488 conjugated secondary antibody	Invitrogen	Cat#A11034
Goat anti-mouse AlexaFluor-488 conjugated secondary antibody	Invitrogen	Cat#A11029
Goat anti-rabbit AlexaFluor-594 conjugated secondary antibody	Invitrogen	Cat#A11037
Goat anti-mouse AlexaFluor-594 conjugated secondary antibody	Invitrogen	Cat#A11032
Donkey anti-sheep AlexaFluor-647 conjugated secondary antibody	Invitrogen	Cat#A21448

Table 2.2: Key Chemicals

CHEMICALS	SOURCE	IDENTIFIER
Okadaic acid	Fisher Scientific	Cat#49560925 UG
Calyculin A	Cell Signaling Technology	Cat#9902
XMU-MP-1	Cayman Chemical	Cat#22083
Lipofectamine^{TM} RNAiMax	Invitrogen	Cat#56532
TransIT-LT1	Mirus	Cat#MIR2300
Paraformadehyde	Sigma-Aldrich	Cat#158127
OmniPur BSA Fraction V	Calbiochem	Cat#2960
DAPI	Roche Diagnostics	Cat#10236276 001
HCS CellMask Deep Red Stain	Invitrogen	Cat#H32721
Fluoromount-G	SouthernBiotech	Cat#0100-01
Protein A sepharose CL-4B	GE Healthcare	Cat#17-0780-01
Lambda Protein Phosphatase	New England Biolabs	Cat#P0753

Table 2.3: Key Cell Lines

CELL LINES	SOURCE	IDENTIFIER
HeLa S3	ATCC	
HeLa S3 stably expressed Golgi localization domain of α-mannosidase II-EGFP (amino acids 1-90) (ManII-GFP Hela)	This study	
HEK293 (AD-293 variant)	Stratagene	Cat#240085
HEK293 stably express ts045-VSVG-GFP	(Farber-Katz et al., 2014)	
Normal Rat kidney cells (NRK cells)	ATCC	
MDA-MB-231	ATCC	
MDA-MB-231-LM2	Dr. Joan Massagué (Memorial Sloan Kettering Cancer Center)	(Minn et al., 2005)
HEK293 LATS1/2DKO	Dr. Kun-liang Guan (University of California, San Diego)	(Meng et al., 2015)

Table 2.4: Key Oligonucleotides

OLIGONUCLEOTIDES	SOURCE	IDENTIFIER
siRNA targeting sequence for MYO18A: Forward 5'-UGGAGGUUAUGGAAAUGGAGGUGAU-3' Reverse 5'-AUCACCUCCAUUUCCAUAACCUCCA-3'	Stealth modified siRNA, Invitrogen, (Dippold et al., 2009)	
siRNA targeting sequence for GOLPH3: Forward 5'-AAAUGAUGUGUAACCCUCGCGGUCC-3' Reverse 5'-GGACCGCGAGGGUUACACAUCAUUU-3'	Stealth modified siRNA, Invitrogen, (Dippold et al., 2009)	
The first siRNA targeting sequence for STRN3 Forward 5'-GGAACUGAACCAAGGUGACUUGAAA-3' Reverse 5'-UUUCAAGUCACCUUGGUUCAGUUCC-3'	Stealth modified siRNA, Invitrogen, this study	

Table 2.4: Key Oligonucleotides, cont.

OLIGONUCLEOTIDES	SOURCE	IDENTIFIER
The second siRNA targeting sequence for STRN3 Forward 5'- UUGCUUAGGAGAUUCACCUCCAUUC-3' Reverse 5'- GAAUGGAGGUGAAUCUCCUAAGCAA-3'	Stealth modified siRNA, Invitrogen, this study	
The third siRNA targeting sequence for STRN3 Forward 5'- GCCAAAUGUUCUAGCUGGCACUUUA-3' Reverse 5'- UAAAGUGCCAGCUAGAACAUUUGGC-3'	Stealth modified siRNA, Invitrogen, this study	
The fourth siRNA targeting sequence for STRN3 Forward 5'- GGAGACCUUGCAGACUUGACGGUAA-3' Reverse 5'- UUACCGUCAAGUCUGCAAGGUCUCC-3'	Stealth modified siRNA, Invitrogen, this study	
The fifth siRNA targeting sequence for STRN3 Forward 5'- CAAGUCAUUUAUUAUGGGUUCUGAU-3' Reverse 5'- AUCAGAACCCAUAAUAAAUGACUUG-3'	Stealth modified siRNA, Invitrogen, this study	
The first siRNA targeting sequence for CTTNBP2NL Forward 5'- CCACUCCUGCUUACUCAUAUGCAAA -3' Reverse 5'- UUUGCAUAUGAGUAAGCAGGAGUGG -3'	Stealth modified siRNA, Invitrogen, this study	
The first siRNA targeting sequence for CTTNBP2NL Forward 5'- CCACUCCUGCUUACUCAUAUGCAAA -3' Reverse 5'- UUUGCAUAUGAGUAAGCAGGAGUGG -3'	Stealth modified siRNA, Invitrogen, this study	

Table 2.4: Key Oligonucleotides, cont.

OLIGONUCLEOTIDES	SOURCE	IDENTIFIER
The second siRNA targeting sequence for CTTNBP2NL Forward 5'- GCAAGCCUGAACUCCUGACACUAUU -3' Reverse 5'- AAUAGUGUCAGGAGUUCAGGCUUGC -3'	Stealth modified siRNA, Invitrogen, this study	
The third siRNA targeting sequence for CTTNBP2NL Forward 5'- CCAAUACUGUUGUAGCAAAUGGUAA -3' Reverse 5'- UUACCAUUUGCUACAACAGUAUUGG -3'	Stealth modified siRNA, Invitrogen, this study	
The first siRNA targeting sequence for MST1 Forward 5'- GACAGCCCUCAUGUAGUCAAAUAUU -3' Reverse 5'- AAUAUUUGACUACAUGAGGGCUGUC -3'	Stealth modified siRNA, Invitrogen, this study	
The second siRNA targeting sequence for MST1 Forward 5'- GGCUGGUUCUGUAUCUGAUAUCAUU -3' Reverse 5'- AAUGAUAUCAGAUACAGAACCAGCC -3'	Stealth modified siRNA, Invitrogen, this study	
The third siRNA targeting sequence for MST1 Forward 5'- GGAGUGUCAAUACUGCGAGACUUAA -3' Reverse 5'- UUAAGUCUCGCAGUAUUGACACUCC -3'	Stealth modified siRNA, Invitrogen, this study	
The first siRNA targeting sequence for MST2 Forward 5'- CCUGUUGAAUCAGAUCUUCAGGAAA -3' Reverse 5'- UUUCCUGAAGAUCUGAUUCAACAGG -3'	Stealth modified siRNA, Invitrogen, this study	

Table 2.4: Key Oligonucleotides, cont.

OLIGONUCLEOTIDES	SOURCE	IDENTIFIER
The second siRNA targeting sequence for MST2 Forward 5'- GGUCAGUUAACAGAUACAAUGGCAA -3' Reverse 5'- UUGCCAUUGUAUCUGUUAACUGACC -3'	Stealth modified siRNA, Invitrogen, this study	
The third siRNA targeting sequence for MST2 Forward 5'- CAAGAAUGCCAAACCUGUAUCAAUA -3' Reverse 5'- UAUUGAUACAGGUUUGGCAUUCUUG -3'	Stealth modified siRNA, Invitrogen, this study	
Negative control siRNA, 48% GC content, designed to have no cognate site in mammalian transcriptomes	Stealth modified siRNA, Invitrogen	Cat# 12935300
Primer for site-directed mutagenesis to make siRNA resistant STRN3 Forward 5'- CACAAATTAAAATATGGCACAGAGCTTAATCAGGGCGATCTAAAGATGCCAACCTTTGAGTCAGA-3' Reverse 5'- TGACTCAAAGGTTGGCATCTTTAGATCGCCCTGATTAAGCTCTGTGCCATATTTTAATTT-3'	This study	
Primer for site-directed mutagenesis to make siRNA resistant MST2 and MST2KR Forward 5'- CCGGTCAAGTTGTCGCAATTCGACAAGTACCTGTTGAATCAGATCTTC-3' Reverse 5'- GAAGATCTGATTCAACAGGTACTTGTCGAATTGCGACAACTTGACCGG-3'	This study	

Table 2.5: Key Recombinant DNA

RECOMBINANT DNA	SOURCE	IDENTIFIER
ts045-VSVG-GFP vector	Dr. Jennifer Lippincott-Schwartz (NIH)	(Presley et al., 1997)
pcDNA3.1(+)-Myc-STRN3	This study	
pcDNA3.1(+)-Myc-STRN3 siRNA-resistant	This study	
pcDNA3.1(+)-STRN3	This study	
pcDNA3.1(+)-STRN3 siRNA-resistant	This study	
pGEX-4T3-GST-STRN3	This study	
pGEX-4T3-GST-GOLPH3	(Dippold et al., 2009)	
pCMV-FLAG-MST1	Dr. Joe Avruch (Harvard University)	
pCMV-FLAG-MST1-K59R	Dr. Joe Avruch (Harvard University)	
pcDNA 3.1(+)-HA-MST2	Dr. Kun-Liang Guan (University of California, San Diego)	
pcDNA 3.1(+)-HA-MST2 siRNA-resistant	This study	
pcDNA 3.1(+)-HA-MST2-K56R	Dr. Kun-Liang Guan (University of California, San Diego)	
pcDNA 3.1(+)-HA-MST2-K56R siRNA-resistant	This study	

Table 2.6: Key Software and Algorithms

SOFTWARE AND ALGORITHMS	SOURCE	IDENTIFIER
Cell Profiler		(Carpenter et al., 2006)
Slidebook	Intelligent Imaging Innovations	
Image Studio Lite Ver. 5.2	LI-COR biosciences	https://www.licor.com/bio/products/software/image_studio_lite/

2.4.2 Cell cultures

HeLa S3, HEK293, MDA-MB-231, and NRK cells were cultured in Dulbecco's Modified Eagle Medium (DMEM) (DMEM 1x, Gibco, Cat#10-013-CV) supplemented with 10% (v/v) fetal bovine serum (FBS) and 100 units/ml Penicillin and 100 µg/ml Streptomycin at 37°C in a humidified, 10% carbon dioxide atmosphere. The stable cell lines HeLa S3 expressing ManII-GFP and HEK293 expressing ts045-VSVG-GFP were grown in media supplemented with 800 µg/mL G418. Experiments are performed in HeLa cells unless indicated otherwise.

2.4.3 Western blot

Cells were lysed at 95^{o}C for 10 min in SDS sample buffer composed of 34.7 mM Tris-HCl, pH 6.8, 6.9% glycerol, 0.5 M β-mercaptoethanol, 1.7% SDS, and 0.04% bromophenol blue. Lysates were run on SDS-PAGE (10% acrylamide), then wet transferred to polyvinylidene difluoride (PVDF) membrane for 3.5 hr at 100 V in 4^{o}C. The membranes were then blocked with 5% (w/v) non-fat milk in tris buffered saline (TBS)/0.1% Tween-20 for one hour before incubation with primary antibody in 5% (w/v) bovine serum albumin (BSA) in TBS/0.1% Tween-20 at 4°C overnight. After that, membranes were washed with TBS/0.1% Tween-20 then incubated with horse radish

peroxidase-conjugated secondary antibody at room temperature for one hour, followed by washing with TBS 0.1% Tween-20. Membranes were then incubated with enhanced chemiluminescence substrates and exposed to film.

2.4.4 siRNA transfection

Cells were incubated with 300 µl of DMEM with 10% FBS and without any antibiotics per well of a 24-well plate (24-well plate, Thermo Scientific, Cat#930186) for 30 min prior to transfection with RNAiMax (Invitrogen, Cat#56532), according to manufacturer's instructions. Cells were incubated with siRNA transfection mixture overnight before replacing with regular growth media. Cells were harvested after 66 hr from first contact with siRNA. The final concentration of siRNA in each well is 20 nM.

2.4.5 DNA transformation

Cells were incubated with 500 µl of DMEM with 10% FBS and without any antibiotics per well of a 24-well plate for 30 min prior to addition of DNA transformation mixture using LT1 (Mirus, Cat#MIR2300), according to manufacturer's instructions. Cells were harvested after 24 hr.

2.4.6 Immunofluorescence

For IF, cells were grown on glass coverslips (Fisherbrand, Microscope Cover Glass, Cat#12-545-81). Cells were fixed with 4^{o}C freshly made 3.7% paraformaldehyde in phosphate buffered saline (PBS) pH 7.5 and gently rocked for 20 min at room temperature. After fixing, cells were washed with PBS then permeabilized with 0.1% TritonX-100 in PBS for 10 min, then washed with PBS. After that, cells were blocked with 5% (w/v) BSA in PBS for one hour at room temperature. Next, cells were immunostained with primary antibody in 1% (w/v) BSA and 500 ng/ml DAPI in PBS overnight at 4°C. The

next day, cells were washed with PBS then immunostained with secondary antibody in 1% (w/v) BSA and 500 ng/ml DAPI in PBS for 2 hr at room temperature. When appropriate, cells were then stained with HCS CellMask Deep Red Stain at 50 ng/ml in PBS for 30 min at room temperature to allow automated image segmentation. After that, cells were washed with PBS and mounted onto glass slides (FisherScientific, Premium Microscope Slides Superfrost, Cat#12-544-7) using Fluoromount-G and sealed with clear nail polish.

2.4.7 Immunoprecipitation

Adherent cells were scraped down and rotated for 1 hr at 4^{o}C in lysis buffer containing 150 mM NaCl, 10 mM 3-[(3-cholamidopropyl)dimethylammonio]-1-propanesulfonate (CHAPS), 2 mM EDTA, 10 mM Na_2PO_4 (pH 7.0), 5 mM dithiothreitol (DTT), 100 µM leupeptin, 1 mM 4-(2-Aminoethyl)benzenesulfonyl fluoride hydrochloride (AEBSF), 1 µg/mL pepstatin A, 40 µM bestatin, 1 mM sodium orthovanadate, 20 mM sodium fluoride, 5 mM β-glycerophosphate, and 2.5 mM sodium pyrophosphate. Lysates were precleared at 12,000 rpm for 10 min and then incubated with appropriate antibody and corresponding pre-immune serum, rotating for 2 hr at 4^{o}C. Protein A Sepharose beads were then added to the mixture and rotated for another hour at 4^{o}C. Finally, beads were recovered at 3,000 rpm for two minutes and decanting. Beads were washed three times with lysis buffer and protein eluted by boiling in SDS sample buffer, followed by WB.

2.4.8 Treatment of cell lysates with Lambda protein phosphatase

Adherent cells were scraped down and rotated for 1 hr at 4^{o}C in lysis buffer containing 150 mM NaCl, 10 mM 3-[(3-cholamidopropyl)dimethylammonio]-1-propanesulfonate (CHAPS), 10 mM Na_2PO_4 (pH 7.0), 5 mM dithiothreitol (DTT), 100 µM

leupeptin, 1 mM 4-(2-Aminoethyl)benzenesulfonyl fluoride hydrochloride (AEBSF), 1 μg/mL pepstatin A, and 40 μM bestatin. After precleared by spinning at 12,000 rpm for 10 min, lysates were added with 1 mM $MnCl_2$ then 800 U/ml Lambda protein phosphatase before incubating at 30°C for 1 hr. Subsequent immunoprecipitation steps followed what described above.

2.4.9 ts045-VSVG-GFP trafficking assay

HEK293 cells engineered to stably express ts045-VSVG-GFP protein were transfected with appropriate siRNAs. After 49 hr, cells were moved to 40°C. After 15.5 hr at 40°C, cells were shifted to the permissive temperature of 32°C. After 90 min incubation at 32°C, cells were fixed and stained. Immunofluorescence was performed without permeablizing the cells, using an anti-VSV-G antibody to detect the extracellular domain of VSVG protein at the PM. Images were analyzed using CellProfiler for image segmentation and quantification of PM VSVG relative to total VSVG-GFP per cell.

2.4.10 ^{35}S-amino acid pulse chase assay

Cells were plated at high or low density and/or transfected with appropriate siRNAs. One hour prior to harvest, cells were washed once with the modified DMEM without L-methionine, L-cystine, and L-glutamine (Corning, DMEM 1x, Cat#17-204-CIR), then pulse-labeled for 30 min at 37°C with 25 μCi/mL ^{35}S-amino acid mixture (PerkinElmer, EasyTag™ EXPRESS^{35}S Protein Labeling Mix, [^{35}S], 2 mCi, NEG772002MC) in modified DMEM and 10% dialyzed FBS (GE Healthcare Life Sciences, Dialyzed Fetal Bovine Serum, Cat#SH30079.02). Afterward, cells were washed twice with regular DMEM (Corning, DMEM 1x, Cat#10-0130CV) and chased for 10 min with regular DMEM supplemented with 10% regular FBS. The ‘chase’ media was

harvested and proteins from the media and cell lysate were precipitated with 10% trichloroacetic acid (TCA) at -20°C overnight followed by centrifugation, and washing twice with cold 10% TCA. Pellets were re-dissolved in 1 M Tris pH 8.8 buffer and counted in a scintillation counter. Protein secretion was calculated as the ratio of labeled protein in the media to total labeled proteins.

2.4.11 *In vitro* pulldown assay

GOLPH3**,** GST, and GST-STRN3 were bacterially expressed and purified. The pull-down buffer contained 150 mM NaCl, 10 mM Na_2PO_4 (pH 7.0), 10 mM CHAPS, and 2 mM EDTA, 5 mM DTT, 100 μM leupeptin, 1 mg/ml AEBSF, 10 μM pepstatin A, and 40 μM bestatin. Equimolar amounts of GOLPH3 and GST or GOLPH3 and GST-STRN3 were mixed, rocked at 4^{o}C for 2 hr, and added to GSH beads (Sigma, Glutathione−Agarose, Cat#G4510), rocking for another 2 hr. The beads were recovered by centrifuging at 500 g for 20 s and then washed three times with pull-down buffer. Proteins were recovered from the beads by boiling in sample buffer for 10 min. Proteins were analyzed by WB.

2.4.12 Treatment of cells with MST1/2 inhibitors XMU-MP-1

Cells were plated at high or low density on coverslips. XMU-MP-1 was then added at 1 μM, 3 μM, or 10 μM, versus addition of DMSO (vehicle control). After 6 hr cells were fixed with paraformaldehyde and processed for IF with antibodies to YAP and GM130, and stained with DAPI and HCS CellMask Deep Red.

2.4.13 Treatment with PP2A inhibitors Okadaic acid (OKA) and Calyculin A (CalA)

Cells were plated on coverslips at low or high density. Treatment with OKA (10 nM, 30 nM, or 50 nM), CalA (1 nM), or DMSO (vehicle control) was performed for 4 hr, followed by fixation with paraformaldehyde and processing for IF.

2.4.14 PDGFA secretion assay

LM2 cells were plated at high or low density and/or transfected with appropriate siRNAs. 40 hr after siRNA transfection cells were washed twice with DMEM and incubated in DMEM without serum for 16 hr. The conditioned media was collected, precleared at 1500 rpm for 3 min, passed through a 0.45 μM filter, and then concentrated 20 fold using an Amicon Ultra-4 centrifugal device (Fisher, Ultra-4 Amicon, 3000NMWL, Cat#UFC800308). The cells were trypsinized, counted, washed two times with PBS, and lysed with RIPA buffer (150 mM NaCl, 2 mM EDTA, 10 mM sodium phosphate pH 7.2, 1%(w/v) NP-40, 1% (w/v) sodium deoxycholate, 0.1% (w/v) SDS, protease inhibitors). Concentrated conditioned media was normalized according to cell count of corresponding samples. Conditioned media and cell lysates were examined by Western blot.

2.4.15 Fluorescence microscopy

Images of stained cells were acquired with an Olympus IX81-ZDC spinning-disk confocal microscope using a 40X/NA 1.30 objective lens. Images were captured using a Photometrics CoolSnap HQ2 cooled CCD camera. The microscope was controlled by and images captured using Slidebook software (Intelligent Imaging Innovations). Automated image segmentation and analysis were performed using CellProfiler software (Carpenter et al., 2006). Additional image analysis was performed using ImageJ software

(Schneider et al., 2012). Images shown in figures are maximum projections in z of confocal z-stacks, unless noted otherwise.

2.4.16 Measurement of Golgi area

An automated pipeline was built in CellProfiler software for automated image segmentation to identify individual cells and to measure the area of the Golgi per cell. Golgi area was determined as the area of an ellipse with the same second moment as the Golgi within that cell (similar to the area of the smallest encircling ellipse). Measurements of Golgi area per cell across treatments and replicate experiments were further analyzed in Microsoft Excel and PAST.

2.4.17 Statistical analysis

Bar graph indicate mean ± SEM. p-values were calculated using the indicated statistical test, using Microsoft Excel or PAST software (Hammer et al., 2001).

Acknowledgements

Chapter 2 is the complete text and figures of the manuscript by Tran, T.T.T, Dippold, H.C., Makowski, S.L., Buschman, M.D., Tanaka, H., Guan, K.-L., and Field, S.J. (2018). Cell Density Regulates the Golgi Through Hippo, the STRIPAK Complex, and GOLPH3. Manuscript is in review with Developmental Cell. I, Thuy Thi Thu Tran, is the primary investigator and author of this paper.

Figure 2.1: Increasing Cell Density Inhibits the GOLPH3 Complex to Cause Reduced Golgi Trafficking and Compact Golgi Morphology.
(A) HeLa cells plated at increasing cell density, examined by IF to Golgi marker GM130 and stained with DAPI to mark nuclei. Differential interference contrast (DIC) images provide an overview of cell density. White box indicates the region shown in lower images to observe Golgi morphology. High cell density results in Golgi compaction. (B) Quantification of (A) reveals reduced Golgi area with increasing cell density. (C) Similar to (A), showing high cell density causes Golgi compaction in HEK293 cells. See also Figures S2.1A-D for additional cell types. (D) Quantification of (C) reveals reduced Golgi area with increasing cell density. (E) Analysis of overall secretion of endogenous proteins by ^{35}S-amino acid pulse-chase assay to detect total protein secretion into the media relative to total protein synthesis. For each cell line, HEK293, HeLa, and NIH3T3, plating cells at high density results in reduced overall secretion. (F) Analysis of trafficking of ts045-VSVG-GFP to the PM in HEK293 cells plated at low versus high density. Delivery of VSVG to the PM is detected using an antibody to the extracellular domain in unpermeabilized cells, occurring only after shift to the permissive temperature of 32ºC. High cell density results in impaired delivery of VSVG to the PM. (G) Quantification of (F) reveals reduced VSVG transport to the PM in cells plated at high density. (H) IP of endogenous GOLPH3 from HeLa cells co-IPs both endogenous MYO18A and endogenous STRN3, and reveals impaired interaction of both proteins with GOLPH3 in cells plated at high density. See also Figures S2.1E-G for related data, including co-IP from HEK293 cells. (I) Quantification of co-IP from (H) reveals impaired GOLPH3-MYO18A interaction in cells at high density. (K) Quantification of co-IP from (H) reveals impaired GOLPH3-STRN3 interaction in cells at high density. Bar graphs show mean ± SEM. Data for (B), (D), and (G) include n cells (as indicated), pooled from three independent experiments for each. (E), (I), and (K) include n (as indicated) independent experiments. p-values calculated for (B), (D), (E), and (G) by t test, for (I) and (K) by one sample t test.

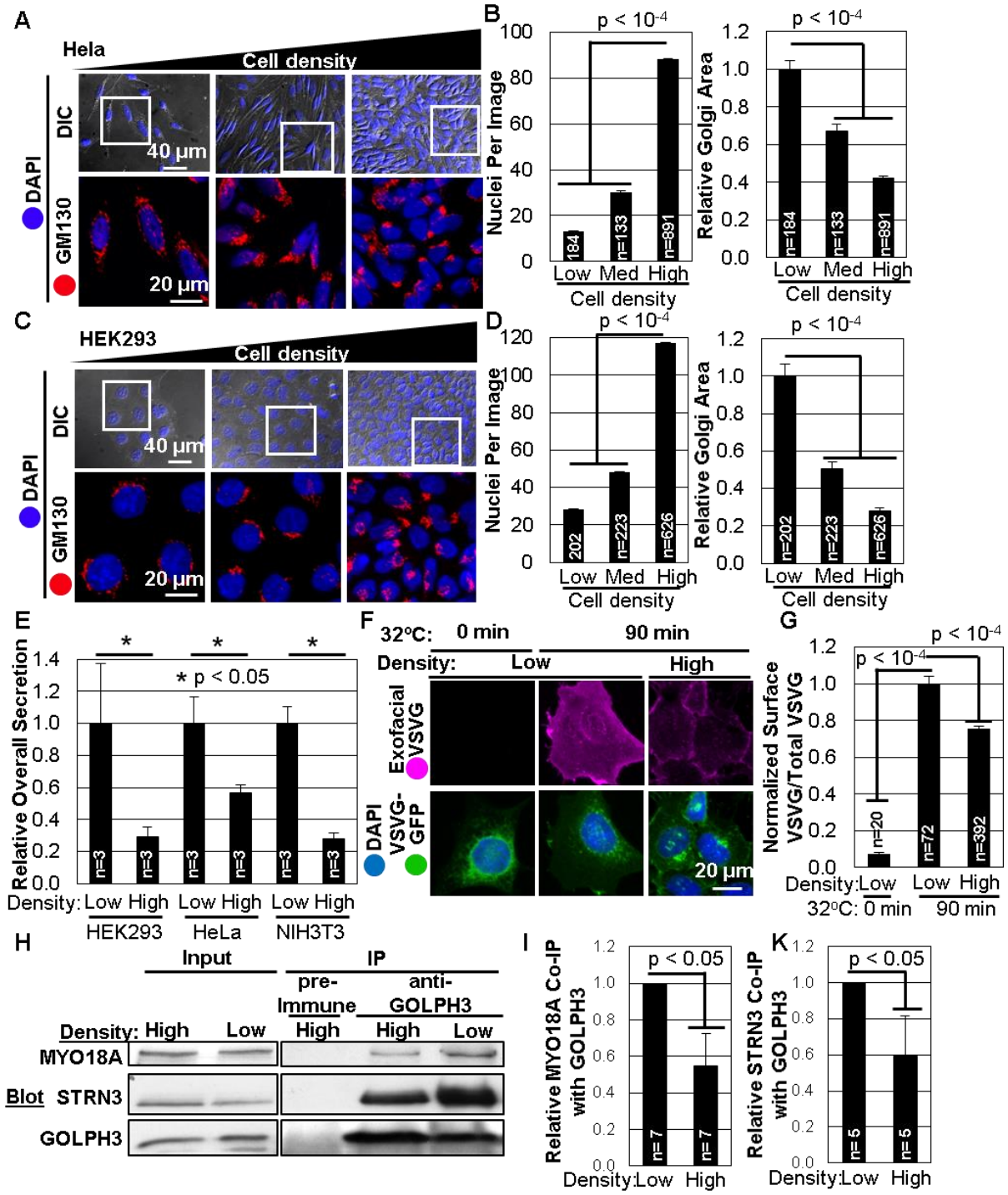
A
Hela
Cell density
DIC
DAPI
GM130
40 μm
20 μm
B
p < 10-4
Nuclei Per Image
Relative Golgi Area
n=184
n=133
n=891
Low Med High
Cell density
C
HEK293
D
n=202
n=223
n=626
E
Relative Overall Secretion
* p < 0.05
Density: Low High Low High Low High
HEK293 HeLa NIH3T3
F
32°C: 0 min 90 min
Density: Low High
Exofacial VSVG
VSVG-GFP
G
Normalized Surface VSVG/Total VSVG
n=20
n=72
n=392
Density:Low Low High
32°C: 0 min 90 min
H
Input
IP
pre-Immune
anti-GOLPH3
Density: High Low High High Low
MYO18A
Blot STRN3
GOLPH3
I
Relative MYO18A Co-IP with GOLPH3
p < 0.05
n= 7
Density:Low High
K
Relative STRN3 Co-IP with GOLPH3
n= 5

Figure 2.2: STRN3 Interacts with GOLPH3 to Regulate Golgi Morphology and Trafficking.
(A) IP of endogenous GOLPH3 robustly co-IPs both endogenous MYO18A and endogenous STRN3. Neither is observed with the pre-immune control. Dashed line indicates omission of irrelevant intervening lanes. (B) IF detects endogenous STRN3 partially colocalizing with the Golgi marker GM130 (red) in HeLa cells. Knockdown of STRN3 by each of three different siRNAs validates the specificity of the STRN3 IF, and demonstrates compaction of the Golgi relative to cells transfected with a control siRNA. See Figure S2.3A for parallel WB to further validate knockdown of STRN3. (C) Quantification of (B) demonstrating significant compaction of the Golgi with STRN3 knockdown. (D) WB demonstrates successful knockdown of GOLPH3, MYO18A, and STRN3 in blots performed in parallel with (E). (E) Partial localization of STRN3 to the Golgi (marked by TGN46), as detected by IF to the endogenous protein. Specificity of IF is validated by siRNA knockdown of STRN3. STRN3 localization to the Golgi is dependent on GOLPH3, but independent of MYO18A. (F) Endogenous STRN3 and MYO18A robustly co-IP with endogenous GOLPH3. Knockdown of MYO18A does not affect the interaction of STRN3 with GOLPH3. (G) siRNA knockdown of STRN3 results in reduced levels of STRN3 and compaction of the Golgi. Expression of siRNA-resistant STRN3 restores STRN3 expression, and restores extended ribbon morphology of the Golgi. See Figure S2.3B for WB. (H) Quantification of (G) demonstrating that knockdown of STRN3 causes Golgi compaction (reduced Golgi area), while expression of siRNA-resistant STRN3 rescues normal Golgi morphology. Bar graphs show mean ± SEM for n cells (as indicated), pooled from three independent experiments for each; p-values calculated by t test.

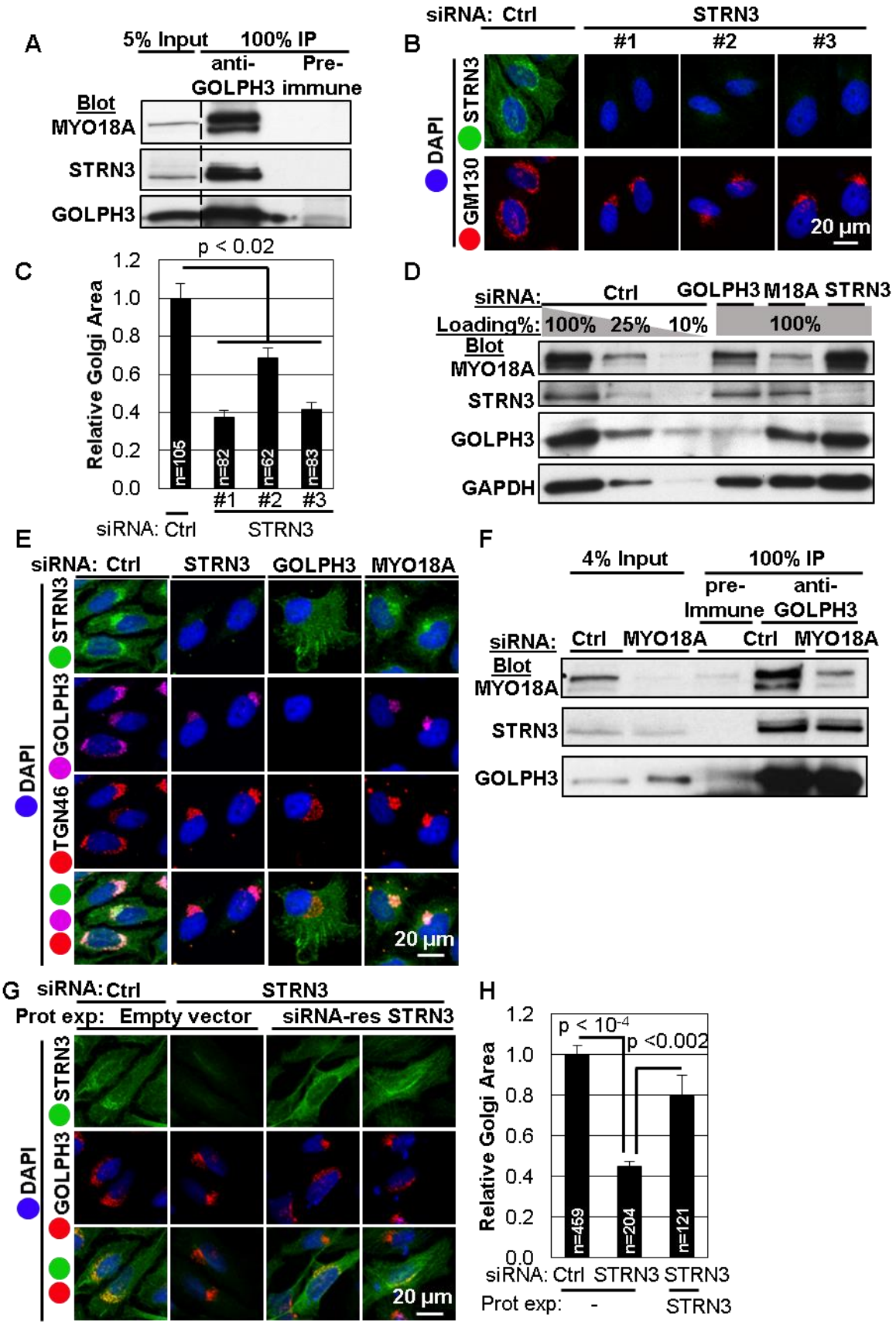
A
5% Input
100% IP
anti-GOLPH3
Pre-immune
Blot
MYO18A
STRN3
GOLPH3
B
siRNA: Ctrl
STRN3
#1
#2
#3
DAPI
STRN3
GM130
20 µm
C
p < 0.02
Relative Golgi Area
1.2
1.0
0.8
0.6
0.4
0.2
0.0
n=105
n=82
n=62
n=83
#1
#2
#3
siRNA: Ctrl
STRN3
D
siRNA:
Ctrl
GOLPH3
M18A
STRN3
Loading%:
100%
25%
10%
100%
Blot
MYO18A
STRN3
GOLPH3
GAPDH
E
siRNA: Ctrl
STRN3
GOLPH3
MYO18A
DAPI
STRN3
GOLPH3
TGN46
20 µm
F
4% Input
100% IP
pre-Immune
anti-GOLPH3
siRNA:
Ctrl
MYO18A
Ctrl
MYO18A
Blot
MYO18A
STRN3
GOLPH3
G
siRNA: Ctrl
STRN3
Prot exp: Empty vector
siRNA-res STRN3
DAPI
STRN3
GOLPH3
20 µm
H
p < 10-4
p <0.002
Relative Golgi Area
1.2
1.0
0.8
0.6
0.4
0.2
0.0
n=459
n=204
n=121
siRNA: Ctrl
STRN3
STRN3
Prot exp:
-
STRN3

Figure 2.3: STRN3 Controls Golgi Form and Function via Regulation of the Interaction of GOLPH3 with MYO18A.
(A) WB of (B) demonstrates successful knockdown of MYO18A and STRN3 (by two independent siRNA oligonucleotides). Dashed line indicates omission of irrelevant intervening lanes.(B) Analysis of overall secretion of endogenous proteins by 35S-amino acid pulse-chase, measuring total protein secretion relative to total protein synthesis, normalized to control. siRNA knockdown of MYO18A or STRN3 (by two independent siRNAs) each cause significant reduction in overall secretion. (C) Trafficking of ts045-VSVG-GFP to the PM in HEK293 cells plated at low versus high density. Delivery of VSVG to the PM is detected by an antibody to extracellular domain in unpermeabilized cells, occurring only after shift to the permissive temperature of 32ºC. siRNA knockdown of STRN3 results in impaired delivery of VSVG to the PM.(D) Quantification of (C) shows significant reduction of VSVG trafficking to the PM in cells plated at high density or upon knockdown of STRN3. (E) siRNA knockdown of STRN3 results in impaired co-IP of endogenous MYO18A with GOLPH3. See also Figure 2.6A.(F) Quantification of (E) shows significant reduction in GOLPH3-MYO18A interaction upon knockdown of STRN3.Bar graphs show mean ± SEM, for (B) and (F) from n (as indicated) independent experiments. (D) from n cells (as indicated), pooled from three independent experiments. p-values are calculated for (B) and (D) by t test, for (F) by one sample t test.

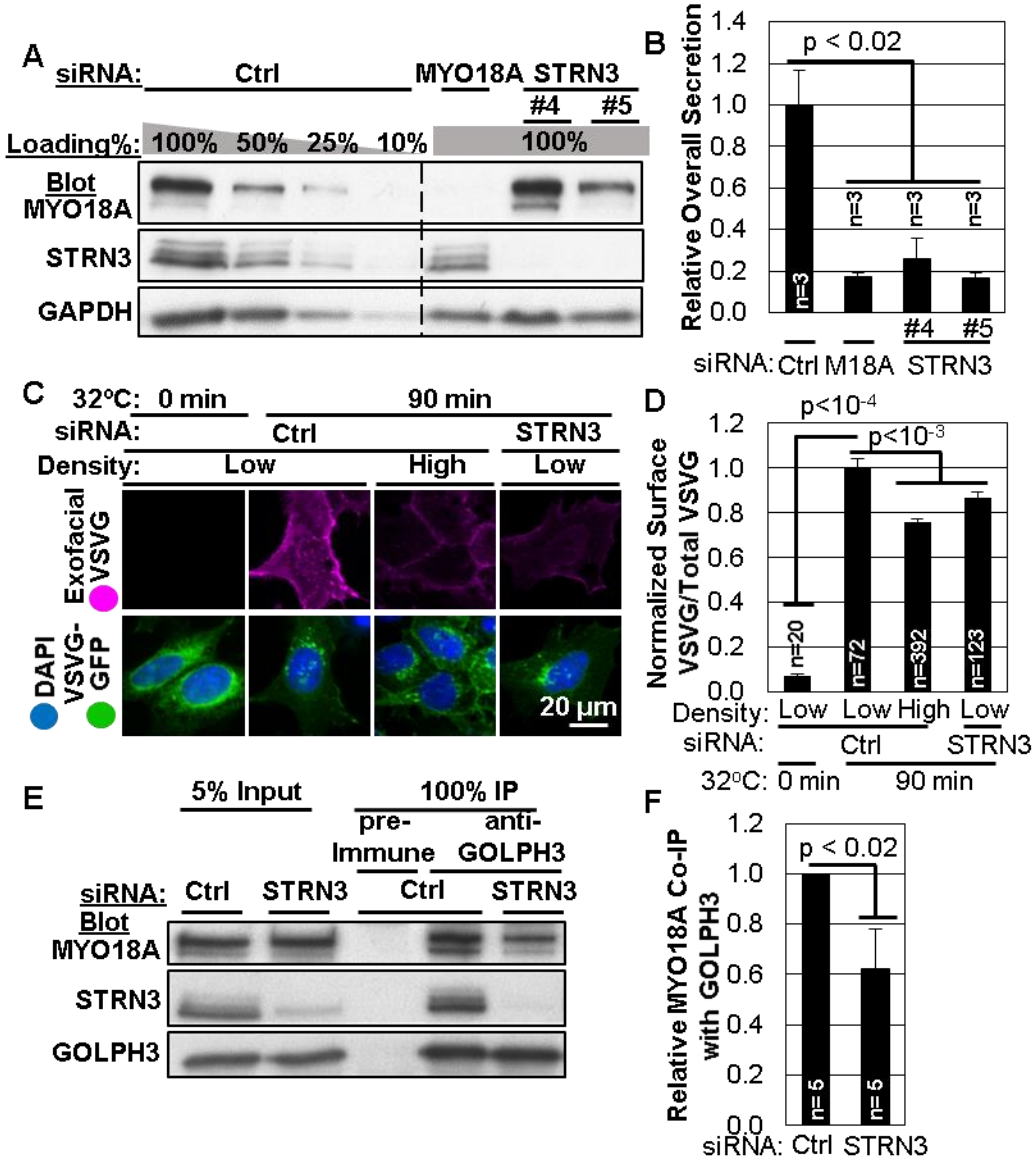
A
siRNA:
Ctrl
MYO18A
STRN3
#4
#5
Loading%:
100%
50%
25%
10%
100%
Blot
MYO18A
STRN3
GAPDH
B
Relative Overall Secretion
p < 0.02
n=3
n=3
n=3
n=3
#4
#5
siRNA: Ctrl M18A STRN3
C
32°C: 0 min
90 min
siRNA:
Ctrl
STRN3
Density:
Low
High
Low
Exofacial VSVG
DAPI
VSVG-GFP
20 µm
D
Normalized Surface VSVG/Total VSVG
p<10-4
p<10-3
n=20
n=72
n=392
n=123
Density: Low Low High Low
siRNA:
Ctrl
STRN3
32°C: 0 min
90 min
E
5% Input
100% IP
pre-Immune
anti-GOLPH3
siRNA:
Ctrl
STRN3
Ctrl
STRN3
Blot
MYO18A
STRN3
GOLPH3
F
Relative MYO18A Co-IP with GOLPH3
p < 0.02
n= 5
n= 5
siRNA: Ctrl STRN3

Figure 2.4: MST1 and MST2 are Required for Normal Golgi Form and Function.

(A) siRNA knockdown of MST1, MST2, or both (using three independent siRNAs for each protein, as indicated), results in compaction of the Golgi ribbon. Shown are IF images of the Golgi marker GM130 (red), together with DAPI to mark the nucleus (blue). See also Figure S2.4A for parallel WB confirming knockdown of MST1 or MST2 by each siRNA. See also Figure S2.5, showing Golgi is unaffected by knockout of LATS1/2. (B) Quantification of (A) shows significant compaction of the Golgi upon knockdown of MST1, MST2, or both. (C) Compaction of the Golgi caused by siRNA knockdown of MST1 is rescued by expression of both WT and kinase-dead (K59R) siRNA-resistant FLAG-MST1. Transfected cells are detected by GFP (control, green) or anti-FLAG IF (FLAG-MST1, green). Golgi morphology is observed by IF to GM130 (red), with nucleus marked by DAPI (blue). See Figure S2.4B for parallel WB to validate expression. (D) Quantification of (C) shows significant compaction of the Golgi upon MST1 knockdown, and rescue of Golgi morphology with re-expression of siRNA-resistant FLAG-MST1, WT or kinase-dead (K59R). (E) Compaction of the Golgi caused by siRNA knockdown of MST2 is rescued by expression of both WT and kinase-dead (K56R) siRNA-resistant HA-MST2. Transfected cells are detected by GFP (control, green) or anti-HA IF (HA-MST2, green). Golgi morphology is observed by IF to GM130 (red), with nucleus marked by DAPI (blue). See Figure S2.4C for parallel WB to validate expression. (F) Quantification of (E) shows significant compaction of the Golgi upon MST2 knockdown, and rescue of Golgi morphology with re-expression of siRNA-resistant HA-MST2, WT or kinase-dead (K56R). (G) Trafficking of ts045-VSVG-GFP to the PM in HEK293 cells is impaired upon knockdown of MST1 or MST2. Delivery to the PM is detected using an antibody to the extracellular domain in unpermeabilized cells. Trafficking occurs upon shift to the permissive temperature of 32ºC. See Figure S2.4D for WB to validate the knockdowns. (H) Quantification of (G) shows significant reduction in VSVG trafficking to the PM upon knockdown of MST1 or MST2. Bar graphs show mean ± SEM for n cells (as indicated), pooled from three independent experiments for each; p-values calculated by t test.

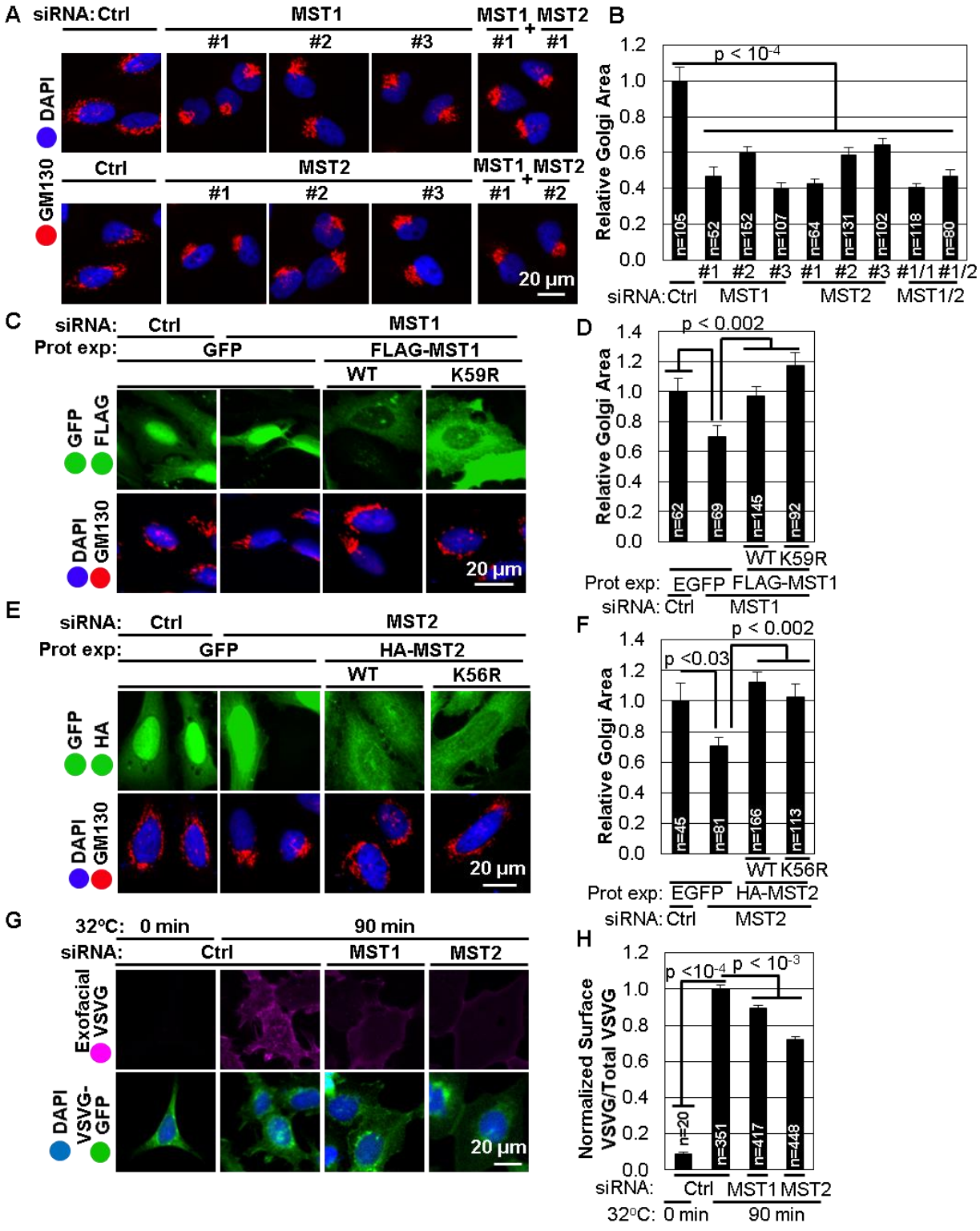
A
siRNA: Ctrl
MST1
MST1+MST2
#1
#2
#3
#1
#1
DAPI
GM130
Ctrl
MST2
MST1+MST2
#1
#2
#3
#1
#2
20 μm
B
Relative Golgi Area
p < 10-4
n=105
n=52
n=152
n=107
n=64
n=131
n=102
n=118
n=80
#1 #2 #3 #1 #2 #3 #1/1 #1/2
siRNA: Ctrl MST1 MST2 MST1/2
C
siRNA: Ctrl
MST1
Prot exp: GFP
FLAG-MST1
WT
K59R
GFP
FLAG
DAPI
GM130
20 μm
D
Relative Golgi Area
p < 0.002
n=62
n=69
n=145
n=92
WT K59R
Prot exp: EGFP FLAG-MST1
siRNA: Ctrl MST1
E
siRNA: Ctrl
MST2
Prot exp: GFP
HA-MST2
WT
K56R
GFP
HA
DAPI
GM130
20 μm
F
Relative Golgi Area
p < 0.002
p <0.03
n=45
n=81
n=166
n=113
WT K56R
Prot exp: EGFP HA-MST2
siRNA: Ctrl MST2
G
32°C: 0 min
90 min
siRNA: Ctrl
MST1
MST2
Exofacial VSVG
DAPI
VSVG-GFP
20 μm
H
Normalized Surface VSVG/Total VSVG
p <10-4
p < 10-3
n=20
n=351
n=417
n=448
siRNA: Ctrl MST1 MST2
32°C: 0 min 90 min

Figure 2.5: MST1 and MST2 Act on the Golgi Independently of Their Kinase Activity, Through STRN3, GOLPH3, and MYO18A.
(A) HeLa treated with MST1/2 kinase inhibitor XMU-MP-1 or DMSO (vehicle control), followed by IF to YAP (green) and the Golgi marker GM130 (red) and stained with DAPI to mark nuclei (blue). In control cells, increasing cell density leads to loss of YAP from the nucleus and compaction of the Golgi. Treatment with MST1/2 kinase inhibitor XMU-MP-1 abrogates regulation of YAP, but has no effect on the Golgi. (B) Quantification of (A) shows Golgi area is unaffected by increasing XMU-MP-1. (C) Overexpression of FLAG-MST1-K59R or HA-MST2-K56R causes expansion of the Golgi, but this effect depends on GOLPH3, MYO18A, and STRN3. Transfected cells are detected by expression of GFP (control), FLAG-MST1-K59R, or HA-MST2-K56R IF (all green). The Golgi is observed by IF to GM130 (red), and nuclei are stained with DAPI (blue). See also Figure S2.5D for WB to assess protein levels. (D) Quantification of (C) shows significant expansion of the Golgi upon overexpression of FLAG-MST1-K59R or HA-MST2-K56R, but not after knockdown of GOLPH3, MYO18A, or STRN3. (E) Sparsely plated cells transfected with siRNAs to knockdown MST1 or MST2 (or control), followed by IF to endogenous STRN3 (green) and Golgi marker GM130 (red), and stained with DAPI to mark nuclei (blue). Partial localization of endogenous STRN3 to the Golgi depends on MST1 and MST2. See also Figure S2.5E for WB to assess protein levels. (F) Quantification of (E) shows significant reduction in STRN3 localization to the Golgi upon MST1 or MST2 knockdown. Bar graphs show mean ± SEM for n cells (as indicated), pooled from three independent experiments for each; p-values calculated by t test.

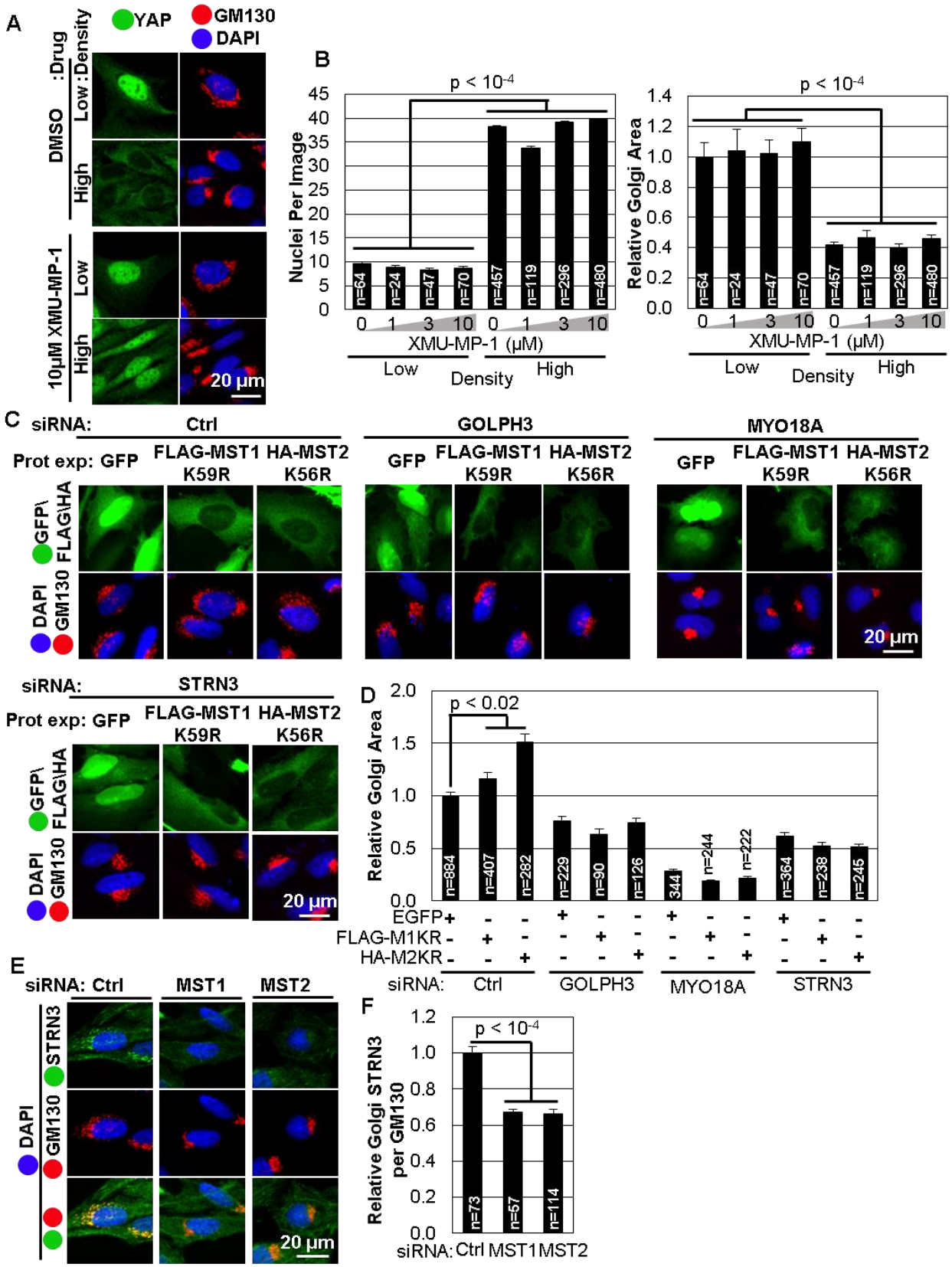
A
YAP
GM130
DAPI
:Drug
:Density
DMSO
Low
High
10μM XMU-MP-1
Low
High
20 μm
B
p < 10-4
Nuclei Per Image
Relative Golgi Area
n=64
n=24
n=47
n=70
n=457
n=119
n=296
n=480
0 1 3 10 0 1 3 10
XMU-MP-1 (μM)
Low
Density
High
C
siRNA:
Ctrl
GOLPH3
MYO18A
Prot exp: GFP
FLAG-MST1 K59R
HA-MST2 K56R
GFP\FLAG\HA
DAPI\GM130
20 μm
siRNA:
STRN3
D
p < 0.02
Relative Golgi Area
n=884
n=407
n=282
n=229
n=90
n=126
344
n=244
n=222
n=364
n=238
n=245
EGFP
FLAG-M1KR
HA-M2KR
siRNA:
Ctrl
GOLPH3
MYO18A
STRN3
E
siRNA: Ctrl
MST1
MST2
STRN3
GM130
DAPI
20 μm
F
p < 10-4
Relative Golgi STRN3 per GM130
n=73
n=57
n=114
siRNA: Ctrl MST1 MST2

Figure 2.6: The STRIPAK Complex Interacts with GOLPH3 via STRN3.
(A) Endogenous STRIPAK proteins CTTNBP2NL, STRIP1, PP2Ac, and STRN3, as well as MYO18A, co-IP with endogenous GOLPH3. Co-IP of STRIPAK proteins is dependent on STRN3, as observed by loss of co-IP after knockdown of STRN3. See also Figure S2.6A for assessment of other STRIPAK proteins. (B) Hela cells transfected with siRNAs to CTTNBP2NL, GOLPH3, STRN3, or MYO18A, followed by IF to CTTNBP2NL (green), Golgi marker GM130 (red) and stained with DAPI (blue) to mark the nuclei. Endogenous CTTNBP2NL is observed to partially localize to the Golgi, validated by siRNA knockdown. CTTNBP2NL localization to the Golgi depends on GOLPH3 and STRN3, but is independent of MYO18A. See also Figure S2.6D for parallel WB confirming knockdowns. See also Figure S2.6B and S6C for additional siRNA validation of IF to CTTNBP2NL. (C) IP of endogenous GOLPH3 co-IPs endogenous STRIP1, CTTNBP2NL, and STRN3. siRNA knockdown of CTTNBP2NL impairs co-IP of STRIP1, but co-IP of STRN3 is unaffected. (D) Bacterially expressed, purified GOLPH3, GST, and GST-STRN3 proteins interact in vitro. GST-STRN3 pulled-down on GSH beads robustly pulls-down GOLPH3, but GST alone does not. (E) Model of STRIPAK interaction with GOLPH3, regulated by MST1/2. In cells at low density STRN3 interacts directly with GOLPH3, dependent on MST1/2. STRN3 bridges to other STRIPAK components including STRIP1, CTTNBP2NL, and PP2A. STRIPAK promotes the interaction between GOLPH3 and MYO18A to promote Golgi-to-plasma membrane trafficking in cells at low density.

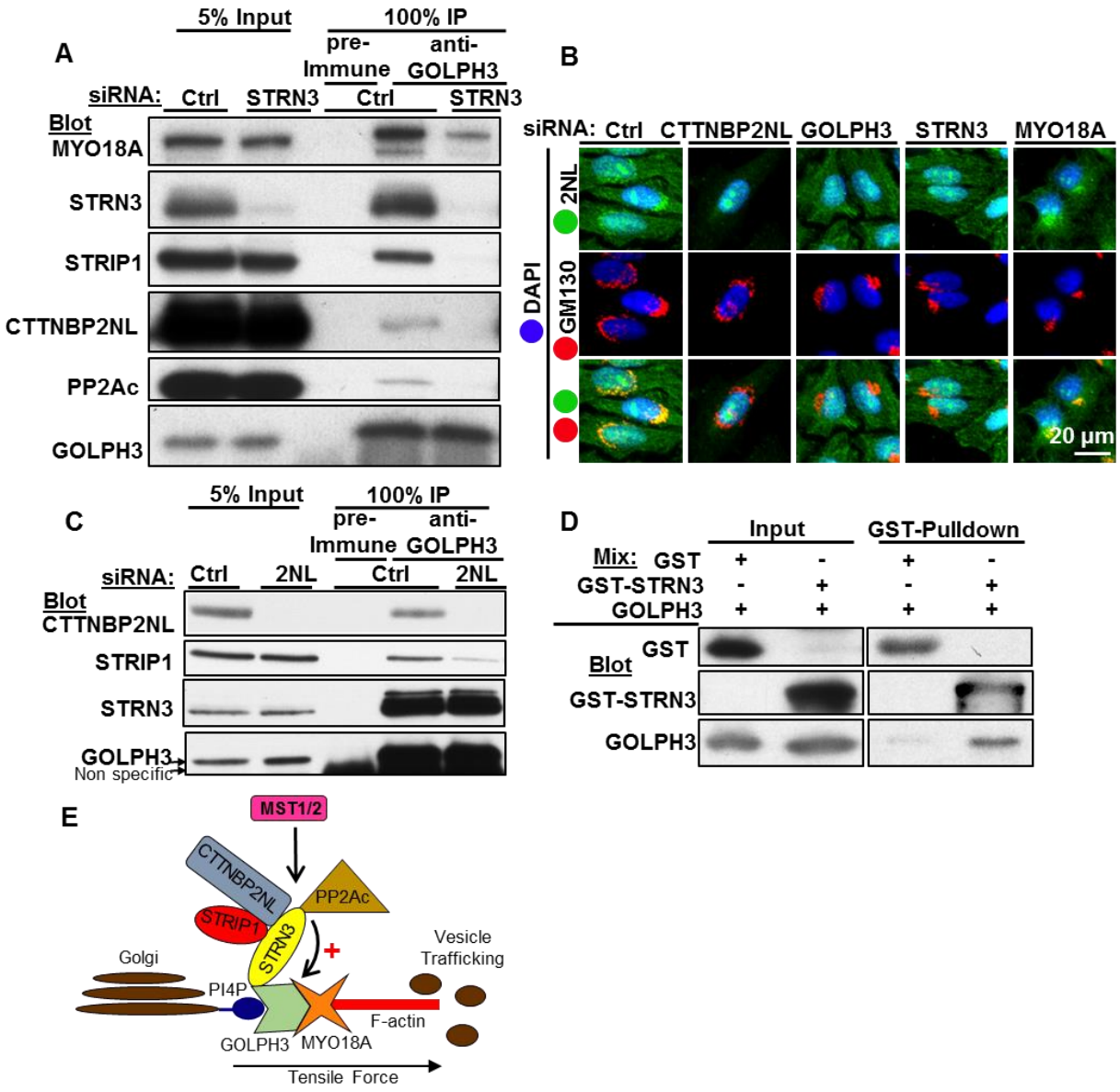
A
5% Input
100% IP
pre-Immune
anti-GOLPH3
siRNA: Ctrl STRN3 Ctrl STRN3
Blot
MYO18A
STRN3
STRIP1
CTTNBP2NL
PP2Ac
GOLPH3
B
siRNA: Ctrl CTTNBP2NL GOLPH3 STRN3 MYO18A
2NL
GM130
DAPI
20 μm
C
5% Input
100% IP
pre-Immune
anti-GOLPH3
siRNA: Ctrl 2NL Ctrl 2NL
Blot
CTTNBP2NL
STRIP1
STRN3
GOLPH3
Non specific
D
Input
GST-Pulldown
Mix: GST + - + -
GST-STRN3 - + - +
GOLPH3 + + + +
Blot
GST
GST-STRN3
GOLPH3
E
MST1/2
CTTNBP2NL
PP2Ac
STRIP1
STRN3
+
Golgi
PI4P
Vesicle Trafficking
F-actin
GOLPH3
MYO18A
Tensile Force

Figure 2.7: STRIPAK PP2Ac Acts on the GOLPH3 Complex in Sparse Cells to Enhance GOLPH3-MYO18A Interaction to Promote Secretion.
(A) HeLa cells plated at low density were treated with PP2A inhibitors Okadaic acid (OKA) or Calyculin A (CalA) or DMSO (vehicle control), followed by IF to the Golgi marker GM130 (red) and stained with DAPI to mark nuclei (blue). OKA and CalA cause Golgi compaction compared to the control. (B) Quantification of (A) shows significant compaction of the Golgi with OKA or CalA treatment. (C) Co-IP of endogenous MYO18A with endogenous GOLPH3 is enhanced by phosphatase treatment of the lysate. Effective phosphatase activity is detected by loss of AKT phosphorylation (on Ser473) in the input lysate. Dashed lines indicate omission of irrelevant intervening lanes. (D) WB detects significantly reduced PDGFA secretion into the media when LM2 cells are plated at high density despite similar expression of PDGFA. Re-blotting for GAPDH provides a loading control for the cell lysates, and demonstrates lack of contamination of the media with cells. (E) Quantification of (D) shows significantly reduced secretion of PDGFA from cells at high density. (F) Knockdown of GOLPH3 or STRN3 in LM2 cells does not affect cellular PDGFA expression, but significantly reduces the amount secreted into the media. Re-blotting for GAPDH provides a loading control for the cell lysates, and demonstrates lack of contamination of the media with cells. See also Figure S2.7 for parallel WB confirming knockdown of GOLPH3 and STRN3. (G) Quantification of (F) shows significant reduction of PDGFA secretion following siRNA knockdown of GOLPH3 or STRN3. Bar graphs show mean ± SEM for n cells (as indicated), in (B) pooled from three independent experiments. (E) and (G) are from n (as indicated) independent experiments. p-values calculated for (B) by t test, for (E) and (G) by one sample t test.

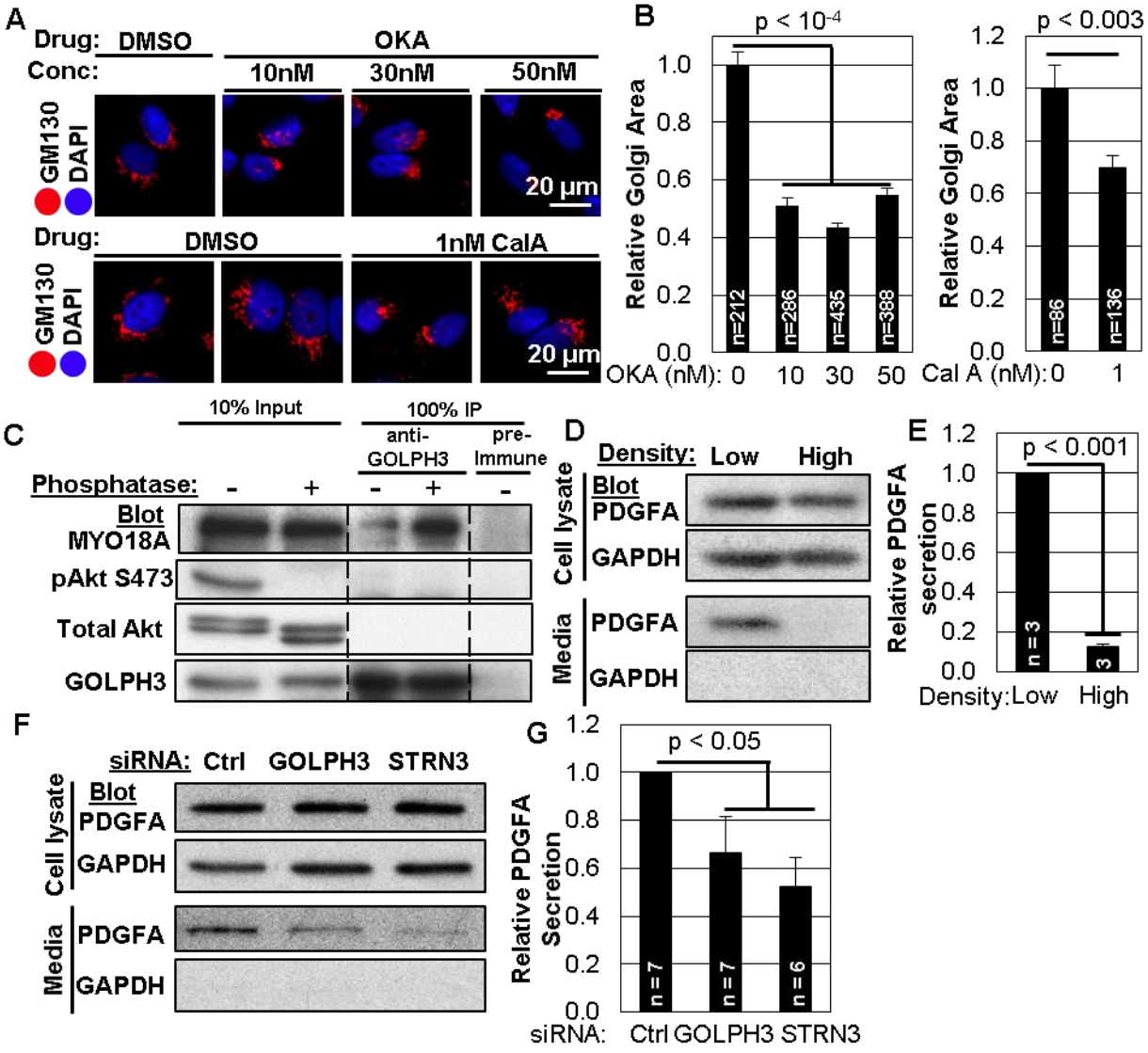
A
Drug: DMSO
OKA
Conc:
10nM
30nM
50nM
GM130
DAPI
20 µm
Drug:
DMSO
1nM CalA
GM130
DAPI
20 µm
B
p < 10-4
Relative Golgi Area
1.0
0.8
0.6
0.4
0.2
0.0
n=212
n=286
n=435
n=388
OKA (nM): 0 10 30 50
p < 0.003
Relative Golgi Area
1.2
1.0
0.8
0.6
0.4
0.2
0.0
n=86
n=136
Cal A (nM): 0 1
C
10% Input
100% IP
anti-GOLPH3
pre-Immune
Phosphatase: - + - + -
Blot
MYO18A
pAkt S473
Total Akt
GOLPH3
D
Density: Low High
Cell lysate
Blot
PDGFA
GAPDH
Media
PDGFA
GAPDH
E
p < 0.001
Relative PDGFA secretion
1.2
1.0
0.8
0.6
0.4
0.2
0.0
n = 3
3
Density: Low High
F
siRNA: Ctrl GOLPH3 STRN3
Cell lysate
Blot
PDGFA
GAPDH
Media
PDGFA
GAPDH
G
p < 0.05
Relative PDGFA Secretion
1.2
1.0
0.8
0.6
0.4
0.2
0.0
n = 7
n = 7
n = 6
siRNA: Ctrl GOLPH3 STRN3

Figure S2.1: Increasing Cell Density Inhibits the GOLPH3 Complex to Cause Golgi Compaction and Impaired Trafficking.
(A) MDA-MB-231 cells were plated at low, medium, or high cell density, followed by IF to the Golgi marker GM130 (red) to examine Golgi morphology, and stained with DAPI to mark nuclei (blue). DIC images provide an overview of cell density. The white box indicates the region shown in the lower images to observe Golgi morphology. (B) Quantification of (A) shows a decrease in Golgi area when MDA-MB-231 cells are plated at higher density. (C) High cell density causes Golgi compaction in NRK cells. See also Figures 2.1A-D for additional cell types. (D) Quantification of (C) shows a decrease in Golgi area when NRK cells are plated at higher density. (E) Protein levels of MYO18A, STRN3, GOLPH3, CTTNBP2NL, STRIP1, MST1, MST2, PP2Ac, and β-actin are not affected by cell density as detected by WB of lysates from equal numbers of cells, plated at low or high density. Dashed line indicates omission of irrelevant intervening lanes. (F) GOLPH3 remains tightly localized to the Golgi in HeLa cells plated at low or high density. IF to observe GOLPH3 (red) was performed in HeLa cells stably expressing ManII-GFP to mark the Golgi (green), and stained with DAPI to mark nuclei (blue). (G) IP of endogenous GOLPH3 from lysates of HEK293 cells plated at low density robustly co-IPs endogenous MYO18A and STRN3. However, when cells are plated at high density the interaction of MYO18A and STRN3 with GOLPH3 is impaired. See also Figure 1H for similar results in Hela cells. Bar graphs in (B) and (D) represent mean ± SEM n cells (as indicated), pooled from three independent experiments for each; p-values are calculated by t test.

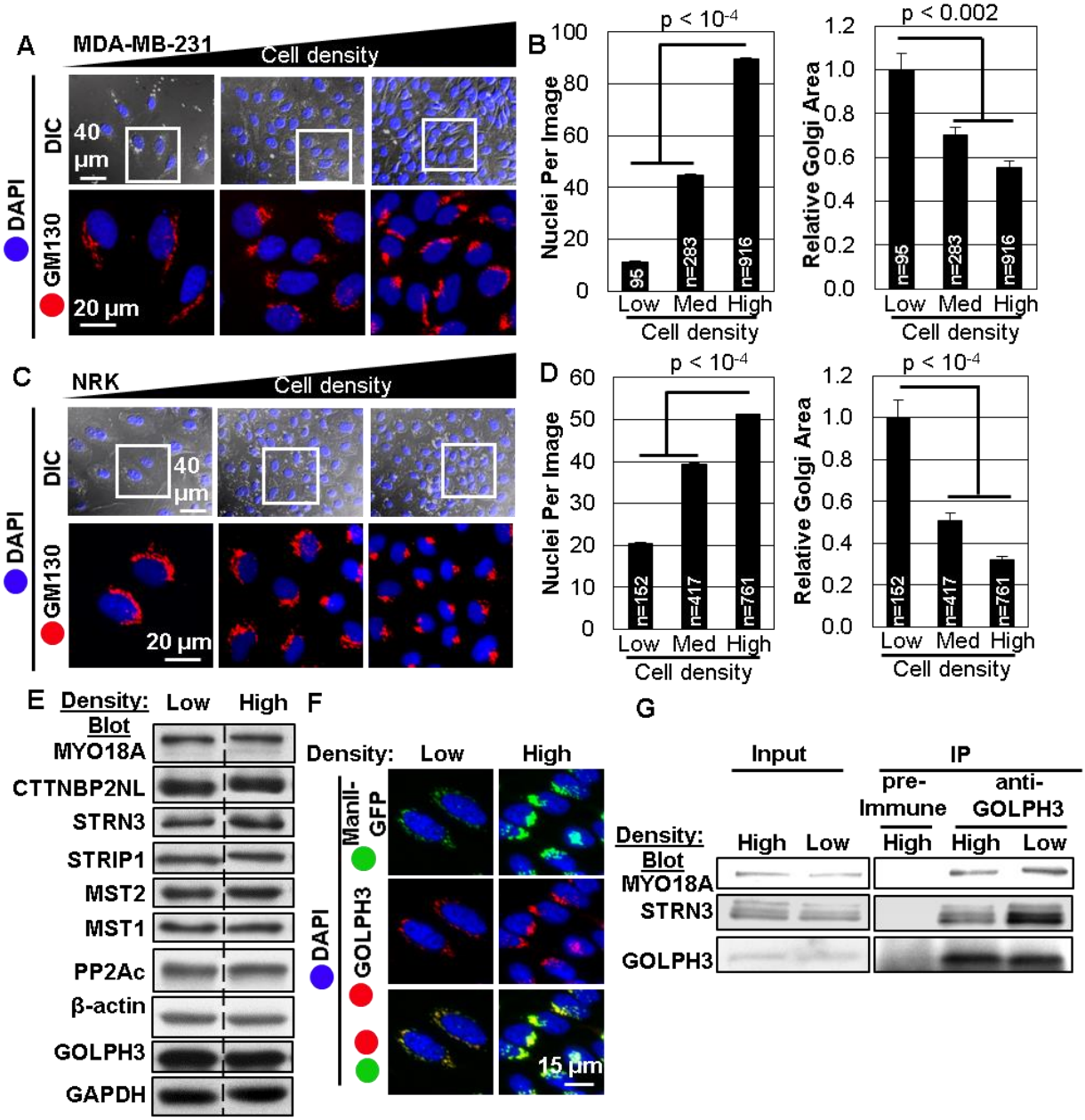
A
MDA-MB-231
Cell density
DIC
DAPI
GM130
40 µm
20 µm
B
p < 10-4
Nuclei Per Image
n=95
n=283
n=916
Low Med High
Cell density
p < 0.002
Relative Golgi Area
C
NRK
D
p < 10-4
n=152
n=417
n=761
E
Density: Low High
Blot
MYO18A
CTTNBP2NL
STRN3
STRIP1
MST2
MST1
PP2Ac
β-actin
GOLPH3
GAPDH
F
Density: Low High
ManII-GFP
GOLPH3
DAPI
15 µm
G
Input
IP
pre-Immune
anti-GOLPH3
Density:
Blot
High Low
High High Low
MYO18A
STRN3
GOLPH3

A

STRN3 mass spectrometry coverage

```
  1 MDELAGGGGG GPGMAAPPRQ QQGPGGNLGL SPGGNGAAGG GGPPASEGAG PAAGPELSRP
 61 QQYTIPGILH YIQHEWARFE MERAHWEVER AELQARIAFL QGERKGQENL KKDLVRRIKM
121 LEYALKQERA KYHKLKYGTE LNQGDLKMPT FESEETKDTE APTAPQNSQL TWKQGRQLLR
181 QYLQEVGYTD TILDVRSQRV RSLLGLSNSE PNGSVETKNL EQILNGGESP KQKGQEIKRS
241 SGDVLETFNF LENADDSDED EENDMIEGIP EGKDKHRMNK HKIGNEGLAA DLTDDPDTEE
301 ALKEFDFLVT AEDGEGAGEA RSSGDGTEWD KDDLSPTAEV WDVDQGLISK LKEQYKKERK
361 GKKGVKRANR TKLYDMIADL GDDELPHIPS GIINQSRSAS TRMTDHEGAR AEEAEPITFP
421 SGGGKSFIMG SDDVLLSVLG LGDLADLTVT NDADYSYDLP ANKDAFRKTW NPKYTLRSHF
481 DGVRALAFHP VEPVLVTASE DHTLKLWNLQ KTVPAKKSAS LDVEPIYTFR AHIGPVLSLA
541 ISSNGEQCFS GGIDATIQWW NMPSPSVDPY DTYEPNVLAG TLVGHTDAVW GLAYSGIKNQ
601 LLSCSADGTV RLWNPQEKLP CICTYNGDKK HGIPTSVDFI GCDPAHMVTS FNTGSAVIYD
661 LETSQSLVIL SSQVDSGLQS NNHINRVVSH PTLPVTITAH EDRHIKFFDN KTGKMIHSMV
721 AHLDAVTSLA VDPNGIYLMS GSHDCSIRLW NLDSKTCVQE ITAHRKKLDE SIYDVAFHSS
781 KAYIASAGAD ALAKVFV
```

B

CTTNBP2NL mass spectrometry coverage

```
  1 MNLEKLSKPE LLTLFSILEG ELEARDLVIE ALKAQHRDTF IEERYGKYNI SDPLMALQRD
 61 FETLKEKNDG EKQPVCTNPL SILKVVMKQC KNMQERMLSQ LAAAESRHRK VILDLEEERQ
121 RHAQDTAEGD DVTYMLEKER ERLTQQLEFE KSQVKKFEKE QKKLSSQLEE ERSRHKQLSS
181 MLVLECKKAT NKAAEEGQKA GELSLKLEKE KSRVSKLEEE LAAERKRGLQ TEAQVEKQLS
241 EFDIEREQLR AKLNREENRT KTLKEEMESL KKIVKDLEAS HQHSSPNEQL KKPVTVSKGT
301 ATEPLMLMSV FCQTESFPAE RTHGSNIAKM TNTGLPGPAT PAYSYAKTNG HCDPEIQTTR
361 ELTAGNNVEN QVPPREKSVA LAQEKPVENG GCPVGIETPV PMPSPLSSSG SSLSPSSTAS
421 SSLTSSPCSS PVLTKRLLGS SASSPGYQSS YQVGINQRFH AARHKFQSQA DQDQQASGLQ
481 SPPSRDLSPT LIDNSAAKQL ARNTVTQVLS RFTSQQGPIK PVSPNSSPFG TDYRNLANTA
541 NPRGDTSHSP TPGKVSSPLS PLSPGIKSPT IPRAERGNPP PIPPKKPGLT PSPSATTPLT
601 KTHSQAASLT TAEDLASSCS SNTVVANGKD VELLLPTSS
```

Figure S2.2: Mass Spectrometry of IP of GOLPH3 Detects STRN3 and CTTNBP2NL.

(A) Large-scale IP of GOLPH3 from HeLa cell lysate was separated on SDS-PAGE and compared to IP with pre-immune serum. A specific, prominent band observed at 100 kDa was trypsinized and analyzed by mass spectrometry. Multiple peptides corresponding to STRN3 were detected, highlighted in red and shown in the context of the full amino acid sequence of human STRN3 (NP_001077362.1). See also Figures 2.1H, 2.2A, 2.2F, 2.3E, 2.6A, and 2.6C for confirmatory IP/WB. (B) A second band from (A) was also analyzed by mass spectrometry. Multiple peptides corresponding to CTTNBP2NL were detected, highlighted in red and shown in the context of the full amino acid sequence of human CTTNBP2NL (NP_061174.1). See also Figures 2.6A and 2.6C for confirmatory IP/WB.

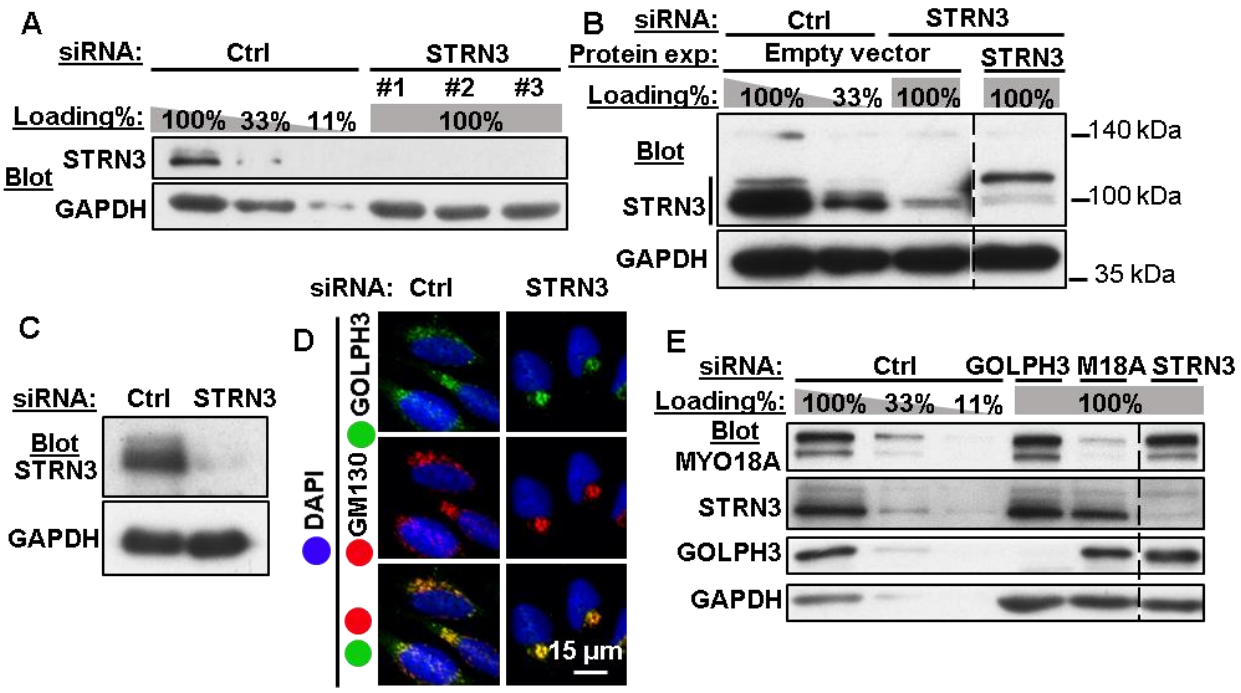

Figure S2.3: STRN3 Regulates Golgi Morphology and Trafficking.
(A) WB shows efficient knockdown of STRN3 by three different siRNAs in the experiment in Figure 2.2B. Blot for GAPDH provides a loading control. (B) WB validating the knockdown and rescue of expression of STRN3 for the experiment in Figure 2.2G. Blot for GAPDH provides a loading control. Dashed line indicates omission of irrelevant intervening lanes. (C) WB shows efficient knockdown of STRN3 in the experiment in Figure 2.3C. (D) Knockdown of STRN3 causes Golgi compaction, but GOLPH3 remains tightly localized to the Golgi. IF was performed to observe GOLPH3 (green) and the Golgi marker GM130 (red), together with staining by DAPI to mark nuclei (blue). (E) WB shows efficient knockdown of STRN3 for the experiment in Figure S2.3D. Knockdown of STRN3 does not affect GOLPH3 or MYO18A protein levels. Dashed line indicates omission of irrelevant intervening lanes.

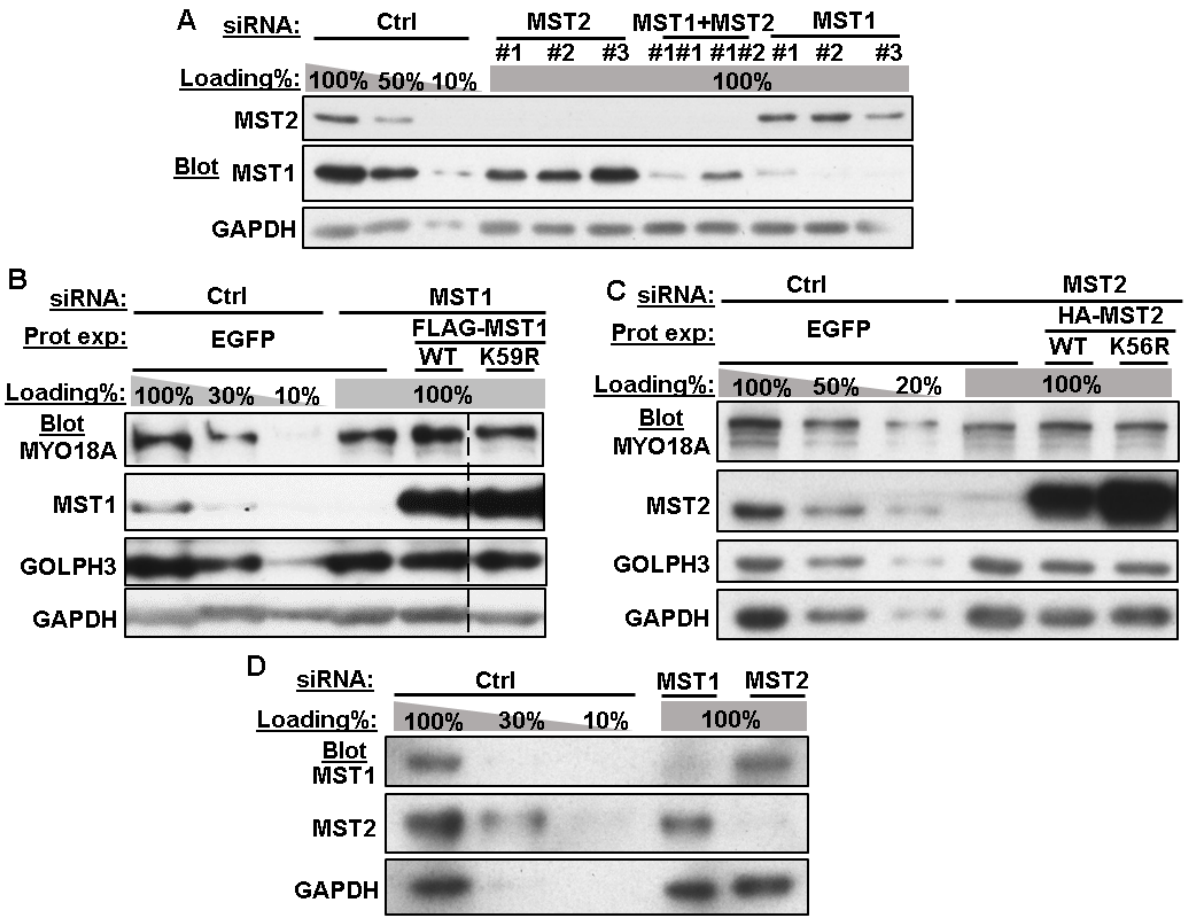

Figure S2.4: MST1 and MST2 Control Golgi Morphology and Trafficking.
(A) WB validating siRNA knockdown for the experiments in Figures 2.4A-B. HeLa cells were transfected with control siRNA, one of three independent siRNAs against MST1 or MST2, or combinations of them, as indicated. SDS lysates were analyzed by WB to detect MST1, MST2, and GAPDH (as a loading control). (B) WB validating siRNA knockdown and rescue of expression of MST1 for the experiments in Figures 2.4C-D. siRNA to MST1 significantly reduces MST1 expression. Transfection with an expression vector for siRNA-resistant FLAG-MST1, either WT or the kinase-dead K59R mutant, restores MST1 expression. GOLPH3 and MYO18A levels are unaffected by knockdown or rescue of MST1 expression. GAPDH serves as a loading control. Dashed line indicates omission of irrelevant intervening lanes. (C) WB validating siRNA knockdown and rescue of expression of MST2 for the experiments in Figures 2.4E-F. siRNA to MST2 significantly reduces MST2 expression. Transfection with an expression vector for siRNA-resistant HA-MST2, either WT or the kinase-dead K56R mutant, restores MST2 expression. GOLPH3 and MYO18A levels are unaffected by knockdown or rescue of MST2 expression. GAPDH serves as a loading control. (D) WB validating siRNA knockdown of MST1 or MST2 for the experiments in Figures 2.4G-H. GAPDH serves as a loading control.

Figure S2.5: MST1 and MST2 Act on the Golgi Independently of LATS1/2, Through GOLPH3, MYO18A, and STRN3.
(A) WB validating knockout of both LATS1 and LATS2 for the experiments in Figures S2.5B-C. SDS lysates were analyzed by WB for LATS1 and LATS2. GAPDH provides a loading control. (B) IF demonstrates an extended Golgi in cells at low density and a compact Golgi in cells at high density, in both WT and LATS1/2 double-knockout (DKO) cells. Images show IF to the Golgi marker GM130 (red), together with DAPI staining to mark the nucleus (blue). (C) Quantification of (B) shows similar compaction of the Golgi in response to high cell density for control and LATS1/2 DKO cells. See also Figure 2.5 for additional evidence that MST1/2 act on the Golgi independently of canonical Hippo signaling. (D) WB validating overexpression of FLAG-MST1-K59R or HA-MST2-K56R, together with siRNA knockdown of GOLPH3, MYO18A, or STRN3 for experiments in Figures 2.5C-D. GAPDH provides a loading control. (E) WB validating siRNA knockdown of MST1 or MST2 for the experiments in Figures 2.5E-F. GAPDH serves as a loading control. Dashed line indicates omission of irrelevant intervening lanes. Bar graphs in (C) show mean ± SEM n cells (as indicated), pooled from three independent experiments; p-values are calculated by t test.

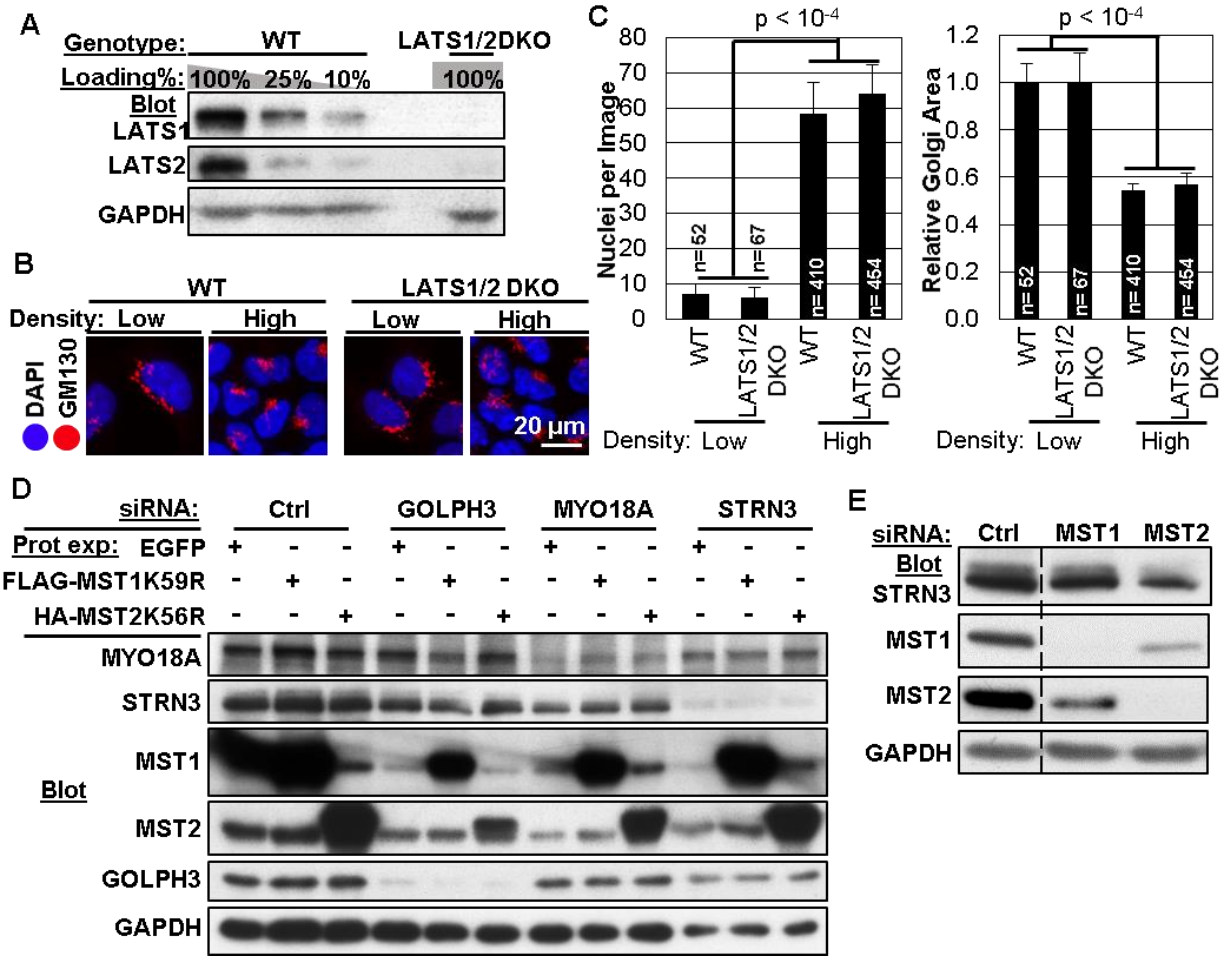
A
Genotype: WT LATS1/2DKO
Loading%: 100% 25% 10% 100%
Blot
LATS1
LATS2
GAPDH
B
WT
LATS1/2 DKO
Density: Low High Low High
DAPI
GM130
20 µm
C
p < 10-4
Nuclei per Image
n=52
n=67
n= 410
n= 454
WT
LATS1/2 DKO
Density: Low High
p < 10-4
Relative Golgi Area
D
siRNA: Ctrl GOLPH3 MYO18A STRN3
Prot exp: EGFP
FLAG-MST1K59R
HA-MST2K56R
Blot
MYO18A
STRN3
MST1
MST2
GOLPH3
GAPDH
E
siRNA: Ctrl MST1 MST2
Blot
STRN3
MST1
MST2
GAPDH

Figure S2.6: The STRIPAK Complex Localizes to the Golgi via STRN3 and GOLPH3.

(A) Unlike CTTNBP2NL, STRIP1, and PP2Ac (Figure 2.6A), CTTNBP2 and SLMAP do not co-IP with GOLPH3, demonstrating that only one of the mutually exclusive STRIPAK complexes (Goudreault et al., 2009) associates with GOLPH3. IP of endogenous GOLPH3 was analyzed by WB to detect endogenous MYO18A, CTTNBP2, and SLMAP. As expected, MYO18A robustly co-IPs with GOLPH3. However, CTTNBP2 and SLMAP do not. (B) WB validates knockdown of CTTNBP2NL by three independent siRNAs for the experiment in Figure S2.6C. GAPDH provides a loading control. (C) siRNA validation of IF detection of CTTNBP2NL (2NL) at the Golgi. Images show IF to CTTNBP2NL (green) and the Golgi marker GM130 (red), together with DAPI to stain the nucleus (blue). In control cells, CTTNBP2NL IF is observed partially at the Golgi (overlapping GM130), and the Golgi IF signal is lost upon knockdown of CTTNBP2NL with each of three independent siRNAs. (D) WB validation of siRNA knockdown of GOLPH3, MYO18A, STRN3, and CTTNBP2NL for the experiment in Figure 2.6B. (E) IP of endogenous STRN3 co-IPs endogenous CTTNBP2NL, STRIP1, and PP2Ac, unaffected by changing cell density.

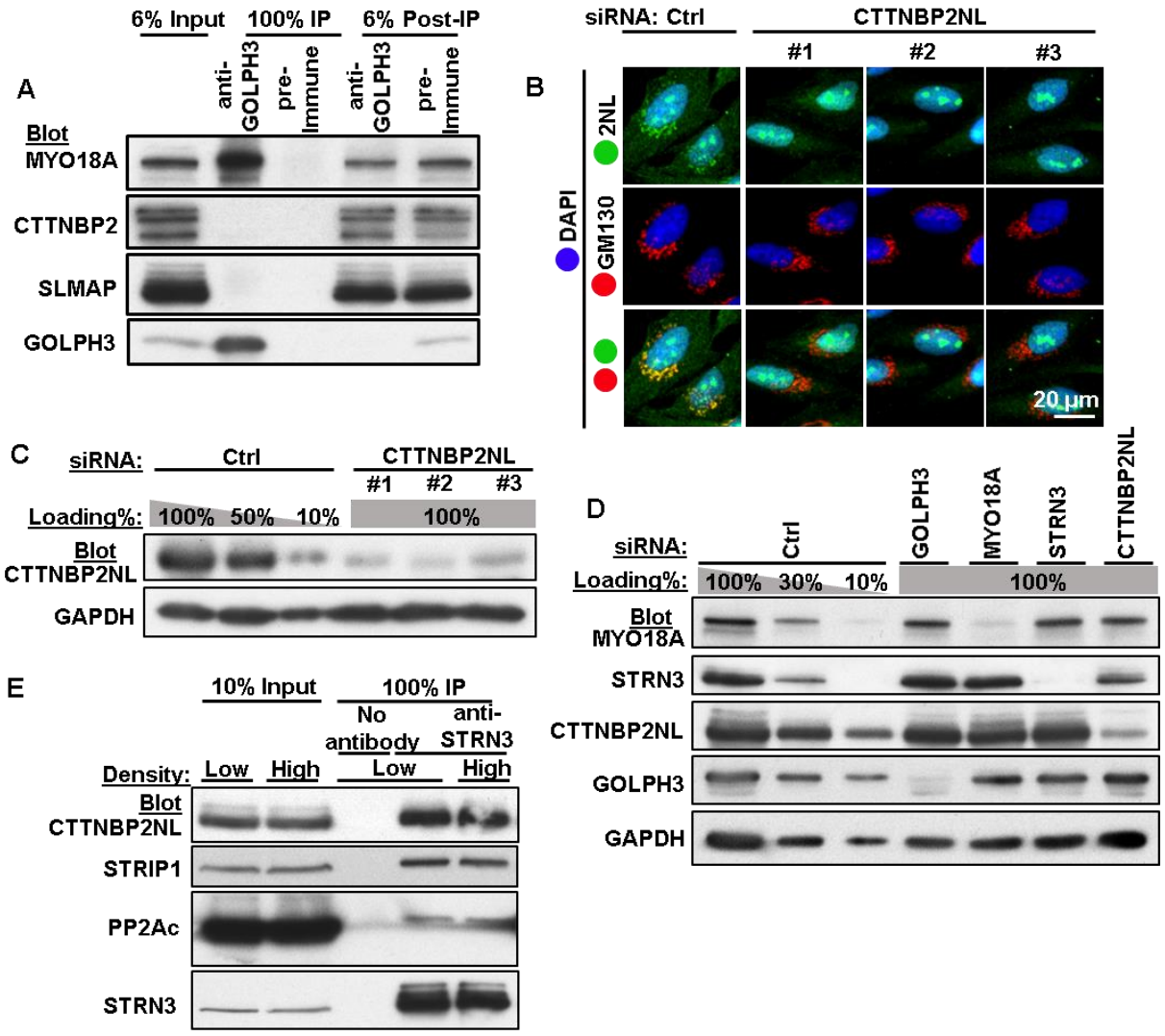
A
6% Input
100% IP
6% Post-IP
anti-GOLPH3
pre-Immune
anti-GOLPH3
pre-Immune
Blot
MYO18A
CTTNBP2
SLMAP
GOLPH3
B
siRNA: Ctrl
CTTNBP2NL
#1
#2
#3
2NL
GM130
DAPI
20 μm
C
siRNA:
Ctrl
CTTNBP2NL
#1
#2
#3
Loading%:
100%
50%
10%
100%
Blot
CTTNBP2NL
GAPDH
D
siRNA:
Ctrl
GOLPH3
MYO18A
STRN3
CTTNBP2NL
Loading%:
100%
30%
10%
100%
Blot
MYO18A
STRN3
CTTNBP2NL
GOLPH3
GAPDH
E
10% Input
100% IP
No antibody
anti-STRN3
Density:
Low
High
Low
High
Blot
CTTNBP2NL
STRIP1
PP2Ac
STRN3

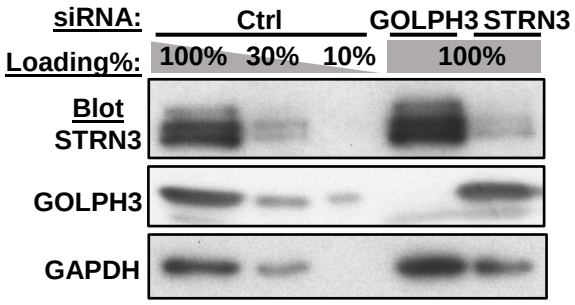

Figure S2.7: Cell Density-Regulated Secretion of PDGFA Depends on GOLPH3 and STRN3.
WB validation of the siRNA knockdown of GOLPH3 and STRN3 for the experiment in Figure 2.7F. GAPDH provides a loading control.

CHAPTER 3: THE MODEL, DISCUSSION, AND FUTURE EXPERIMENTS

THE MODEL

The Golgi plays a critical role in protein transport and secretion, and most cytokines and growth factors depend on the Golgi for secretion out of the cells, but very little is known about regulation of Golgi trafficking. There is scattered evidence showing inhibition of COPI and COPII vesicles or mutating some of Golgi enzymes which can eventually lead to inhibition of secretion due to lack of cargo formation, but very little is known about mechanisms that could affect Golgi trafficking in response to extracellular signals.

Here we report that in low cell density, the MST1 and MST2 protein kinases, independent of their kinase activity, trigger STRIPAK complex localization to the Golgi. The STRIPAK complex docks at the Golgi through direct interaction between GOLPH3 and STRN3. There, dephosphorylation by PP2A of the STRIPAK/GOLPH3-MYO18A complex leads to enhanced interaction between GOLPH3 and MYO18A. GOLPH3 interaction with MYO18A creates a pulling force applied onto Golgi membrane, which aids vesicle budding for forward trafficking. A consequence of that pulling force is that the Golgi ribbon is stretched around the nucleus. On the other hand, high cell density decouples the effect of MST1/2 on the STRIPAK complex, making STRIPAK delocalize from the Golgi, which leads to weakening of GOLPH3-MYO18A interaction. This results in inhibition of forward trafficking, and a compact Golgi (Figure 3.1).

DISCUSSION

Although cell density signaling to the Golgi also relies on the ability of MST1/2 to transduce cell density signals, available data show that MST1/2 regulate the Golgi independent from the canonical Hippo pathway. There are discrepancies in our

observation of Hippo MST1/2 involvement in Golgi trafficking versus the canonical Hippo pathway. First, our model shows MST1/2 function in sparse cells, whereas in the canonical Hippo pathway, MST1/2 function at high cell density. Second, our data show that MST1/2 function independent of their kinase activity, while with the Hippo pathway, MST1/2 need to be kinase activated to activate downstream effectors. Third, MST1/2 have been shown to be redundant to each other and to other kinases in activating downstream effectors LATS1/2 in mammals (Meng et al., 2015), while in our model, MST1/2 are both required for Golgi function. Fourth, disabling downstream effectors of the canonical Hippo pathways such as LATS1/2 does not affect regulation of the Golgi. Therefore, our data report a novel function for the Hippo protein MST1/2.

There is evidence showing the STRIPAK complex regulates kinase activity of MST1/2 in the Hippo pathway (Bae et al., 2017; Couzens et al., 2013; Hauri et al., 2013; Ribeiro et al., 2010; Zheng et al., 2017). Besides, our model (Figure 3.1) proposes that MST1/2, independent of their kinase activity, localize the STRIPAK complex to the Golgi in sparse cells. The question is, whether MST1/2-STRIPAK interaction in canonical Hippo pathway is similar to MST1/2-STRIPAK interaction in cell density signaling at the Golgi. Recent findings by two groups (Bae et al., 2017; Zheng et al., 2017) showed MST1/2 kinase activity being inhibited by PP2A. They showed that the protein SLMAP of the STRIPAK complex links STRIPAK, and thus PP2A to MST1/2 through direct binding of SLMAP to the phosphorylated linker region of MST1/2. In our proteomic screen for GOLPH3 interacting partners as well as in our co-IPs, we did not detect SLMAP but CTTNBP2NL. CTTNBP2NL has been shown to form a complex with STRIPAK in a mutually exclusive manner from SLMAP (Couzens et al., 2013; Kean et al., 2011).

Therefore, STRIPAK complex may interact differently with MST1/2 in the context of the canonical Hippo pathway versus Golgi signaling. In addition, (Bae et al., 2017; Zheng et al., 2017) showed that in mammalian cells SLMAP does not bind to kinase-dead MST2. This finding is in line with our data, since we found that MST1/2 act on the Golgi independent of their kinase activity. Therefore, our signaling pathway involving MST1/2, STRIPAK, and GOLPH3 complex are independent from the canonical Hippo pathway.

The Hippo pathway has been shown to exert both autonomous and non-cell autonomous effects on cell proliferation. The non-cell autonomous effect of the Hippo pathway causes reduction in growth factor secretion. This effect was often attributed to the probable reduction in transcription level due to inhibition of YAP (Del Re et al., 2010; Sarikaya and Extavour, 2015; Zhang et al., 2009). However, our data reveal the level of growth factors such as PDGFA is unchanged in cells, but reduced secretion into media. Here, we report a novel mechanism for non-cell autonomous effect of the Hippo pathway, in which Hippo MST1/2 regulate Golgi secretion, thus regulate growth factors secretion into media.

Figuring out upstream effectors that send cell density signal to MST1/2 is a topic being studied by many different labs that study the Hippo pathway. Some research groups have published data on upstream signaling to MST1/2. The neurofibromatosis type 2 (NF2) gene encodes for protein Merlin. Examination of NIH3T3, Rat1 fibroblasts, normal rat kidney (NRK), and human osteosarcoma (MG63 and U20S) cells showed that high cell density or serum starvation leads to an increase in Merlin protein level. In low cell density or addition of serum, Merlin level is reduced. Especially, the faster running, unphosphorylated form of the Merlin doublet reduced even further (Morrison et al., 2001;

Shaw et al., 1998). In primary normal rat Schwann cells, cells at high cell density express more Merlin than cells at low density. In the transformed Schwannoma cells, which do not cease division at high density but continue to form foci, Merlin levels do not increase. Inducible expression of wild type Merlin but not an inactive Merlin mutant reduce Schwannoma foci formation (cell growth) in soft agar and tumor volume when nude mice are injected with those cells (Morrison et al., 2001).

On the cell surface, the polymorphic glycoprotein CD44 is a receptor for hyaluronic acid (HA), an important component of the extracellular matrix (Aruffo et al., 1990; Lesley et al., 2000; Sherman et al., 1995). (Morrison et al., 2001) showed that only the hypophosphorylated form of Merlin (high cell density merlin form) could bind to CD44 but not the related Ezrin, Radixin, and Moesin (ERM) family of membrane/cytoskeletal linker proteins. When only the cytoplasmic tail of CD44 is expressed to neutralize Merlin, the growth inhibition effect is blocked. On the other hand, phosphorylated Merlin and the ERM family protein bind to CD44 in low density cells. To confirm that cell density signals through extracellular matrix HA binding to CD44 receptor then signaling to Merlin, (Morrison et al., 2001) grew cells in the presence of soluble extracellular domain of CD44 (apparently depleted HA binding to cell surface, full length CD44) and saw that Merlin overexpression could no longer inhibit cell growth. On the other hand, if the soluble extracellular domain of CD44 carrying mutations that render it unable to bind glycosaminoglycan, Merlin overexpression stills inhibited cell growth. Treating murine NIH3T3, canine MDCK, and rat kangaroo Ptk2 cells with HA caused Merlin dephosphorylation and inhibited cell proliferation. Overexpression of Merlin in human melanoma cells that metastasized to the lymph node (MeWo) cells led to increased

phosphorylation of MST1/2 and further pre-disposed MST1/2 to phosphorylation by stress stimuli such as H_2O_2 treatment (Murray et al., 2012)

Clearly, these studies provide a compelling example of a pathway that responsed to cell density, through HA, CD44, and Merlin and transduces signal to MST1/2. It presents an example of annotated signal transduction upstream of the Hippo pathway, involving substrates, receptors, and effectors. Of course, many more signaling pathways upstream of MST1/2 are believed to exist and remained to be elucidated.

Although our model highlights different steps of the signaling pathway, there are still details to fill in the picture.

FUTURE EXPERIMENTS

How do MST1 and MST2 work together to affect the Golgi?

Our data show MST1/2 function independent of their kinase activity. They together promote Golgi trafficking in sparse cells. Unlike in the canonical Hippo pathway, MST1/2 are not functionally redundant. Our data showed that MST1/2 are both required for extended Golgi and Golgi trafficking. There have been reports that MST1/2 form homodimer through the SARAH domain (Jin et al., 2012; Ni et al., 2013), however, heterodimer formation between MST1/2, although very likely, has not been reported. MST1/2 forming heterodimer to function at the Golgi is a likely explanation for why they are both required for Golgi function. The ability of MST1/2 to form heterodimer could be tested *in vitro* by mixing purified, differently labeled kinase-dead MST1/2 together to see if heterodimers form. The reason kinase-dead versions of MST1/2 need to be used is because our model points away from relevance of kinase activity; however, WT versions of MST1/2 can also be used. SARAH domain-truncated mutant of MST1 could be mixed

with full length MST2 and vice versa to test the role of SARAH domain in heterodimer formation. *In vivo* experiments such as fluorescence resonance energy transfer (FRET) (Sekar and Periasamy, 2003) could be done with kinase-dead MST1/2 to determine their ability to form heterodimer.

How do MST1/2 promote STRIPAK localization to the Golgi?

Detailed mechanisms of how kinase-dead MST1/2 interact with STRIPAK in sparse cells and how that interaction promote STRIPAK localization to the Golgi remain to be elucidated. In that context, MST1/2 could either act as scaffold or they themselves regulate other kinases/phosphatases upstream of STRIPAK. To figure out this interaction network, conventional IP-MS or BioID (Roux et al., 2012, 2013) could be done in sparse cells using each protein kinase-dead MST1/2 or STRIPAK as baits. It must be noted that IP-MS and BioID have been done with MST1/2 before, but not with kinase dead MST1/2 specifically in sparse cells. Analysis of acquired data should give some hints on possible proteins that link MST1/2 to STRIPAK. Hits found on IP-MS or BioID with kinase-dead MST1/2 as baits could also give hints for upstream signaling that transduces cell density signal to MST1/2.

What are regulatory phosphorylation events that affect GOLPH3-MYO18A interaction?

Our data showed that when the GOLPH3-MYO18A/STRIPAK complex is dephosphorylated, the interaction between GOLPH3 and MYO18A is enhanced. It would be interesting to identify such regulatory phosphorylation sites on GOLPH3, MYO18A, and STRN3. To identify those sites, stable isotope labeling by amino acids in cell culture (SILAC) (Ong et al., 2002) accompanied by phosphopeptide isolation could be done on

GOLPH3, MYO18A, or STRN3 in sparse versus confluent cells. Alternatively, such SILAC experiments could be done in cells with PP2A inhibition versus controls. Either PP2A inhibitor used in our experiments, OKA or Cal A, could be used to treat the cells. Because our model predicts that the absence of STRN3 falls to direct PP2A to the Golgi, and our data showed reduction of GOLPH3 interaction with MYO18A upon STRN3 knockdown, another possibility is to use SILAC experiments to look at differences in GOLPH3 or MYO18A phosphorylation in STRN3 knockdown cells versus controls, which could reveal regulatory phosphorylation sites on both proteins. Upon identification of phosphorylation sites, phosphomimetic and unphosphorylatable mutants can be made, and tested their ability to rescue Golgi function in respective knockdowns.

How does STRN3 interact with GOLPH3?

Since our data show a direct interaction between GOLPH3 and STRN3, it would be interesting to define structurally how STRN3 binds to GOLPH3. To find out binding sites on STRN3, in vitro pull-down could be done with purified truncations of STRN3 mixing with full-length GOLPH3. Truncations of STRN3 could be made by truncating each domain of STRN3, the CaV, CaM, C-C, and six WD repeats (STRN3 domains are depicted in Figure 1.5). If the binding site to GOLPH3 falls in one of the domains, alanine scanning of that domain could reveal the binding sequence. If the binding site to GOLPH3 does not fall in any domains, alanine scans could be done on linker regions between each domain to find binding sequence. To define the binding site on GOLPH3, since GOLPH3 is a globular protein with relatively short sequence of 298 amino acids, alanine scanning can be performed on each segment of GOLPH3 sequence, from N-terminal to C-terminal. Once binding sites on GOLPH3 and STRN3 are identified, mutations can be made and

expressed in cells with knockdown of GOLPH3 or STRN3 respectively to see if they could rescue Golgi phenotypes.

CONCLUDING REMARKS

Our study reports a regulatory pathway that transduces cell density signals through MST1/2, STRIPAK, to GOLPH3 complex to regulate Golgi trafficking. This result provides further evidences that the GOLPH3 pathway is a hub for signals that regulate the Golgi. In normal condition, the GOLPH3 complex receives cell density signals to regulate forward trafficking. GOLPH3 complex contributes to Golgi reorientation toward the leading edge to direct forward trafficking (Xing et al., 2016). In the context of DNA damage, GOLPH3 was phosphorylated at T143 and T148. GOLPH3-MYO18A interaction leads to Golgi dispersal throughout cytoplasm, which gives the cells a survival advantage after the catastrophe event (Farber-Katz et al., 2014). PITPNC1, a member of PI transfer protein family, whose gene is amplified in a large fraction of cancer, is capable of binding to PI4P and drives vesicular secretion of pro-invasive and pro-angiogenic factors. PITPNC1's effect is dependent on GOLPH3 at the Golgi (Halberg et al., 2016). GOLPH3L, a paralog of GOLPH3, only expressed in high secretory cells, could antagonize the action of GOLPH3, probably to keep the GOLPH3 complex and Golgi secretion in check (Ng et al., 2013). In this current report, we show regulation of growth factor secretion at the Golgi dependent on GOLPH3 complex as a mechanism for non-cell autonomous effects of Hippo. Hence, the GOLPH3 complex is important in regulation of Golgi function in response to different cellular signals.

GOLPH3 and MYO18A have both been identified as oncogenic cancer drivers for many types of cancer (Buschman and Field, 2017; Buschman et al., 2015a; Kuna and

Field, 2018; Makowski et al., 2017; Scott et al., 2009; Xing et al., 2016). PITPNC1 is an oncogenic cancer driver found to act via GOLPH3 (Halberg et al., 2016). Since its discovery, the STRIPAK complex has fascinated researchers with its diverse structures and functions. STRIPAK in its full form carries both phosphatases and kinases, but could also exist in partial STRIPAK complex, without full complement of members, but carries specialized functions (Hwang and Pallas, 2014; Shi et al., 2016). STRIPAK function in cancer. STRN3 has been implicated in cancer (Kelly et al., 2014). The dysregulation of many STRIPAK members, such as CCM3, is linked to cerebral cavernous malformation (Cavalcanti et al., 2012); CTTNBP2 is related to autism (Cheung et al., 2001). STRN3 has been shown to be the regulator subunit of the PP2A holoenzyme. PP2A inactivation is observed in many tumors (Seshacharyulu et al., 2013).

Trafficking from the Golgi is essential to life, and thus its regulation in homeostasis. My study will contribute to our understanding of how Golgi trafficking is regulated in response to extracellular factors, cell density in particular. Therefore, my study will not only contribute to the knowledge of Golgi trafficking regulation, but also insights on different pathophysiology.

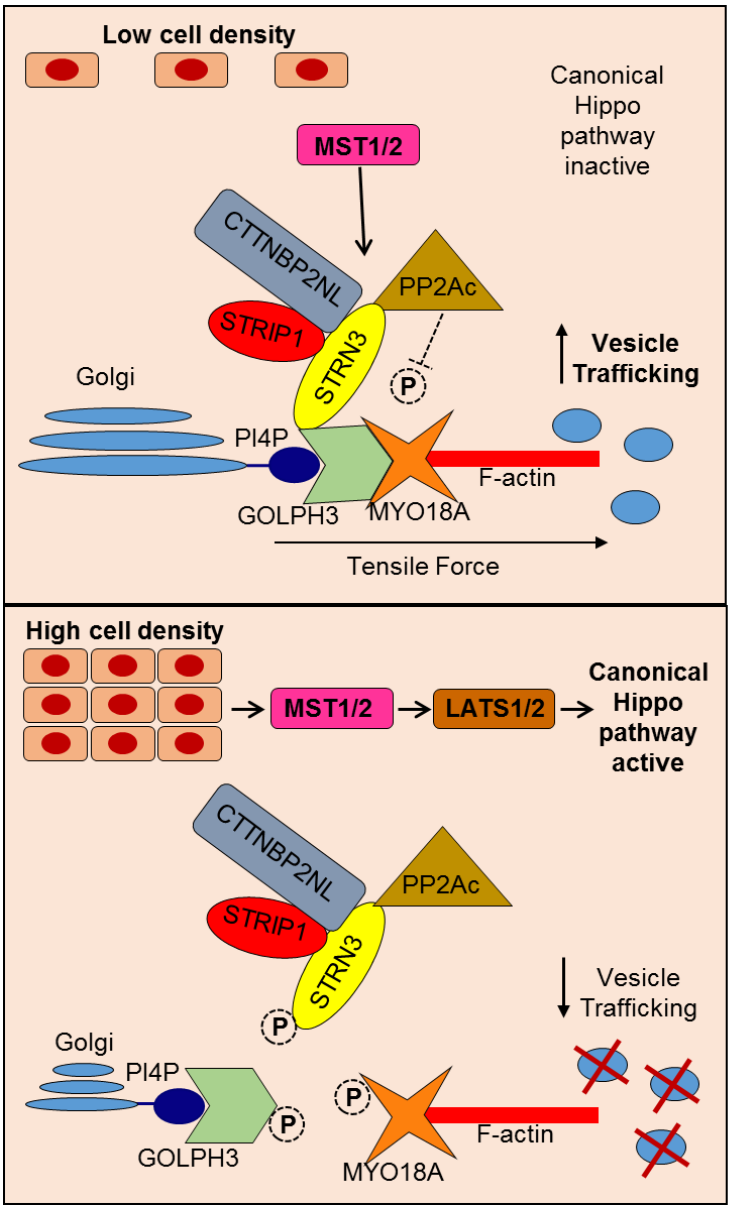

Figure 3.1: The Model of Cell Density Regulation of Golgi Morphology and Forward Trafficking.
In low cell density MST1 and MST2 act non-redundantly and independent of their kinase activity to promote STRN3 interaction with GOLPH3 at the Golgi. STRN3 brings along other STRIPAK components, including STRIP1, CTTNBP2NL, and PP2A. The phosphatase activity of PP2A serves to enhance the interaction of MYO18A with GOLPH3, increasing the tensile force that promotes vesicle budding for forward trafficking and stretching the Golgi into an extended ribbon. At high cell density, MST1/2 protein kinases activate the canonical Hippo pathway. MST1/2 no longer promote STRN3/STRIPAK interaction with GOLPH3, eliminating PP2A phosphatase activity from the complex, and thus impairing the interaction of MYO18A with GOLPH3. This results in compaction of the Golgi, and arrest of trafficking to the PM

CHAPTER 4: REFERENCES

Appenzeller-Herzog, C., and Hauri, H.-P. (2006). The ER-Golgi intermediate compartment (ERGIC): in search of its identity and function. Journal of Cell Science *119*, 2173–2183.

Aruffo, A., Stamenkovic, I., Melnick, M., Underhill, C.B., and Seed, B. (1990). CD44 is the principal cell surface receptor for hyaluronate. Cell *61*, 1303–1313.

Avruch, J., Zhou, D., Fitamant, J., Bardeesy, N., Mou, F., and Barrufet, L.R. (2012). Protein kinases of the Hippo pathway: regulation and substrates. Semin. Cell Dev. Biol. *23*, 770–784.

Bae, S.J., Ni, L., Osinski, A., Tomchick, D.R., Brautigam, C.A., and Luo, X. (2017). SAV1 promotes Hippo kinase activation through antagonizing the PP2A phosphatase STRIPAK. ELife Sciences *6*, e30278.

Baillat, G., Moqrich, A., Castets, F., Baude, A., Bailly, Y., Benmerah, A., and Monneron, A. (2001). Molecular cloning and characterization of phocein, a protein found from the Golgi complex to dendritic spines. Mol. Biol. Cell *12*, 663–673.

Bajaj Pahuja, K., Wang, J., Blagoveshchenskaya, A., Lim, L., Madhusudhan, M.S., Mayinger, P., and Schekman, R. (2015). Phosphoregulatory protein 14-3-3 facilitates SAC1 transport from the endoplasmic reticulum. Proc Natl Acad Sci U S A *112*, E3199–E3206.

Balla, A., Tuymetova, G., Barshishat, M., Geiszt, M., and Balla, T. (2002). Characterization of type II phosphatidylinositol 4-kinase isoforms reveals association of the enzymes with endosomal vesicular compartments. J. Biol. Chem. *277*, 20041–20050.

Barylko, B., Gerber, S.H., Binns, D.D., Grichine, N., Khvotchev, M., Südhof, T.C., and Albanesi, J.P. (2001). A Novel Family of Phosphatidylinositol 4-Kinases Conserved from Yeast to Humans. J. Biol. Chem. *276*, 7705–7708.

Bell, A.W., Ward, M.A., Blackstock, W.P., Freeman, H.N., Choudhary, J.S., Lewis, A.P., Chotai, D., Fazel, A., Gushue, J.N., Paiement, J., et al. (2001). Proteomics characterization of abundant Golgi membrane proteins. J. Biol. Chem. *276*, 5152–5165.

Bialojan, C., and Takai, A. (1988). Inhibitory effect of a marine-sponge toxin, okadaic acid, on protein phosphatases. Specificity and kinetics. Biochem. J. *256*, 283–290.

Billington, N., Beach, J.R., Heissler, S.M., Remmert, K., Guzik-Lendrum, S., Nagy, A., Takagi, Y., Shao, L., Li, D., Yang, Y., et al. (2015). Myosin 18A coassembles with nonmuscle myosin 2 to form mixed bipolar filaments. Curr. Biol. *25*, 942–948.

Bishé, B., Syed, G.H., Field, S.J., and Siddiqui, A. (2012). Role of phosphatidylinositol 4-phosphate (PI4P) and its binding protein GOLPH3 in hepatitis C virus secretion. J. Biol. Chem. *287*, 27637–27647.

Blagoveshchenskaya, A., Cheong, F.Y., Rohde, H.M., Glover, G., Knödler, A., Nicolson, T., Boehmelt, G., and Mayinger, P. (2008). Integration of Golgi trafficking and growth factor signaling by the lipid phosphatase SAC1. J Cell Biol *180*, 803–812.

Boggiano, J.C., Vanderzalm, P.J., and Fehon, R.G. (2011). Tao-1 Phosphorylates Hippo/MST Kinases to Regulate the Hippo-Salvador-Warts Tumor Suppressor Pathway. Developmental Cell *21*, 888–895.

Buschman, M.D., and Field, S.J. (2017). MYO18A: An unusual myosin. Advances in Biological Regulation.

Buschman, M.D., Rahajeng, J., and Field, S.J. (2015a). GOLPH3 links the Golgi, DNA damage, and cancer. Cancer Res. *75*, 624–627.

Buschman, M.D., Xing, M., and Field, S.J. (2015b). The GOLPH3 pathway regulates Golgi shape and function and is activated by DNA damage. Front. Neurosci. *9*, 362.

Carpenter, A.E., Jones, T.R., Lamprecht, M.R., Clarke, C., Kang, I.H., Friman, O., Guertin, D.A., Chang, J.H., Lindquist, R.A., Moffat, J., et al. (2006). CellProfiler: image analysis software for identifying and quantifying cell phenotypes. Genome Biology *7*, R100.

Cavalcanti, D.D., Kalani, M.Y.S., Martirosyan, N.L., Eales, J., Spetzler, R.F., and Preul, M.C. (2012). Cerebral cavernous malformations: from genes to proteins to disease. J. Neurosurg. *116*, 122–132.

Cerami, E., Gao, J., Dogrusoz, U., Gross, B.E., Sumer, S.O., Aksoy, B.A., Jacobsen, A., Byrne, C.J., Heuer, M.L., Larsson, E., et al. (2012). The cBio Cancer Genomics Portal: An Open Platform for Exploring Multidimensional Cancer Genomics Data. Cancer Discovery *2*, 401–404.

Chan, E.H.Y., Nousiainen, M., Chalamalasetty, R.B., Schäfer, A., Nigg, E.A., and Silljé, H.H.W. (2005). The Ste20-like kinase Mst2 activates the human large tumor suppressor kinase Lats1. Oncogene *24*, 2076–2086.

Cheung, J., Petek, E., Nakabayashi, K., Tsui, L.C., Vincent, J.B., and Scherer, S.W. (2001). Identification of the human cortactin-binding protein-2 gene from the autism candidate region at 7q31. Genomics *78*, 7–11.

Cohen, P., Klumpp, S., and Schelling, D.L. (1989). An improved procedure for identifying and quantitating protein phosphatases in mammalian tissues. FEBS Lett. *250*, 596–600.

Cohen, P., Holmes, C.F.B., and Tsukitani, Y. (1990). Okadaic acid: a new probe for the study of cellular regulation. Trends in Biochemical Sciences *15*, 98–102.

Couzens, A.L., Knight, J.D.R., Kean, M.J., Teo, G., Weiss, A., Dunham, W.H., Lin, Z.-Y., Bagshaw, R.D., Sicheri, F., Pawson, T., et al. (2013). Protein interaction network of the

mammalian Hippo pathway reveals mechanisms of kinase-phosphatase interactions. Sci Signal *6*, rs15.

Creasy, C.L., and Chernoff, J. (1995a). Cloning and Characterization of a Human Protein Kinase with Homology to Ste20. J. Biol. Chem. *270*, 21695–21700.

Creasy, C.L., and Chernoff, J. (1995b). Cloning and characterization of a member of the MST subfamily of Ste20-like kinases. Gene *167*, 303–306.

Creasy, C.L., Ambrose, D.M., and Chernoff, J. (1996). The Ste20-like protein kinase, Mst1, dimerizes and contains an inhibitory domain. J. Biol. Chem. *271*, 21049–21053.

Dalton, A.J., and Felix, M.D. (1954). Cytologic and cytochemical characteristics of the Golgi substance of epithelial cells of the epididymis in situ, in homogenates and after isolation. Am. J. Anat. *94*, 171–207.

Del Re, D.P., Matsuda, T., Zhai, P., Gao, S., Clark, G.J., Van Der Weyden, L., and Sadoshima, J. (2010). Proapoptotic Rassf1A/Mst1 signaling in cardiac fibroblasts is protective against pressure overload in mice. J. Clin. Invest. *120*, 3555–3567.

Deng, Y., Pang, A., and Wang, J.H. (2003). Regulation of mammalian STE20-like kinase 2 (MST2) by protein phosphorylation/dephosphorylation and proteolysis. J. Biol. Chem. *278*, 11760–11767.

Di Paolo, G., and De Camilli, P. (2006). Phosphoinositides in cell regulation and membrane dynamics. Nature *443*, 651–657.

Dippold, H.C., Ng, M.M., Farber-Katz, S.E., Lee, S.-K., Kerr, M.L., Peterman, M.C., Sim, R., Wiharto, P.A., Galbraith, K.A., Madhavarapu, S., et al. (2009). GOLPH3 bridges phosphatidylinositol-4- phosphate and actomyosin to stretch and shape the Golgi to promote budding. Cell *139*, 337–351.

Dong, J., Feldmann, G., Huang, J., Wu, S., Zhang, N., Comerford, S.A., Gayyed, M.F., Anders, R.A., Maitra, A., and Pan, D. (2007). Elucidation of a universal size-control mechanism in Drosophila and mammals. Cell *130*, 1120–1133.

Dröscher, A. (1998). Camillo Golgi and the discovery of the Golgi apparatus. Histochem. Cell Biol. *109*, 425–430.

Dupree, P., and Sherrier, D.J. (1998). The plant Golgi apparatus. Biochimica et Biophysica Acta (BBA) - Molecular Cell Research *1404*, 259–270.

Eagle, H., and Levine, E.M. (1967). Growth Regulatory Effects of Cellular Interaction. Nature *213*, 1102–1106.

Fan, F., He, Z., Kong, L.-L., Chen, Q., Yuan, Q., Zhang, S., Ye, J., Liu, H., Sun, X., Geng, J., et al. (2016). Pharmacological targeting of kinases MST1 and MST2 augments tissue repair and regeneration. Sci Transl Med *8*, 352ra108.

Farber-Katz, S.E., Dippold, H.C., Buschman, M.D., Peterman, M.C., Xing, M., Noakes, C.J., Tat, J., Ng, M.M., Rahajeng, J., Cowan, D.M., et al. (2014). DNA damage triggers Golgi dispersal via DNA-PK and GOLPH3. Cell *156*, 413–427.

Farhan, H., and Rabouille, C. (2011). Signalling to and from the secretory pathway. J. Cell. Sci. *124*, 171–180.

Furusawa, T., Ikawa, S., Yanai, N., and Obinata, M. (2000). Isolation of a novel PDZ-containing myosin from hematopoietic supportive bone marrow stromal cell lines. Biochem. Biophys. Res. Commun. *270*, 67–75.

Gaillard, S., Bartoli, M., Castets, F., and Monneron, A. (2001). Striatin, a calmodulin-dependent scaffolding protein, directly binds caveolin-1. FEBS Lett. *508*, 49–52.

Gao, J., Aksoy, B.A., Dogrusoz, U., Dresdner, G., Gross, B., Sumer, S.O., Sun, Y., Jacobsen, A., Sinha, R., Larsson, E., et al. (2013). Integrative analysis of complex cancer genomics and clinical profiles using the cBioPortal. Sci Signal *6*, pl1.

Glantschnig, H., Rodan, G.A., and Reszka, A.A. (2002). Mapping of MST1 kinase sites of phosphorylation. Activation and autophosphorylation. J. Biol. Chem. *277*, 42987–42996.

Godi, A., Pertile, P., Meyers, R., Marra, P., Di Tullio, G., Iurisci, C., Luini, A., Corda, D., and De Matteis, M.A. (1999). ARF mediates recruitment of PtdIns-4-OH kinase-beta and stimulates synthesis of PtdIns(4,5)P2 on the Golgi complex. Nat. Cell Biol. *1*, 280–287.

Godi, A., Di Campli, A., Konstantakopoulos, A., Di Tullio, G., Alessi, D.R., Kular, G.S., Daniele, T., Marra, P., Lucocq, J.M., and De Matteis, M.A. (2004). FAPPs control Golgi-to-cell-surface membrane traffic by binding to ARF and PtdIns(4)P. Nat. Cell Biol. *6*, 393–404.

Goudreault, M., D'Ambrosio, L.M., Kean, M.J., Mullin, M.J., Larsen, B.G., Sanchez, A., Chaudhry, S., Chen, G.I., Sicheri, F., Nesvizhskii, A.I., et al. (2009). A PP2A Phosphatase High Density Interaction Network Identifies a Novel Striatin-interacting Phosphatase and Kinase Complex Linked to the Cerebral Cavernous Malformation 3 (CCM3) Protein. Mol Cell Proteomics *8*, 157–171.

Graves, J.D., Gotoh, Y., Draves, K.E., Ambrose, D., Han, D.K., Wright, M., Chernoff, J., Clark, E.A., and Krebs, E.G. (1998). Caspase-mediated activation and induction of apoptosis by the mammalian Ste20-like kinase Mst1. EMBO J *17*, 2224–2234.

Guzik-Lendrum, S., Heissler, S.M., Billington, N., Takagi, Y., Yang, Y., Knight, P.J., Homsher, E., and Sellers, J.R. (2013). Mammalian myosin-18A, a highly divergent myosin. J. Biol. Chem. *288*, 9532–9548.

Halberg, N., Sengelaub, C.A., Navrazhina, K., Molina, H., Uryu, K., and Tavazoie, S.F. (2016). PITPNC1 Recruits RAB1B to the Golgi Network to Drive Malignant Secretion. Cancer Cell *29*, 339–353.

Halder, G., and Johnson, R.L. (2011). Hippo signaling: growth control and beyond. Development *138*, 9–22.

Hama, H., Schnieders, E.A., Thorner, J., Takemoto, J.Y., and DeWald, D.B. (1999). Direct involvement of phosphatidylinositol 4-phosphate in secretion in the yeast Saccharomyces cerevisiae. J. Biol. Chem. *274*, 34294–34300.

Hammer, Ø., Harper, D.A.T., and Ryan, P.D. (2001). PAST: Paleontological statistics software package for education and data analysis. Palaeontologia Electronica *4*, 1–9.

Hanahan, D., and Weinberg, R.A. (2000). The hallmarks of cancer. Cell *100*, 57–70.

Hardie, D.G., Haystead, T.A.J., and Sim, A.T.R. (1991). Use of okadaic acid to inhibit protein phosphatases in intact cells. In Methods in Enzymology, (Academic Press), pp. 469–476.

Hariharan, I.K. (2015). Organ Size Control: Lessons from Drosophila. Dev. Cell *34*, 255–265.

Harvey, K.F., Pfleger, C.M., and Hariharan, I.K. (2003). The Drosophila Mst Ortholog, hippo, Restricts Growth and Cell Proliferation and Promotes Apoptosis. Cell *114*, 457–467.

Hauri, S., Wepf, A., van Drogen, A., Varjosalo, M., Tapon, N., Aebersold, R., and Gstaiger, M. (2013). Interaction proteome of human Hippo signaling: modular control of the co-activator YAP1. Mol Syst Biol *9*.

Haystead, T.A., Sim, A.T., Carling, D., Honnor, R.C., Tsukitani, Y., Cohen, P., and Hardie, D.G. (1989). Effects of the tumour promoter okadaic acid on intracellular protein phosphorylation and metabolism. Nature *337*, 78–81.

Holley, R.W. (1975). Control of growth of mammalian cells in cell culture. Nature *258*, 487–490.

Hwang, J., and Pallas, D.C. (2014). STRIPAK complexes: structure, biological function, and involvement in human diseases. Int. J. Biochem. Cell Biol. *47*, 118–148.

Hwang, E., Ryu, K.-S., Pääkkönen, K., Güntert, P., Cheong, H.-K., Lim, D.-S., Lee, J.-O., Jeon, Y.H., and Cheong, C. (2007). Structural insight into dimeric interaction of the SARAH domains from Mst1 and RASSF family proteins in the apoptosis pathway. Proc Natl Acad Sci U S A *104*, 9236–9241.

Hwang, E., Cheong, H.-K., Ul Mushtaq, A., Kim, H.-Y., Yeo, K.J., Kim, E., Lee, W.C., Hwang, K.Y., Cheong, C., and Jeon, Y.H. (2014). Structural basis of the heterodimerization of the MST and RASSF SARAH domains in the Hippo signalling pathway. Acta Crystallogr. D Biol. Crystallogr. *70*, 1944–1953.

Ishihara, H., Martin, B.L., Brautigan, D.L., Karaki, H., Ozaki, H., Kato, Y., Fusetani, N., Watabe, S., Hashimoto, K., Uemura, D., et al. (1989). Calyculin A and okadaic acid: Inhibitors of protein phosphatase activity. Biochemical and Biophysical Research Communications *159*, 871–877.

Isogawa, Y., Kon, T., Inoue, T., Ohkura, R., Yamakawa, H., Ohara, O., and Sutoh, K. (2005). The N-terminal domain of MYO18A has an ATP-insensitive actin-binding site. Biochemistry *44*, 6190–6196.

Jang, S.-W., Yang, S.-J., Srinivasan, S., and Ye, K. (2007). Akt Phosphorylates MstI and Prevents Its Proteolytic Activation, Blocking FOXO3 Phosphorylation and Nuclear Translocation. J. Biol. Chem. *282*, 30836–30844.

Jin, Y., Dong, L., Lu, Y., Wu, W., Hao, Q., Zhou, Z., Jiang, J., Zhao, Y., and Zhang, L. (2012). Dimerization and cytoplasmic localization regulate Hippo kinase signaling activity in organ size control. J. Biol. Chem. *287*, 5784–5796.

John, M.A.R.S., Tao, W., Fei, X., Fukumoto, R., Carcangiu, M.L., Brownstein, D.G., Parlow, A.F., McGrath, J., and Xu, T. (1999). Mice deficient of Lats1 develop soft-tissue sarcomas, ovarian tumours and pituitary dysfunction. Nature Genetics *21*, 182–186.

Jung, S., Kang, J.G., Lee, J.H., Song, K.J., Ko, J.-H., and Kim, Y.-S. (2014). PHLPP1 regulates contact inhibition by dephosphorylating Mst1 at the inhibitory site. Biochem. Biophys. Res. Commun. *443*, 1263–1269.

Kaji, D.M., and Tsukitani, Y. (1991). Role of protein phosphatase in activation of KCl cotransport in human erythrocytes. American Journal of Physiology-Cell Physiology *260*, C176–C180.

Kean, M.J., Ceccarelli, D.F., Goudreault, M., Sanches, M., Tate, S., Larsen, B., Gibson, L.C.D., Derry, W.B., Scott, I.C., Pelletier, L., et al. (2011). Structure-Function Analysis of Core STRIPAK Proteins A SIGNALING COMPLEX IMPLICATED IN GOLGI POLARIZATION. J. Biol. Chem. *286*, 25065–25075.

Kelly, L.M., Barila, G., Liu, P., Evdokimova, V.N., Trivedi, S., Panebianco, F., Gandhi, M., Carty, S.E., Hodak, S.P., Luo, J., et al. (2014). Identification of the transforming STRN-ALK fusion as a potential therapeutic target in the aggressive forms of thyroid cancer. Proc Natl Acad Sci U S A *111*, 4233–4238.

Kuna, R.S., and Field, S.J. (2018). GOLPH3: A Golgi phosphatidylinositol(4)phosphate effector that directs vesicle trafficking and drives cancer. J. Lipid Res. jlr.R088328.

Lee, K.K., Ohyama, T., Yajima, N., Tsubuki, S., and Yonehara, S. (2001). MST, a physiological caspase substrate, highly sensitizes apoptosis both upstream and downstream of caspase activation. J. Biol. Chem. *276*, 19276–19285.

Lesley, J., Hascall, V.C., Tammi, M., and Hyman, R. (2000). Hyaluronan Binding by Cell Surface CD44. J. Biol. Chem. *275*, 26967–26975.

Makowski, S.L., Tran, T.T.T., and Field, S.J. (2017). Emerging themes of regulation at the Golgi. Curr. Opin. Cell Biol. *45*, 17–23.

van Meer, G., Voelker, D.R., and Feigenson, G.W. (2008). Membrane lipids: where they are and how they behave. Nat Rev Mol Cell Biol *9*, 112–124.

Meng, Z., Moroishi, T., Mottier-Pavie, V., Plouffe, S.W., Hansen, C.G., Hong, A.W., Park, H.W., Mo, J.-S., Lu, W., Lu, S., et al. (2015). MAP4K family kinases act in parallel to MST1/2 to activate LATS1/2 in the Hippo pathway. Nat Commun *6*, 8357.

Meng, Z., Moroishi, T., and Guan, K.-L. (2016). Mechanisms of Hippo pathway regulation. Genes Dev. *30*, 1–17.

Millward, T.A., Zolnierowicz, S., and Hemmings, B.A. (1999). Regulation of protein kinase cascades by protein phosphatase 2A. Trends in Biochemical Sciences *24*, 186–191.

Minn, A.J., Gupta, G.P., Siegel, P.M., Bos, P.D., Shu, W., Giri, D.D., Viale, A., Olshen, A.B., Gerald, W.L., and Massagué, J. (2005). Genes that mediate breast cancer metastasis to lung. Nature *436*, 518–524.

Minogue, S., Anderson, J.S., Waugh, M.G., dos Santos, M., Corless, S., Cramer, R., and Hsuan, J.J. (2001). Cloning of a human type II phosphatidylinositol 4-kinase reveals a novel lipid kinase family. J. Biol. Chem. *276*, 16635–16640.

Mo, J.-S., Park, H.W., and Guan, K.-L. (2014). The Hippo signaling pathway in stem cell biology and cancer. EMBO Rep. *15*, 642–656.

Moreno, C.S., Park, S., Nelson, K., Ashby, D., Hubalek, F., Lane, W.S., and Pallas, D.C. (2000). WD40 repeat proteins striatin and S/G(2) nuclear autoantigen are members of a novel family of calmodulin-binding proteins that associate with protein phosphatase 2A. J. Biol. Chem. *275*, 5257–5263.

Moreno, C.S., Lane, W.S., and Pallas, D.C. (2001). A mammalian homolog of yeast MOB1 is both a member and a putative substrate of striatin family-protein phosphatase 2A complexes. J. Biol. Chem. *276*, 24253–24260.

Morrison, H., Sherman, L.S., Legg, J., Banine, F., Isacke, C., Haipek, C.A., Gutmann, D.H., Ponta, H., and Herrlich, P. (2001). The NF2 tumor suppressor gene product, merlin, mediates contact inhibition of growth through interactions with CD44. Genes Dev. *15*, 968–980.

Munro, S. (2005). The Golgi apparatus: defining the identity of Golgi membranes. Curr. Opin. Cell Biol. *17*, 395–401.

Muro, Y., Chan, E., Landberg, G., and Tan, E. (1995). A Cell-Cycle Nuclear Autoantigen Containing Wd-40 Motifs Expressed Mainly in S-Phase and G(2)-Phase Cells. Biochemical and Biophysical Research Communications *207*, 1029–1037.

Murray, L.B., Lau, Y.-K.I., and Yu, Q. (2012). Merlin is a negative regulator of human melanoma growth. PLoS ONE *7*, e43295.

Nehme, N.T., Schmid, J.P., Debeurme, F., André-Schmutz, I., Lim, A., Nitschke, P., Rieux-Laucat, F., Lutz, P., Picard, C., Mahlaoui, N., et al. (2012). MST1 mutations in autosomal recessive primary immunodeficiency characterized by defective naive T-cell survival. Blood *119*, 3458–3468.

Ng, M.M., Dippold, H.C., Buschman, M.D., Noakes, C.J., and Field, S.J. (2013). GOLPH3L antagonizes GOLPH3 to determine Golgi morphology. Mol. Biol. Cell *24*, 796–808.

Ni, L., Li, S., Yu, J., Min, J., Brautigam, C.A., Tomchick, D.R., Pan, D., and Luo, X. (2013). Structural basis for autoactivation of human Mst2 kinase and its regulation by RASSF5. Structure *21*, 1757–1768.

Ong, S.-E., Blagoev, B., Kratchmarova, I., Kristensen, D.B., Steen, H., Pandey, A., and Mann, M. (2002). Stable isotope labeling by amino acids in cell culture, SILAC, as a simple and accurate approach to expression proteomics. Mol. Cell Proteomics *1*, 376–386.

Pan, D. (2007). Hippo signaling in organ size control. Genes Dev. *21*, 886–897.

Park, H.W., and Guan, K.-L. (2013). Regulation of the Hippo pathway and implications for anticancer drug development. Trends Pharmacol. Sci. *34*, 581–589.

Penzo-Méndez, A.I., and Stanger, B.Z. (2015). Organ-Size Regulation in Mammals. Cold Spring Harb Perspect Biol *7*, a019240.

Polesello, C., Huelsmann, S., Brown, N.H., and Tapon, N. (2006). The Drosophila RASSF homolog antagonizes the hippo pathway. Curr. Biol. *16*, 2459–2465.

Praskova, M., Khoklatchev, A., Ortiz-Vega, S., and Avruch, J. (2004). Regulation of the MST1 kinase by autophosphorylation, by the growth inhibitory proteins, RASSF1 and NORE1, and by Ras. Biochem. J. *381*, 453–462.

Praskova, M., Xia, F., and Avruch, J. (2008). MOBKL1A/MOBKL1B phosphorylation by MST1 and MST2 inhibits cell proliferation. Curr. Biol. *18*, 311–321.

Presley, J., Cole, N., Schroer, T., Hirschberg, K., Zaal, K., and Lippincott-Schwartz, J. (1997). ER to Golgi transport visualized in living cells. Nature *389*, 81–85.

Puthenveedu, M.A., and Linstedt, A.D. (2005). Subcompartmentalizing the Golgi apparatus. Current Opinion in Cell Biology *17*, 369–375.

Qiao, M., Wang, Y., Xu, X., Lu, J., Dong, Y., Tao, W., Stein, J., Stein, G.S., Iglehart, J.D., Shi, Q., et al. (2010). Mst1 is an interacting protein that mediates PHLPPs' induced apoptosis. Mol. Cell *38*, 512–523.

Rawat, S.J., and Chernoff, J. (2015). Regulation of mammalian Ste20 (Mst) kinases. Trends in Biochemical Sciences *40*, 149–156.

Record, C.J., Chaikuad, A., Rellos, P., Das, S., Pike, A.C.W., Fedorov, O., Marsden, B.D., Knapp, S., and Lee, W.H. (2010). Structural Comparison of Human Mammalian Ste20-Like Kinases. PLOS ONE *5*, e11905.

Ribeiro, P.S., Josué, F., Wepf, A., Wehr, M.C., Rinner, O., Kelly, G., Tapon, N., and Gstaiger, M. (2010). Combined functional genomic and proteomic approaches identify a PP2A complex as a negative regulator of Hippo signaling. Mol. Cell *39*, 521–534.

Rossanese, O.W., Soderholm, J., Bevis, B.J., Sears, I.B., O'Connor, J., Williamson, E.K., and Glick, B.S. (1999). Golgi Structure Correlates with Transitional Endoplasmic Reticulum Organization in Pichia pastoris and Saccharomyces cerevisiae. The Journal of Cell Biology *145*, 69–81.

Roux, K.J., Kim, D.I., Raida, M., and Burke, B. (2012). A promiscuous biotin ligase fusion protein identifies proximal and interacting proteins in mammalian cells. J Cell Biol *196*, 801–810.

Roux, K.J., Kim, D.I., and Burke, B. (2013). BioID: A Screen for Protein-Protein Interactions. Current Protocols in Protein Science *74*, 19.23.1-19.23.14.

Sarikaya, D.P., and Extavour, C.G. (2015). The Hippo Pathway Regulates Homeostatic Growth of Stem Cell Niche Precursors in the Drosophila Ovary. PLOS Genetics *11*, e1004962.

Scales, S.J., Pepperkok, R., and Kreis, T.E. (1997). Visualization of ER-to-Golgi Transport in Living Cells Reveals a Sequential Mode of Action for COPII and COPI. Cell *90*, 1137–1148.

Schmitz, K.R., Liu, J., Li, S., Setty, T.G., Wood, C.S., Burd, C.G., and Ferguson, K.M. (2008). Golgi localization of glycosyltransferases requires a Vps74p oligomer. Dev. Cell *14*, 523–534.

Schneider, C.A., Rasband, W.S., and Eliceiri, K.W. (2012). NIH Image to ImageJ: 25 years of image analysis. Nat. Methods *9*, 671–675.

Scott, K.L., Kabbarah, O., Liang, M.-C., Ivanova, E., Anagnostou, V., Wu, J., Dhakal, S., Wu, M., Chen, S., Feinberg, T., et al. (2009). GOLPH3 modulates mTOR signalling and rapamycin sensitivity in cancer. Nature *459*, 1085–1090.

Sekar, R.B., and Periasamy, A. (2003). Fluorescence resonance energy transfer (FRET) microscopy imaging of live cell protein localizations. J Cell Biol *160*, 629–633.

Seshacharyulu, P., Pandey, P., Datta, K., and Batra, S.K. (2013). Phosphatase: PP2A structural importance, regulation and its aberrant expression in cancer. Cancer Lett. *335*, 9–18.

Shaw, R.J., McClatchey, A.I., and Jacks, T. (1998). Regulation of the Neurofibromatosis Type 2 Tumor Suppressor Protein, Merlin, by Adhesion and Growth Arrest Stimuli. J. Biol. Chem. *273*, 7757–7764.

Sherman, L., Skroch-Angel, P., Moll, J., Schwechheimer, K., Ponta, H., Herrlich, P., and Hofmann, M. (1995). Schwann cell tumors express characteristic patterns of CD44 splice variants. J. Neurooncol. *26*, 171–184.

Shi, Z., Jiao, S., and Zhou, Z. (2016). STRIPAK complexes in cell signaling and cancer. Oncogene *35*, 4549–4557.

Sjöstrand, F.S., and Hanzon, V. (1954). Electron microscopy of the golgi apparatus of the exocrine pancreas cells. Experientia *10*, 367–369.

Smith, T.F. (2008). Diversity of WD-Repeat proteins. In The Coronin Family of Proteins, (Springer, New York, NY), pp. 20–30.

Snyder, C.M., Mardones, G.A., Ladinsky, M.S., and Howell, K.E. (2006). GMx33 Associates with the Trans-Golgi Matrix in a Dynamic Manner and Sorts within Tubules Exiting the Golgi. Mol Biol Cell *17*, 511–524.

Staehelin, L.A., and Kang, B.-H. (2008). Nanoscale Architecture of Endoplasmic Reticulum Export Sites and of Golgi Membranes as Determined by Electron Tomography. Plant Physiology *147*, 1454–1468.

Stoker, M.G., and Rubin, H. (1967). Density dependent inhibition of cell growth in culture. Nature *215*, 171–172.

Strating, J.R.P.M., and Martens, G.J.M. (2009). The p24 family and selective transport processes at the ER—Golgi interface. Biology of the Cell *101*, 495–509.

Tachibana, K., Scheuer, P.J., Tsukitani, Y., Kikuchi, H., Van Engen, D., Clardy, J., Gopichand, Y., and Schmitz, F.J. (1981). Okadaic acid, a cytotoxic polyether from two marine sponges of the genus Halichondria. J. Am. Chem. Soc. *103*, 2469–2471.

Taft, M.H., Behrmann, E., Munske-Weidemann, L.-C., Thiel, C., Raunser, S., and Manstein, D.J. (2013). Functional Characterization of Human Myosin-18A and its Interaction with F-actin and GOLPH3. J. Biol. Chem. jbc.M113.497180.

Taylor, L.K., Wang, H.C., and Erikson, R.L. (1996). Newly identified stress-responsive protein kinases, Krs-1 and Krs-2. Proc Natl Acad Sci U S A *93*, 10099–10104.

Thyberg, J., and Moskalewski, S. (1985). Microtubules and the organization of the Golgi complex. Exp. Cell Res. *159*, 1–16.

Udan, R.S., Kango-Singh, M., Nolo, R., Tao, C., and Halder, G. (2003). Hippo promotes proliferation arrest and apoptosis in the Salvador/Warts pathway. Nat. Cell Biol. *5*, 914–920.

Valm, A.M., Cohen, S., Legant, W.R., Melunis, J., Hershberg, U., Wait, E., Cohen, A.R., Davidson, M.W., Betzig, E., and Lippincott-Schwartz, J. (2017). Applying systems-level spectral imaging and analysis to reveal the organelle interactome. Nature *546*, 162–167.

Wang, Y.J., Wang, J., Sun, H.Q., Martinez, M., Sun, Y.X., Macia, E., Kirchhausen, T., Albanesi, J.P., Roth, M.G., and Yin, H.L. (2003). Phosphatidylinositol 4 Phosphate Regulates Targeting of Clathrin Adaptor AP-1 Complexes to the Golgi. Cell *114*, 299–310.

Wehland, J., Henkart, M., Klausner, R., and Sandoval, I.V. (1983). Role of microtubules in the distribution of the Golgi apparatus: effect of taxol and microinjected anti-alpha-tubulin antibodies. Proc. Natl. Acad. Sci. U.S.A. *80*, 4286–4290.

Weinstein, J.N., Collisson, E.A., Mills, G.B., Shaw, K.M., Ozenberger, B.A., Ellrott, K., Shmulevich, I., Sander, C., and Stuart, J.M. (2013). The Cancer Genome Atlas Pan-Cancer Analysis Project. Nat Genet *45*, 1113–1120.

Wise, G.E., and Flickinger, C.J. (1970). Cytochemical staining of the Golgi apparatus in Amoeba Proteus. J Cell Biol *46*, 620–626.

Wood, C.S., Schmitz, K.R., Bessman, N.J., Setty, T.G., Ferguson, K.M., and Burd, C.G. (2009). PtdIns4P recognition by Vps74/GOLPH3 links PtdIns 4-kinase signaling to retrograde Golgi trafficking. J. Cell Biol. *187*, 967–975.

Wu, C.C., Taylor, R.S., Lane, D.R., Ladinsky, M.S., Weisz, J.A., and Howell, K.E. (2000). GMx33: a novel family of trans-Golgi proteins identified by proteomics. Traffic *1*, 963–975.

Wu, S., Huang, J., Dong, J., and Pan, D. (2003). hippo Encodes a Ste-20 Family Protein Kinase that Restricts Cell Proliferation and Promotes Apoptosis in Conjunction with salvador and warts. Cell *114*, 445–456.

Xing, M., Peterman, M.C., Davis, R.L., Oegema, K., Shiau, A.K., and Field, S.J. (2016). GOLPH3 drives cell migration by promoting Golgi reorientation and directional trafficking to the leading edge. Mol. Biol. Cell *27*, 3828–3840.

Yabuta, N., Mukai, S., Okamoto, A., Okuzaki, D., Suzuki, H., Torigata, K., Yoshida, K., Okada, N., Miura, D., Ito, A., et al. (2013). N-terminal truncation of Lats1 causes abnormal cell growth control and chromosomal instability. J Cell Sci *126*, 508–520.

Yasumoto, T., Murata, M., Oshima, Y., Matsumoto, G.K., and Clardy, J. (1984). Diarrhetic Shellfish Poisoning. In Seafood Toxins, (American Chemical Society), pp. 207–214.

Yoon, S., Choi, J., Yoon, J., Huh, J.-W., and Kim, D. (2006). Okadaic acid induces JNK activation, bim overexpression and mitochondrial dysfunction in cultured rat cortical neurons. Neuroscience Letters *394*, 190–195.

Zhang, X., and Wang, Y. (2016). GRASPs in Golgi Structure and Function. Front. Cell Dev. Biol. *3*.

Zhang, J., Ji, J.-Y., Yu, M., Overholtzer, M., Smolen, G.A., Wang, R., Brugge, J.S., Dyson, N.J., and Haber, D.A. (2009). YAP-dependent induction of amphiregulin identifies a non-cell-autonomous component of the Hippo pathway. Nature Cell Biology *11*, 1444–1450.

Zhao, B., Wei, X., Li, W., Udan, R.S., Yang, Q., Kim, J., Xie, J., Ikenoue, T., Yu, J., Li, L., et al. (2007). Inactivation of YAP oncoprotein by the Hippo pathway is involved in cell contact inhibition and tissue growth control. Genes Dev *21*, 2747–2761.

Zhao, B., Tumaneng, K., and Guan, K.-L. (2011). The Hippo pathway in organ size control, tissue regeneration and stem cell self-renewal. Nature Cell Biology *13*, 877–883.

Zheng, Y., Liu, B., Wang, L., Lei, H., Prieto, K.D.P., and Pan, D. (2017). Homeostatic Control of Hpo/MST Kinase Activity through Autophosphorylation-Dependent Recruitment of the STRIPAK PP2A Phosphatase Complex. Cell Reports *21*, 3612–3623.

Zhou, D., Medoff, B.D., Chen, L., Li, L., Zhang, X., Praskova, M., Liu, M., Landry, A., Blumberg, R.S., Boussiotis, V.A., et al. (2008). The Nore1B/Mst1 complex restrains antigen receptor-induced proliferation of naïve T cells. PNAS *105*, 20321–20326.

Zhou, D., Conrad, C., Xia, F., Park, J.-S., Payer, B., Yin, Y., Lauwers, G.Y., Thasler, W., Lee, J.T., Avruch, J., et al. (2009). Mst1 and Mst2 maintain hepatocyte quiescence and suppress hepatocellular carcinoma development through inactivation of the Yap1 oncogene. Cancer Cell *16*, 425–438.